Top quark pair production and decay at hadron colliders

W. Bernreuther [a,*]**, A. Brandenburg** [a,b,†]**, Z. G. Si** [c,‡] **and P. Uwer** [d]

[a]Institut für Theoretische Physik, RWTH Aachen, 52056 Aachen, Germany
[b]DESY-Theorie, 22603 Hamburg, Germany
[c]Department of Physics, Shandong University, Jinan, Shandong 250100, China
[d]Institut für Theoretische Teilchenphysik, Universität Karlsruhe, 76128 Karlsruhe, Germany and
Department of Physics, TH Division, CERN, CH-1211 Geneva 23, Switzerland

Abstract

In ongoing and upcoming hadron collider experiments, top quark physics will play an important rôle in testing the Standard Model and its possible extensions. In this work we present analytic results for the differential cross sections of top quark pair production in hadronic collisions at next-to-leading order in the QCD coupling, keeping the full dependence on the spins of the top quarks. These results are combined with the corresponding next-to-leading order results for the decay of polarized top quarks into dilepton, lepton plus jets, and all jets final states. As an application we predict double differential angular distributions which are due to the QCD-induced top quark spin correlations in the intermediate state. In addition to the analytic results, we give numerical results in terms of fit functions that can easily be used in an experimental analysis.

I. Introduction

A large number of top quarks will be produced at the Fermilab Tevatron and at the CERN Large Hadron Collider (LHC). This makes the exploration of the interactions of these quarks one of the main physics issues at these facilities. Top quark spin phenomena are expected to play an important rôle in these efforts: the spin-polarization and spin-correlation phenomena reflect in detail the interactions involved in top quark production and decay, thus give an opportunity for precise tests of these interactions. In contrast to light quarks the top quark polarization/correlation effects are not washed out by hadronization. This is because these quarks are extremely short-lived and thus decay weakly before hadronization can take place [1].

As far as theoretical predictions on top quark pair production are concerned, the cross sections for spin-averaged top quark pair production have been known for quite some time to next-to-leading order (NLO) in QCD [2, 3, 4, 5]. The NLO results were refined later by resummation of soft gluon and threshold logarithms; see Refs. [6, 7, 8, 9], and the review Ref. [10] and references therein. As to top quark spin phenomena at hadron colliders there exists an extensive literature on theoretical investigations within the standard model (SM) [11, 12, 13, 14, 15, 16, 17, 18, 19] and beyond [20, 21, 22, 23, 24, 25, 26, 27, 28, 29, 30, 31, 32]. Yet the precision of these analyses — in particular within the SM — must be increased for the data samples that will be recorded at the Tevatron and at the LHC to be fully explored.

In this paper we study hadronic top quark pair production and decay at NLO QCD by taking the spin of the top and antitop quarks into account. In particular we present the differential cross sections to order α_s^3, describing the $t\bar{t} + X$ production in a general spin configuration. Short reports on parts of this work were given in Refs. [33, 34, 35].

The theoretical description of top quark pair production in proton–proton and proton–antiproton collisions at next-to-leading order in the QCD coupling involves the following parton reactions: quark–antiquark annihilation

$$q + \bar{q} \rightarrow t + \bar{t}, \tag{I.1}$$

$$q + \bar{q} \rightarrow t + \bar{t} + g, \tag{I.2}$$

which is the dominant production mechanism at the Tevatron, gluon–gluon fusion

$$g + g \rightarrow t + \bar{t}, \tag{I.3}$$

$$g + g \rightarrow t + \bar{t} + g, \tag{I.4}$$

which dominates at the LHC, and

$$g + q \rightarrow t + \bar{t} + q, \tag{I.5}$$

$$g + \bar{q} \rightarrow t + \bar{t} + \bar{q}, \tag{I.6}$$

which gives, in general, only a tiny correction.

As mentioned earlier the top quarks decay before they can form hadronic bound states. To construct realistic observables, the decays of the top and antitop quarks have to be taken into account. We consider the SM decays of polarized (anti)top quarks both into semileptonic and non-leptonic final states, taking into account the order α_s QCD corrections [36, 37]. The main SM top decay modes at that order are:

$$t \rightarrow bW \rightarrow b\ell\nu_\ell(g), bq\bar{q}'(g) \tag{I.7}$$

where $q\bar{q}' = u\bar{d}, c\bar{s}$. A complete next-to-leading order QCD analysis of top quark production *and* decay thus involves the parton reactions

$$gg, q\bar{q} \xrightarrow{t\bar{t}} b\bar{b} + 4f, \tag{I.8}$$

$$gg, q\bar{q} \xrightarrow{t\bar{t}} b\bar{b} + 4f + g, \tag{I.9}$$

$$g + q(\bar{q}) \xrightarrow{t\bar{t}} b\bar{b} + 4f + q(\bar{q}), \tag{I.10}$$

where $f = q, \ell, \nu_\ell$. In view of the fact that the total width Γ_t of the top quark is much smaller than its mass, $\Gamma_t/m_t = O(1\%)$, one may expand the amplitudes of the reactions Eqs. (I.8)–(I.10) around the poles of the unstable top and antitop quarks, which corresponds to an expansion in powers of Γ_t/m_t. Only the leading term of this expansion, i.e. the residue of the double poles, is considered here. In this framework the radiative corrections to Eq. (I.8) can be classified into so-called factorizable and non-factorizable corrections — and, likewise, the contributions to the squared matrix elements of Eq. (I.9). We compute the factorizable corrections in the narrow width approximation $\Gamma_t/m_t \rightarrow 0$. In this approximation the squared matrix element $|\mathcal{M}|^2$ of the respective reaction is of the form

$$|\mathcal{M}|^2 \propto \text{Tr}\,[\rho R \bar{\rho}] = \rho_{\alpha'\alpha} R_{\alpha\alpha',\beta\beta'} \bar{\rho}_{\beta'\beta}. \tag{I.11}$$

Here R denotes the density matrix that describes the production of on-shell top quark pairs in a specific spin configuration by one of the six reactions Eqs. (I.1)–(I.6). The matrices $\rho, \bar{\rho}$ are the density matrices describing the decay of polarized top and antitop quarks into specific final states. The subscripts in Eq. (I.11) denote the top and antitop spin indices. Both the production and decay density matrices are gauge invariant. The production density matrices are determined from the NLO results for the reactions Eq. (I.1)–Eq. (I.6). The decay density matrices are derived from the results for the reactions shown in Eq. (I.7).

With these building blocks the factorizable NLO QCD corrections to top quark pair production and decay can be computed, keeping the full information on the spin configuration of the intermediate $t\bar{t}$ state. As far as applications of these results are concerned, our primary aim in this paper is the study of final-state angular correlations of the top quark and antiquark decay products, which reflect the spin properties of the top and antitop quarks. For this purpose we consider the following channels:

$$p\bar{p}, pp \rightarrow t\bar{t} + X \rightarrow \ell^+ \ell'^- + X, \tag{I.12}$$

$$p\bar{p}, pp \rightarrow t\bar{t} + X \rightarrow \ell^+ j_2 + X, \tag{I.13}$$

$$p\bar{p}, pp \rightarrow t\bar{t} + X \rightarrow j_1 \ell'^- + X, \tag{I.14}$$

$$p\bar{p}, pp \rightarrow t\bar{t} + X \rightarrow j_1 j_2 + X, \tag{I.15}$$

where $\ell = e, \mu, \tau$, and j_1, j_2 denote jets originating from top and antitop decays. For these final states we study the following distributions at NLO in the coupling α_s:

i. The double distributions

$$\frac{1}{\sigma}\frac{d\sigma}{d\cos\theta_1 d\cos\theta_2} = \frac{1}{4}\left(1 + B_1\cos\theta_1 + B_2\cos\theta_2 - C\cos\theta_1\cos\theta_2\right), \tag{I.16}$$

where σ denotes the cross section for the channel under consideration. Here θ_1 (θ_2) describes the angle between the direction of flight of the lepton ℓ^+ or jet j_1 (ℓ'^- or j_2) in the t ($\bar{t}$) rest frame and

2

a reference direction $\hat{\mathbf{a}}$ ($\hat{\mathbf{b}}$). In particular we will discuss three specific choices for the reference directions $\hat{\mathbf{a}}, \hat{\mathbf{b}}$ which allow a simple physical interpretation.

ii. The opening angle distributions

$$\frac{1}{\sigma}\frac{d\sigma}{d\cos\varphi} = \frac{1}{2}(1 - D\cos\varphi) , \tag{I.17}$$

where φ denotes the angle between the direction of flight of the lepton ℓ^+ (or jet j_1) and of ℓ'^- (or j_2), defined in the t or $\bar{t}$ rest frames, respectively.

The functional forms of the r.h.s. of Eqs. (I.16) and (I.17) hold if no kinematic cuts are applied and will be derived in Section VI.

The results presented in this work are definite predictions of QCD. Specifically, comparison of our results for the above distributions with future measurements will allow for detailed investigations of top quark production and decay dynamics.

The paper is organized as follows. In Section II we present the differential cross sections for the $2 \to 2$ processes Eq. (I.1) and Eq. (I.3) to order α_s^3. In Section III we treat the real gluon radiation Eq. (I.2), Eq. (I.4) and the qg ($\bar{q}g$) fusion processes. In particular, we compute the differential cross sections in the soft and collinear limits and perform the mass factorization. In Section IV we discuss the QCD-induced top and antitop spin effects at NLO, and we treat the issue of constructing infrared and collinear safe $t, \bar{t}$ spin observables at the parton level. Specifically, we compute, for all relevant parton reactions $i \to t\bar{t}X$, the expectation values of four different spin observables. These observables correspond to different choices of the directions $\hat{\mathbf{a}}, \hat{\mathbf{b}}$ used to define the angles in Eq. (I.16). We also show that the spin observables have a simple interpretation as double spin asymmetries with respect to a given quantization axis. The spin observables serve as one building block for the calculation of the distributions Eq. (I.16), Eq. (I.17). The other building blocks are given in Section V: these are the one-particle inclusive angular distributions of the semileptonic [36] and non-leptonic [37] decays of polarized top quarks and antiquarks to order α_s. In Section VI we show that the functional form of the distributions (I.16), (I.17) is indeed as given in (I.16), (I.17). In addition we give NLO formulae for the coefficients C and D defined in Eq. (I.16) and Eq. (I.17). We further investigate the important question of whether the distributions Eqs. (I.16), (I.17) are affected by non-factorizable QCD corrections. In particular we show, using the results of Refs. [38, 39, 40, 41, 42], that the non-factorizable corrections at order α_s^3 do not contribute to Eqs. (I.16), (I.17). In Section VII we present our NLO predictions for these distributions for the dilepton, for the lepton+jet, and for the jet+jet decay channels, both at the Tevatron and the LHC. Section VIII contains our conclusions. Appendix A contains a collection of one-loop integrals that appear in the virtual corrections to the squared matrix elements of $q\bar{q} \to t\bar{t}$ and $gg \to t\bar{t}$, which are given in Appendices B and C, respectively. In Appendix D we give the amplitudes for the processes Eqs. (I.2), (I.4), (I.5), and (I.6), for arbitrary spins of the t and $\bar{t}$ and arbitrary helicities of the massless partons. Appendix E contains fit functions for the NLO results for the expectation values of the four spin observables computed in Section IV.

II. One-loop QCD corrections to qq̄ annihilation and to gg fusion

In this section we present the differential cross sections of the parton processes

$$q(p_1) + \bar{q}(p_2) \to t(k_1, s_t) + \bar{t}(k_2, s_{\bar{t}}), \tag{II.1}$$

$$g(p_1) + g(p_2) \to t(k_1, s_t) + \bar{t}(k_2, s_{\bar{t}}). \tag{II.2}$$

at NLO in α_s. Here p_1, p_2, k_1, and k_2 denote the parton momenta, and the vectors s_t, $s_{\bar{t}}$, with

$$s_t^2 = s_{\bar{t}}^2 = -1 \quad \text{and} \quad k_1 \cdot s_t = k_2 \cdot s_{\bar{t}} = 0, \tag{II.3}$$

describe the spin of the top and antitop quarks. All quarks but the top quark are taken to be massless. The top quark mass is denoted by m. In the calculation of the radiative corrections, ultraviolet as well as soft/collinear singularities are encountered. The singularities are regulated by using dimensional regularization. We keep the spin vectors in 4 dimensions. Note that no scheme dependence is introduced in this way, in particular no 'γ_5 problem' arises. This is because the cancellation of the UV singularities is independent of the external spin state and the soft/collinear singularities are cancelled in a universal way.

In the (anti)top rest frame, the spin of the (anti)top is described by a unit vector $\hat{\mathbf{s}}_t$ ($\hat{\mathbf{s}}_{\bar{t}}$). We define the t ($\bar{t}$) rest frame by a rotation-free Lorentz boost from the zero momentum frame of the $t\bar{t}$ quarks ($t\bar{t}$-ZMF). In this frame

$$(k_1 + k_2)^\mu = \left(\sqrt{(k_1 + k_2)^2}, 0, 0, 0 \right). \tag{II.4}$$

As we will see in Section IV, choosing this frame simplifies the definition of infrared and collinear safe observables at the parton level. For the $2 \to 2$ processes Eqs. (II.1) and (II.2), the $t\bar{t}$-ZMF coincides with the centre-of-mass frame of the initial partons. Note that in principle the $t\bar{t}$-ZMF is only defined up to an arbitrary rotation. One can resolve this, for instance, as done in an experiment where the direction of one of the initial hadron beams is chosen as z-axis and one orthogonal direction as x-axis. After having measured the 4-momenta of the t and $\bar{t}$ in this laboratory frame, the $t\bar{t}$-ZMF can be defined unambiguously by a rotation-free boost. The observables that we consider in Sections IV and VI are actually the same for any choice of the $t\bar{t}$-ZMF.

In the $t\bar{t}$-ZMF we have

$$s_t^\mu = \left(\frac{\mathbf{k} \cdot \hat{\mathbf{s}}_t}{m}, \hat{\mathbf{s}}_t + \frac{\mathbf{k}(\mathbf{k} \cdot \hat{\mathbf{s}}_t)}{m(m+E)} \right), \tag{II.5}$$

$$s_{\bar{t}}^\mu = \left(-\frac{\mathbf{k} \cdot \hat{\mathbf{s}}_{\bar{t}}}{m}, \hat{\mathbf{s}}_{\bar{t}} + \frac{\mathbf{k}(\mathbf{k} \cdot \hat{\mathbf{s}}_{\bar{t}})}{m(m+E)} \right), \tag{II.6}$$

where E and $\mathbf{k}$ are the energy and the 3-momentum of the top quark in the $t\bar{t}$-ZMF.

In $d = 4 - 2\varepsilon$ dimensions the Born+virtual parts of the cross sections of the processes Eqs. (II.1), (II.2) are, to order α_s^3, of the following form:

$$d\sigma^i(s_t, s_{\bar{t}}) = d\sigma_B^i + d\sigma_V^i = \frac{1}{2\hat{s}} \Phi_i d\Gamma_2 \left[|\mathcal{M}_B^i|^2 + \mathcal{M}_B^{*i}\mathcal{M}_V^i + \mathcal{M}_V^{*i}\mathcal{M}_B^i \right], \tag{II.7}$$

4

where $i = q\bar{q}, gg$, and $\hat{s} = (p_1 + p_2)^2$. The factors

$$\Phi_{q\bar{q}} = \frac{1}{4N^2}, \qquad \Phi_{gg} = \frac{1}{(N^2-1)^2(d-2)^2} \tag{II.8}$$

arise from averaging over the colours ($N = 3$) and spins of the initial partons. The 2-particle phase-space measure is denoted by $d\Gamma_2$, $\mathcal{M}_B^i$ are the Born amplitudes and $\mathcal{M}_V^i$ those of the virtual corrections. As indicated earlier, Eq. (II.7) still contains soft and collinear singularities regulated in the framework of conventional dimensional regularization. The production spin density matrices R^i that enter the formula (I.11) are obtained from the identity

$$d\sigma^i(s_t, s_{\bar{t}}) = \frac{1}{2\hat{s}} \Phi_i d\Gamma_2 \frac{1}{4} \text{Tr} \left[R^i (\mathbb{1} + \hat{\mathbf{s}}_t \cdot \boldsymbol{\tau}) \otimes (\mathbb{1} + \hat{\mathbf{s}}_{\bar{t}} \cdot \boldsymbol{\tau}) \right], \tag{II.9}$$

where τ_i are the Pauli matrices.

II.1. Born matrix elements

II.1.1. q$\bar{q}$ initial states

For the sake of fixing our notation, we present the squared Born matrix element for the reaction (II.1) in two ways, which prove useful in the presentation of the virtual, soft, and collinear contributions to the cross sections.

The squared Born matrix element reads

$$|\mathcal{M}_B^{q\bar{q}}|^2 = 4\pi^2 \alpha_s^2 (N^2 - 1) \left\{ A_0^{q\bar{q}} + C_{\mu\nu}^{q\bar{q}} s_t^\mu s_{\bar{t}}^\nu \right\}, \tag{II.10}$$

where

$$A_0^{q\bar{q}} = 2 - \beta^2 \left(1 - y^2 \right) - 2\varepsilon. \tag{II.11}$$

Here

$$\beta = \sqrt{1 - \frac{4m^2}{\hat{s}}}, \tag{II.12}$$

and y is the cosine of the scattering angle in the $t\bar{t}$-ZMF, i.e. $y = \hat{\mathbf{p}} \cdot \hat{\mathbf{k}}$, where $\hat{\mathbf{p}}$ is the direction of the initial quark (or one of the gluons in the case of gg fusion) in that frame. The spin-dependent term can be decomposed as follows:

$$\begin{aligned} C_{\mu\nu}^{q\bar{q}} s_t^\mu s_{\bar{t}}^\nu &= C_0^{q\bar{q}} (s_t \cdot s_{\bar{t}}) + D_0^{q\bar{q}} \left[(p_1 \cdot s_t)(p_1 \cdot s_{\bar{t}}) + (p_2 \cdot s_t)(p_2 \cdot s_{\bar{t}}) \right] \\ &+ E_0^{q\bar{q}} (p_1 \cdot s_t)(p_2 \cdot s_{\bar{t}}) + F_0^{q\bar{q}} (p_2 \cdot s_t)(p_1 \cdot s_{\bar{t}}), \end{aligned} \tag{II.13}$$

where

$$\begin{aligned} C_0^{q\bar{q}} &= \beta^2 (1 - y^2) + 2\varepsilon, \\ D_0^{q\bar{q}} &= -\frac{4}{\hat{s}} \varepsilon, \\ E_0^{q\bar{q}} &= -\frac{4}{\hat{s}} \left\{ 1 + \beta y + \varepsilon \right\}, \\ F_0^{q\bar{q}} &= -\frac{4}{\hat{s}} \left\{ 1 - \beta y + \varepsilon \right\}. \end{aligned} \tag{II.14}$$

In view of a compact presentation of the virtual corrections $d\sigma_V^{q\bar{q}}$ (see Section II.2.1), it is useful to write down the spin-dependent term in an alternative way. Defining the two unit vectors $\hat{\mathbf{u}}_1, \hat{\mathbf{u}}_2$ which are orthogonal to each other:

$$
\begin{aligned}
\hat{\mathbf{u}}_1 &= \frac{1}{\sqrt{1-y^2+\gamma^2 y^2}}\left[-\sqrt{1-y^2}\,\hat{\mathbf{q}} - \gamma y\,\hat{\mathbf{k}}\right], \\
\hat{\mathbf{u}}_2 &= \frac{1}{\sqrt{1-y^2+\gamma^2 y^2}}\left[\sqrt{1-y^2}\,\hat{\mathbf{k}} - \gamma y\,\hat{\mathbf{q}}\right],
\end{aligned}
\tag{II.15}
$$

where $\hat{\mathbf{q}} = (\hat{\mathbf{p}} - y\hat{\mathbf{k}})/\sqrt{1-y^2}$ and $\gamma = E/m$, we obtain

$$
C_{\mu\nu}^{q\bar{q}} s_t^\mu s_{\bar{t}}^\nu = \tilde{C}_{ij}^{q\bar{q}} \hat{s}_t^i \hat{s}_{\bar{t}}^j,
\tag{II.16}
$$

with

$$
\tilde{C}_{ij}^{q\bar{q}} = \frac{1}{3}e_0\delta_{ij} + \left(\hat{u}_{1i}\hat{u}_{1j} - \frac{1}{3}\delta_{ij}\right)e_1 + \left(\hat{u}_{2i}\hat{u}_{2j} - \frac{1}{3}\delta_{ij}\right)e_2 + (\hat{u}_{1i}\hat{u}_{2j} + \hat{u}_{2i}\hat{u}_{1j})e_3,
\tag{II.17}
$$

and

$$
\begin{aligned}
e_0 &= A_0^{q\bar{q}} - 4\varepsilon, \\
e_1 &= 2, \\
e_2 &= 2\beta^2(1-y^2), \\
e_3 &= 0.
\end{aligned}
\tag{II.18}
$$

II.1.2. gg initial state

The squared Born matrix element is given by

$$
|\mathcal{M}_B^{gg}|^2 = 2\left[N^2(1+\beta^2 y^2) - 2\right]|\tilde{\mathcal{M}}_B^{gg}|^2,
\tag{II.19}
$$

where

$$
\begin{aligned}
|\tilde{\mathcal{M}}_B^{gg}|^2 &= \frac{4\pi^2\alpha_s^2(N^2-1)}{N(1-\beta^2 y^2)^2}\Big\{A_0^{gg} + C_0^{gg}(s_t \cdot s_{\bar{t}}) + D_0^{gg}\left[(p_1 \cdot s_t)(p_1 \cdot s_{\bar{t}}) + (p_2 \cdot s_t)(p_2 \cdot s_{\bar{t}})\right] \\
&\quad + E_0^{gg}(p_1 \cdot s_t)(p_2 \cdot s_{\bar{t}}) + E_0^{gg}|_{y\to -y}(p_2 \cdot s_t)(p_1 \cdot s_{\bar{t}})\Big\},
\end{aligned}
\tag{II.20}
$$

and

$$
\begin{aligned}
A_0^{gg} &= 1 + 2\beta^2(1-y^2) - \beta^4\left[1 + (1-y^2)^2\right] + \varepsilon\left[(1+\beta^2 y^2)^2 - 4\right] + 2\varepsilon^2(1-\beta^2 y^2), \\
C_0^{gg} &= 1 - 2\beta^2 + \beta^4\left[1 + (1-y^2)^2\right] - \varepsilon(1-\beta^2 y^2)^2 - 2\varepsilon^2(1-\beta^2 y^2), \\
D_0^{gg} &= \frac{32\varepsilon m^2}{\hat{s}^2}, \\
E_0^{gg} &= \frac{4(1+\beta y)}{\hat{s}}\left\{-\beta^2(1-y^2) + \varepsilon(1-\beta^2 y^2) + 2\varepsilon^2\right\}.
\end{aligned}
\tag{II.21}
$$

The virtual corrections $d\sigma_V^{gg}$ do not simplify when using a decomposition similar to Eq. (II.16).

II.2. Virtual corrections

We now give our results for the order α_s^3 virtual corrections to the Born cross sections of Section II.1. The ultraviolet singularities are removed by using the $\overline{\text{MS}}$ prescription for the QCD coupling and the on-shell definition of the top mass. In the following, α_s denotes the QCD coupling defined in the $\overline{\text{MS}}$ scheme of $N_f = 6$ flavour QCD (5 massless and one massive quark), m denotes the mass of the top quark defined in the on-shell scheme, and μ_R is the renormalization scale. The renormalized differential cross sections $d\sigma_V^i$ still contain single and double poles in $\varepsilon = (4-d)/2$ due to soft and collinear divergences, which we collectively call infrared (IR) singularities in the following. These poles are removed after including the contributions from soft gluon radiation and mass factorization. This will be done in the next section.

The absorptive parts of the one-loop amplitudes induce small polarizations of the t and $\bar{t}$ quarks orthogonal to the $2 \to 2$ scattering plane, i.e. the $d\sigma_V^i$ contain also terms proportional to $\varepsilon_{ijl}\hat{s}_t^i \hat{p}^j \hat{k}^l$ and $\varepsilon_{ijl}\hat{s}_{\bar{t}}^i \hat{p}^j \hat{k}^l$, which are ultraviolet- and infrared-finite at this order in the perturbative expansion. These terms were computed in Refs. [43, 44]. They do not contribute to the observables, which we investigate in Sections IV and VI, so that we omit them in the following.

II.2.1. $q\bar{q}$ initial states

The NLO virtual corrections as defined in Eq. (II.7) can be presented as follows:

$$
\begin{aligned}
d\sigma_V^{q\bar{q}} &= \frac{\alpha_s}{\pi} C_\varepsilon d\sigma_B^{q\bar{q}} \left\{ -\frac{C_F}{\varepsilon^2} + \frac{1}{\varepsilon}\left[-\frac{5C_F}{2} + \frac{1+\beta^2}{4\beta N}\ln(x) + \frac{2}{N}\ln\left(\frac{1+\beta y}{1-\beta y}\right) \right.\right. \\
&\quad + \left.\left. C_F \ln\left(\frac{\hat{s}}{m^2}\right) + \frac{N}{2}\ln\left(\frac{(1-\beta y)^2}{1-\beta^2}\right) \right] \right\} + \frac{1}{2\hat{s}}\Phi_{q\bar{q}}\mathcal{F}_{q\bar{q}}d\Gamma_2,
\end{aligned}
\tag{II.22}
$$

where

$$
C_\varepsilon = \left[\frac{4\pi\mu^2}{m^2}\right]^\varepsilon e^{-\varepsilon\gamma_E},
\tag{II.23}
$$

$C_F = (N^2-1)/(2N)$, γ_E is the Euler constant, μ is an arbitrary mass scale, and

$$
x = \frac{1-\beta}{1+\beta}.
\tag{II.24}
$$

The IR-finite part $\mathcal{F}_{q\bar{q}}$ is of the form

$$
\mathcal{F}_{q\bar{q}} = \mathcal{F}_1 |\mathcal{M}_B^{q\bar{q}}|^2 + 4\pi^2\alpha_s^2(N^2-1)\mathcal{F}_2,
\tag{II.25}
$$

with

$$
\begin{aligned}
\mathcal{F}_1 &= \frac{\alpha_s}{2\pi}\left\{ 2G + \frac{\hat{s}}{N}\overline{C}_0(p_1,p_2,0,0,0) + \frac{N^2-2}{N}\hat{s}(1-\beta y)\overline{C}_0(-p_1,k_1,0,0,m) \right. \\
&\quad + \left. \frac{2\hat{s}(1+\beta y)}{N}\overline{C}_0(-p_1,k_2,0,0,m) + \frac{\hat{s}(1+\beta^2)}{2N}\overline{C}_0(k_1,k_2,m,0,m) \right\}.
\end{aligned}
\tag{II.26}
$$

The contribution G is the finite part of the sum of the gluon self-energy diagram (computed in the Feynman gauge) and the counterterms:

$$G = \frac{11N - 2N_f}{6} \ln\left(\frac{\mu_R^2}{m^2}\right) + \frac{N}{6}\left(5\overline{B}_0(k_1 + k_2, 0, 0) + \frac{1}{3}\right)$$
$$- \frac{1}{3}\left[(N_f - 1)\overline{B}_0(k_1 + k_2, 0, 0) + \left(1 + \frac{2m^2}{\hat{s}}\right)\overline{B}_0(k_1 + k_2, m, m) - \frac{1}{3}N_f\right]. \quad \text{(II.27)}$$

The functions $\overline{C}_0$, $\overline{B}_0$, which appear in Eqs. (II.26), (II.27), are defined in Appendix A. Omitting the contributions from the absorptive parts, the term $\mathcal{F}_2$ can be decomposed as follows:

$$\mathcal{F}_2 = \frac{\alpha_s}{\pi}\left[A_V^{q\bar{q}} + \tilde{C}_{ij}^V \hat{s}_t^i \hat{s}_{\bar{t}}^j\right]. \quad \text{(II.28)}$$

The 3×3 matrix $\tilde{C}_{ij}^V$ has the same structure as Eq. (II.17) with the coefficients e_a being replaced by e_a^V. These coefficients and $A_V^{q\bar{q}}$ are listed in Appendix B.

II.2.2. gg initial state

The one-loop contributions to the differential cross section of the gluon fusion reaction (II.2) are of the following form:

$$d\sigma_V^{gg} = \frac{1}{2\hat{s}}\Phi_{gg}\left\{C_\varepsilon\mathcal{G}_{gg} + \mathcal{H}_{gg}\right\}d\Gamma_2, \quad \text{(II.29)}$$

where the IR-singular term $\mathcal{G}_{gg}$ is given by

$$\mathcal{G}_{gg} = \frac{\alpha_s}{\pi}\left\{\mathcal{V}_A|\mathcal{M}_B^{gg}|^2 + |\tilde{\mathcal{M}}_B^{gg}|^2\left[\mathcal{V}_B + \mathcal{V}_C + \mathcal{V}_C|_{y\to-y}\right]\right\}, \quad \text{(II.30)}$$

with

$$\mathcal{V}_A = -\frac{N}{\varepsilon^2} - \frac{1}{\varepsilon}\frac{11N - 2(N_f - 1)}{6} - \frac{1}{\varepsilon}\left[C_F - N\ln\left(\frac{\hat{s}}{m^2}\right)\right],$$
$$\mathcal{V}_B = -\frac{1 + \beta^2}{2N\beta}\left[2 + N^2(1 - \beta^2 y^2)\right]\frac{\ln(x)}{\varepsilon},$$
$$\mathcal{V}_C = \frac{N}{2\varepsilon}\left[N^2(1 + \beta y)^2 - 4\right]\ln\left(\frac{(1 - \beta y)^2}{1 - \beta^2}\right). \quad \text{(II.31)}$$

The infrared-finite part reads

$$\mathcal{H}_{gg} = \frac{\alpha_s}{\pi}\ln\left(\frac{\mu_R^2}{m^2}\right)\frac{11N - 2N_f}{6}|\mathcal{M}_B^{gg}|^2 + \mathcal{H}_1|\tilde{\mathcal{M}}_B^{gg}|^2 + 4\pi^2\alpha_s^2(N^2 - 1)\mathcal{H}_2, \quad \text{(II.32)}$$

with

$$\mathcal{H}_1 = -\frac{\alpha_s}{\pi}\hat{s}\left\{\overline{C}_0(k_1, k_2, m, 0, m)\frac{(1 + \beta^2)[2 + N^2(1 - \beta^2 y^2)]}{2N}\right.$$

8

$$
\begin{aligned}
+ &\ \overline{C}_0(p_1, p_2, 0, 0, 0) N^3 \left(1 + \beta^2 y^2\right) \\
+ &\ \overline{C}_0(-p_1, k_1, 0, 0, m) \frac{N}{2} \left[4 - N^2 (1 + \beta y)^2\right] (1 - \beta y) \\
+ &\ \overline{C}_0(-p_1, k_2, 0, 0, m) \frac{N}{2} \left[4 - N^2 (1 - \beta y)^2\right] (1 + \beta y) \Bigg\}.
\end{aligned}
\tag{II.33}
$$

The term $\mathcal{H}_2$ has the structure (here too, contributions from absorptive parts are omitted)

$$
\begin{aligned}
\mathcal{H}_2 \ = \ & \frac{\alpha_s}{\pi} \Big\{ A_V^{gg} + C_V^{gg} (s_t \cdot s_{\bar{t}}) + D_V^{gg} \Big[(p_1 \cdot s_t)(p_1 \cdot s_{\bar{t}}) + (p_2 \cdot s_t)(p_2 \cdot s_{\bar{t}}) \Big] \\
& + E_V^{gg} (p_1 \cdot s_t)(p_2 \cdot s_{\bar{t}}) + E_V^{gg}|_{y \to -y} (p_2 \cdot s_t)(p_1 \cdot s_{\bar{t}}) \Big\}.
\end{aligned}
\tag{II.34}
$$

The coefficients $A_V^{gg}, \ldots, E_V^{gg}$ are given in Appendix C.

III. Real gluon radiation and (anti)quark–gluon fusion

In this section we consider the reactions

$$
q(p_1) + \bar{q}(p_2) \to t(k_1, s_t) + \bar{t}(k_2, s_{\bar{t}}) + g(p_3),
\tag{III.1}
$$

$$
g(p_1) + g(p_2) \to t(k_1, s_t) + \bar{t}(k_2, s_{\bar{t}}) + g(p_3),
\tag{III.2}
$$

$$
q(p_1) + g(p_2) \to t(k_1, s_t) + \bar{t}(k_2, s_{\bar{t}}) + q(p_3),
\tag{III.3}
$$

$$
\bar{q}(p_1) + g(p_2) \to t(k_1, s_t) + \bar{t}(k_2, s_{\bar{t}}) + \bar{q}(p_3).
\tag{III.4}
$$

In order to deal with the IR divergences of the corresponding lowest order QCD cross sections, we employ the phase-space slicing method: in the case of the reactions Eq. (III.1), Eq. (III.2), we divide the phase-space into four regions, namely the region where the gluon is soft, the two regions where the gluon is collinear (but not soft) to one of the initial-state massless partons, and the complement of these three regions, where all partons are 'resolved'. The Born cross sections of the reactions in Eqs. (III.3) and (III.4) develop collinear divergences but no soft ones. Thus, in this case, we split the phase-space into the two regions where the outgoing q ($\bar{q}$) becomes collinear to the incoming (anti)quark or gluon, and the complement, which is the resolved region. For convenience we parametrize in this section the 3-parton phase space in terms of angles and momenta defined in the c.m.s. of the initial partons.

III.1. Soft gluon cross sections

For the processes of Eqs. (III.1), and (III.2), we define the soft region by the requirement that the scaled gluon energy in the c.m. frame of the initial partons, $x_g = 2E_g/\sqrt{\hat{s}}$, be smaller than some cut parameter $x_{\min}$, where $x_{\min} \ll 1$. That is, 'hard' and 'soft' gluon refers to the decomposition

$$
1 = \Theta(x_g - x_{\min}) + \Theta(x_{\min} - x_g).
\tag{III.5}
$$

9

In the soft region we use the eikonal approximation for the matrix elements $\mathcal{M}^{q\bar{q},g}$ and $\mathcal{M}^{gg,g}$ of Eqs. (III.1) and (III.2), and the soft limit of the d-dimensional phase-space measure.

For quark–antiquark annihilation, we obtain

$$
\begin{aligned}
|\mathcal{M}_{\text{soft}}^{q\bar{q},g}|^2 &= 4\pi\alpha_s\mu^{2\varepsilon}\left\{-C_F\left[\frac{m^2}{(k_1\cdot p_3)^2}+\frac{m^2}{(k_2\cdot p_3)^2}\right]-\frac{1}{N}\left[\frac{k_1\cdot k_2}{(k_1\cdot p_3)(k_2\cdot p_3)}\right.\right. \\
&\quad +\left.\frac{p_1\cdot p_2}{(p_1\cdot p_3)(p_2\cdot p_3)}-\frac{2k_1\cdot p_2}{(k_1\cdot p_3)(p_2\cdot p_3)}-\frac{2k_2\cdot p_1}{(k_2\cdot p_3)(p_1\cdot p_3)}\right] \\
&\quad +\left.\frac{N^2-2}{N}\left[\frac{k_1\cdot p_1}{(k_1\cdot p_3)(p_1\cdot p_3)}+\frac{k_2\cdot p_2}{(k_2\cdot p_3)(p_2\cdot p_3)}\right]\right\}|\mathcal{M}_B^{q\bar{q}}|^2.
\end{aligned}
\tag{III.6}
$$

Here $|\mathcal{M}_B^{q\bar{q}}|^2$ is the d-dimensional squared Born matrix element (II.10). Integrating the gluon momentum p_3 over the soft region we obtain

$$
\begin{aligned}
d\sigma_{\text{soft}}^{q\bar{q},g} &= \frac{1}{2\hat{s}}\Phi_{q\bar{q}}d\Gamma_2\int|M_{\text{soft}}^{q\bar{q},g}|^2\,\Theta(x_{\min}-x_g)\frac{d^{d-1}p_3}{(2\pi)^{d-1}2E_g} \\
&= d\sigma_B^{q\bar{q}}\frac{\alpha_s}{\pi}\tilde{C}_\varepsilon\left\{\frac{C_F}{\varepsilon^2}+\frac{1}{\varepsilon}\left[C_F-\frac{1+\beta^2}{4\beta N}\ln(x)-\frac{2}{N}\ln\left(\frac{1+\beta y}{1-\beta y}\right)-\frac{N}{2}\ln\left(\frac{(1-\beta y)^2}{1-\beta^2}\right)\right]\right. \\
&\quad -C_F\frac{\pi^2}{6}+\frac{1+\beta^2}{2N\beta}\left\{\mathrm{Li}_2(1-x)+\frac{1}{4}\ln^2(x)\right\}-\frac{C_F}{\beta}\ln(x)-\frac{N}{4}\ln^2(x) \\
&\quad +\left.\frac{N^2-2}{2N}S(y)+\frac{1}{N}S(-y)\right\},
\end{aligned}
\tag{III.7}
$$

where

$$
\tilde{C}_\varepsilon = \left(\frac{4\pi\mu^2}{\hat{s}}\right)^\varepsilon\frac{x_{\min}^{-2\varepsilon}}{\Gamma(1-\varepsilon)}
\tag{III.8}
$$

and

$$
S(y) = 2\mathrm{Li}_2\left(-\frac{\beta(1-y)}{1-\beta}\right)-2\mathrm{Li}_2\left(-\frac{\beta(1+y)}{1-\beta y}\right)+\ln^2\left(\frac{1-\beta y}{1-\beta}\right).
\tag{III.9}
$$

Using again the eikonal approximation the d-dimensional soft gg fusion matrix element squared takes the form

$$
\begin{aligned}
|\mathcal{M}_{\text{soft}}^{gg,g}|^2 &= 4\pi\alpha_s N\mu^{2\varepsilon}\left\{\left[(N^2-1)M_2-M_1-M_{12}\right]\left[\frac{p_2\cdot k_1}{(p_2\cdot p_3)(k_1\cdot p_3)}+\frac{p_1\cdot k_2}{(p_1\cdot p_3)(k_2\cdot p_3)}\right]\right. \\
&\quad +\left[(N^2-1)M_1-M_2-M_{12}\right]\left[\frac{p_2\cdot k_2}{(p_2\cdot p_3)(k_2\cdot p_3)}+\frac{p_1\cdot k_1}{(p_1\cdot p_3)(k_1\cdot p_3)}\right] \\
&\quad +N^2\left[M_1+M_2\right]\frac{p_1\cdot p_2}{(p_1\cdot p_3)(p_2\cdot p_3)}
\end{aligned}
$$

10

$$
\begin{aligned}
&+\ \frac{N^2-1}{2N^2}\Big[M_{12}-(N^2-1)(M_1+M_2)\Big]\Big[\frac{m^2}{(k_1\cdot p_3)^2}+\frac{m^2}{(k_2\cdot p_3)^2}\Big]\\
&+\ \frac{1}{N^2}\Big[M_1+M_2+(N^2+1)M_{12}\Big]\frac{k_1\cdot k_2}{(k_1\cdot p_3)(k_2\cdot p_3)}\Big\},
\end{aligned}
\tag{III.10}
$$

where

$$
\begin{aligned}
M_1 &= (1+\beta y)^2|\tilde{\mathcal{M}}_B^{gg}|^2,\\
M_2 &= (1-\beta y)^2|\tilde{\mathcal{M}}_B^{gg}|^2,\\
M_{12} &= 2(1-\beta^2 y^2)|\tilde{\mathcal{M}}_B^{gg}|^2,
\end{aligned}
\tag{III.11}
$$

and $|\tilde{\mathcal{M}}_B^{gg}|^2$ is given in Section II.1.2. Integrating p_3 over the soft region we obtain

$$
d\sigma_{\text{soft}}^{gg,g} = \frac{1}{2\hat{s}}\Phi_{gg}\,\frac{\alpha_s}{\pi}\tilde{C}_\varepsilon\Big\{\mathcal{S}_A|\mathcal{M}_B^{gg}|^2+|\tilde{\mathcal{M}}_B^{gg}|^2\Big[\mathcal{S}_B+\mathcal{S}_C+\mathcal{S}_C|_{y\to-y}\Big]\Big\}d\Gamma_2,
\tag{III.12}
$$

where

$$
\begin{aligned}
\mathcal{S}_A &= \frac{N}{\varepsilon^2}+\frac{C_F}{\varepsilon}-\frac{N}{6}\pi^2-\frac{C_F}{\beta}\ln(x),\\[4pt]
\mathcal{S}_B &= \frac{1+\beta^2}{2\beta N}\big[N^2(1-\beta^2 y^2)+2\big]\Big[\frac{\ln(x)}{\varepsilon}-2\mathrm{Li}_2(1-x)-\frac{1}{2}\ln^2(x)\Big]\\
&\quad+\ \frac{N}{2}\big[4-N^2(1+\beta^2 y^2)\big]\ln^2(x),\\[4pt]
\mathcal{S}_C &= \frac{N}{2}\big[4-N^2(1+\beta y)^2\big]\Big[\frac{1}{\varepsilon}\ln\Big(\frac{(1-\beta y)^2}{1-\beta^2}\Big)-S(y)\Big].
\end{aligned}
\tag{III.13}
$$

Adding the virtual and soft contributions, we obtain the following results for the remaining singular contribution:

$$
\begin{aligned}
\big[d\sigma_V^{q\bar{q}}+d\sigma_{\text{soft}}^{q\bar{q},g}\big]_{\text{singular}} &= -\frac{\alpha_s}{2\pi}C_F\frac{1}{\varepsilon}\big[3+4\ln(x_{\min})\big]d\sigma_B^{q\bar{q}},\\[4pt]
\big[d\sigma_V^{gg}+d\sigma_{\text{soft}}^{gg,g}\big]_{\text{singular}} &= -\frac{\alpha_s}{2\pi}\frac{1}{\varepsilon}\Big[\frac{11N-2(N_f-1)}{3}+4N\ln(x_{\min})\Big]d\sigma_B^{gg}.
\end{aligned}
\tag{III.14}
$$

III.2. Collinear contributions and mass factorization

The order α_s^3 cross sections of the reactions Eqs. (III.1)–(III.4) develop collinear singularities when the momentum of the outgoing massless parton becomes parallel to the momentum of the incoming massless quark or gluon. We use, for convenience, the parameter $x_{\min}$ for characterizing the collinear regions in phase-space, too. For Eqs. (III.1) and (III.2), we define the two collinear regions by $\{\cos\theta>(1-x_{\min})$ and $x_g>x_{\min}\}$ and $\{\cos\theta<(-1+x_{\min})$ and $x_g>x_{\min}\}$, where θ is the angle between the gluon and one of the initial partons in the c.m. frame of the initial partons. For Eqs. (III.3) and (III.4) the two collinear regions are defined by $\cos\theta>(1-x_{\min})$ and $\cos\theta<(-1+x_{\min})$. Here θ denotes the angle between the outgoing massless (anti)quark and one of the initial partons.

In these regions we use the collinear approximations for both the squared matrix element of the respective reaction and the phase-space measure in d dimensions. We parametrize $p_3 = (1-z)p_i + p_\perp + O(p_\perp^2)$, $p' = zp_i - p_\perp + O(p_\perp^2)$, $p_3 \cdot p_\perp = 0$, where $p_i = p_1, p_2$ is the momentum of one of the initial partons, p_3 is the momentum of the unobserved collinear outgoing parton, and p' is the momentum of parton i after collinear emission. The momentum fraction z varies in the interval $z \in [4m^2/\hat{s}, 1-\delta]$, where $\delta = x_{\min}$ for $q\bar{q}$ and gg initial states, and $\delta = 0$ for the $gq(\bar{q})$ initial state. Integrating over the angles of the parton with momentum p_3 in the collinear region, using the angular measure in $d-1$ spatial dimensions, $d\Omega_{d-1} = (1-\cos^2\theta)^{-\varepsilon} d\cos\theta \, d\Omega_{d-2}$, we obtain for the collinear contribution to the differential cross sections:

$$d\sigma_{\text{coll}}^{q\bar{q},g}(z) = -\frac{\alpha_s C_F}{2\pi} F_\varepsilon \frac{1}{\varepsilon} \frac{1+z^2 - \varepsilon(1-z)^2}{1-z} \left\{ d\sigma_B^{q\bar{q}}(zp_1, p_2) + d\sigma_B^{q\bar{q}}(p_1, zp_2) \right\} dz, \tag{III.15}$$

$$d\sigma_{\text{coll}}^{gg,g}(z) = -\frac{N\alpha_s}{\pi} F_\varepsilon \frac{1}{\varepsilon} \left\{ \frac{1}{1-z} + \frac{1}{z} - z^2 + z - 2 \right\} \left\{ d\sigma_B^{gg}(zp_1, p_2) + d\sigma_B^{gg}(p_1, zp_2) \right\} dz, \tag{III.16}$$

$$\begin{aligned} d\sigma_{\text{coll}}^{gq}(z) = d\sigma_{\text{coll}}^{g\bar{q}}(z) &= -\frac{\alpha_s}{2\pi} F_\varepsilon \frac{1}{\varepsilon} \left\{ \frac{1}{2} \frac{z^2 + (1-z)^2 - \varepsilon}{1-\varepsilon} d\sigma_B^{q\bar{q}}(p_1, zp_2) \right. \\ &\quad + \left. C_F \frac{1+(1-z)^2 - \varepsilon z^2}{z} d\sigma_B^{gg}(zp_1, p_2) \right\} dz, \end{aligned} \tag{III.17}$$

where

$$F_\varepsilon = \left[\frac{8\pi\mu^2}{\hat{s}} \right]^\varepsilon \frac{x_{\min}^{-\varepsilon}(1-z)^{-2\varepsilon}}{\Gamma(1-\varepsilon)}. \tag{III.18}$$

The Born cross sections in Eqs. (III.15)–(III.17) are those given in Section II.1. The z-dependent terms in front of the $d\sigma_B^i$, which appear in these equations are, as expected, proportional to the d-dimensional Altarelli–Parisi splitting functions $P_{qq}^d(z)$, $P_{gg}^d(z)$, $P_{gq}^d(z)$, and $P_{qg}^d(1-z)$. In Eqs. (III.15) and (III.16), the integration over the momentum fraction z can be performed using the relation

$$\begin{aligned} \int_{\frac{4m^2}{\hat{s}}}^{1-x_{\min}} dz \frac{g(z)}{(1-z)^{1+\varepsilon}} &= \int_{\frac{4m^2}{\hat{s}}}^{1} dz\, g(z) \left[\frac{1}{(1-z)_+} - \delta(1-z)\ln(x_{\min}) \right. \\ &\quad - \left. \varepsilon \left[\frac{\ln(1-z)}{1-z} \right]_+ + \frac{1}{2}\varepsilon\delta(1-z)\ln^2(x_{\min}) + O(\varepsilon^2) \right]. \end{aligned} \tag{III.19}$$

The plus prescription defines distributions via

$$[F(z)]_+ = \lim_{\eta\to 0} \left\{ \Theta(1-z-\eta)F(z) - \delta(1-z-\eta)\int_0^{1-\eta} F(y)dy \right\}, \tag{III.20}$$

so that if $g(z)$ is well-behaved at $z = 1$, then

$$\int_x^1 dz \frac{g(z)}{(1-z)_+} = \int_x^1 \frac{g(z) - g(1)}{1-z} + g(1)\ln(1-x), \tag{III.21}$$

$$\int_x^1 dz\, g(z) \left[\frac{\ln(1-z)}{1-z} \right]_+ = \int_x^1 \frac{(g(z) - g(1))\ln(1-z)}{1-z} + \frac{g(1)}{2}\ln^2(1-x). \tag{III.22}$$

12

Adding, in the case of $i = q\bar{q}, gg$, the soft and collinear contributions, the singularities proportional to $\ln(x_{\min})$ cancel for infrared- and collinear-safe observables. The singularities, which remain in $d\sigma_V^i + d\sigma_{\text{soft}}^{i,g}$ and $d\sigma_{\text{coll}}^{i,g}$, are removed by absorbing them into the unphysical bare parton density functions, i.e. by renormalizing these functions at the factorization scale μ_F. At the level of the differential cross sections, this amounts to adding counterterms $d\sigma_c^i$ being composed of mass factorization counterfunctions. Finite Born cross sections for gq and $g\bar{q}$ scattering are obtained in an analogous fashion. Performing the mass factorization in the $\overline{\text{MS}}$ scheme, the counterterms read

$$d\sigma_c^{q\bar{q}}(z) = \frac{1}{\Gamma(1-\varepsilon)}\left(\frac{4\pi\mu^2}{\mu_F^2}\right)^\varepsilon \frac{1}{\varepsilon}\frac{\alpha_s}{2\pi}\left[P_{qq}(z)d\sigma_B^{q\bar{q}}(zp_1,p_2) + P_{\bar{q}\bar{q}}(z)d\sigma_B^{q\bar{q}}(p_1,zp_2)\right]dz, \qquad \text{(III.23)}$$

$$d\sigma_c^{gg}(z) = \frac{1}{\Gamma(1-\varepsilon)}\left(\frac{4\pi\mu^2}{\mu_F^2}\right)^\varepsilon \frac{1}{\varepsilon}\frac{\alpha_s}{2\pi}\left[P_{gg}(z)d\sigma_B^{gg}(zp_1,p_2) + P_{gg}(z)d\sigma_B^{gg}(p_1,zp_2)\right]dz, \qquad \text{(III.24)}$$

$$d\sigma_c^{gq}(z) = \frac{1}{\Gamma(1-\varepsilon)}\left(\frac{4\pi\mu^2}{\mu_F^2}\right)^\varepsilon \frac{1}{\varepsilon}\frac{\alpha_s}{2\pi}\left[P_{gq}(z)d\sigma_B^{gg}(zp_1,p_2) + P_{qg}(z)d\sigma_B^{q\bar{q}}(p_1,zp_2)\right]dz, \qquad \text{(III.25)}$$

and $d\sigma_c^{g\bar{q}}(z) = d\sigma_c^{gq}(z)$. The evolution kernels are given by [45,46,47,48,49]

$$P_{gg}(z) = \delta(1-z)\frac{11N-2(N_f-1)}{6} + 2N\left[\frac{z}{(1-z)_+} + \frac{1-z}{z} + z(1-z)\right], \qquad \text{(III.26)}$$

$$P_{qq}(z) = P_{\bar{q}\bar{q}}(z) = C_F\left[\frac{3}{2}\delta(1-z) + \frac{1+z^2}{(1-z)_+}\right], \qquad \text{(III.27)}$$

$$P_{gq}(z) = P_{g\bar{q}}(z) = C_F\frac{1+(1-z)^2}{z}, \qquad \text{(III.28)}$$

$$P_{qg}(z) = P_{\bar{q}g}(z) = \frac{1}{2}\left[z^2 + (1-z)^2\right]. \qquad \text{(III.29)}$$

III.3. Finite contributions

In the resolved regions the four differential cross sections $d\sigma_{\text{res}}^i$, respectively the corresponding production density matrices R_{res}^i for the final states $t\bar{t}+g$, $t\bar{t}+q$, $t\bar{t}+\bar{q}$, are obtained from the helicity amplitudes given in Appendix D according to formula (D.1). In the resolved regions no singularities arise and it is thus possible to work in $d = 4$ dimensions.

IV. Parton level results for the final states $t\bar{t}X$

Based on the results given in the previous sections we consider in this the inclusive parton reactions

$$i \to t\bar{t}X, \quad i = q\bar{q}, gg, gq, g\bar{q} \qquad \text{(IV.1)}$$

at NLO. From the different contributions $d\sigma_B^i, d\sigma_V^i, d\sigma_{\text{soft}}^{i,g}$, given in Sections II and III, we can extract the corresponding density matrices using Eq. (II.9). For $d\sigma_{\text{coll}}^{i,g}$ and $d\sigma_c^i$ an analogous formula holds. These

13

and the above-mentioned matrices R^i_{res} have the following structure in the spin spaces of the top and antitop quarks:

$$(R^i)_{\alpha\alpha',\beta\beta'} = A^i\delta_{\alpha\alpha'}\delta_{\beta\beta'} + B^i_{ta}(\tau^a)_{\alpha\alpha'}\delta_{\beta\beta'} + B^i_{\bar{t}a}\delta_{\alpha\alpha'}(\tau^a)_{\beta\beta'} + C^i_{ab}(\tau^a)_{\alpha\alpha'}(\tau^b)_{\beta\beta'}\,, \tag{IV.2}$$

where τ^a are the Pauli matrices. The functions A^i determine the spin-averaged production cross section. The functions B^i_{ta} and $B^i_{\bar{t}a}$ are associated with a polarization of the top quarks and antiquarks. As mentioned earlier, parity invariance of QCD only allows top and antitop polarizations that are induced by absorptive parts of the scattering amplitudes. To NLO QCD, the corresponding polarization is orthogonal to the $2 \rightarrow 2$ scattering plane, i.e. the $\mathbf{B}^i_t$ and $\mathbf{B}^i_{\bar{t}}$ have no components in the scattering plane. The functions C^i_{ab} encode the top–antitop spin-spin correlations. For a general decomposition of the $2 \rightarrow 2$ density matrices and their classification with respect to discrete symmetries, see Ref. [25].

In the following we consider a general observable O that may depend on the spins and momenta of the top and antitop quarks and is thus sensitive to the different structures shown in Eq. (IV.2). In particular we study observables of the following form

$$O = 4\,(\mathbf{S}_t \cdot \hat{\mathbf{a}})(\mathbf{S}_{\bar{t}} \cdot \hat{\mathbf{b}})\,, \tag{IV.3}$$

which are sensitive to the correlation C^i_{ab}. The top and antitop spin operators are given by

$$\mathbf{S}_t = \frac{1}{2}(\tau \otimes \mathbb{1}) \tag{IV.4}$$

and

$$\mathbf{S}_{\bar{t}} = \frac{1}{2}(\mathbb{1} \otimes \tau). \tag{IV.5}$$

The unit vectors $\hat{\mathbf{a}}$ and $\hat{\mathbf{b}}$ are arbitrary reference directions. The factor 4 in Eq. (IV.3) is introduced to have a simple relation between the expectation values of the observables defined in Eq. (IV.3) and double spin asymmetries. At the parton level the following relation holds:

$$4\langle(\mathbf{S}_t \cdot \hat{\mathbf{a}})(\mathbf{S}_{\bar{t}} \cdot \hat{\mathbf{b}})\rangle_i = \frac{\sigma^i(\uparrow\uparrow) + \sigma^i(\downarrow\downarrow) - \sigma^i(\uparrow\downarrow) - \sigma^i(\downarrow\uparrow)}{\sigma^i(\uparrow\uparrow) + \sigma^i(\downarrow\downarrow) + \sigma^i(\uparrow\downarrow) + \sigma^i(\downarrow\uparrow)}. \tag{IV.6}$$

The arrows on the right-hand side refer to the spin state of the top and antitop quarks with respect to the quantization axes $\hat{\mathbf{a}}$ and $\hat{\mathbf{b}}$. A prescription of how to construct the correlated top and antitop rest frames in a unique way has to be given. At that point it is important to make sure that the specific prescription is soft and collinear-safe. To illustrate the problem, consider the top–antitop helicity correlation, in which case $\hat{\mathbf{a}}$ and $\hat{\mathbf{b}}$ are the t and $\bar{t}$ directions of flight. An obvious frame in which these directions may be defined is the c.m. frame of the initial partons. In fact, this is how the helicity correlation at parton level is usually defined in Born level calculations for hadron colliders. However, this frame can only be constructed by a measurement of the 4-momenta of all final state particles/jets. In particular, at NLO QCD, one needs to know, apart from the top and antitop momenta, also the momentum of the hard gluon emitted in real radiation. Obviously, this information cannot be obtained if the gluon is collinear to one of the initial partons. Thus the above definition of the helicity correlation is not collinear-safe and cannot be applied beyond the leading order. This applies also to other observables involving the momenta of the

top and antitop defined in the c.m. frame of the initial-state partons. In the situation at hand, a suitable frame is the $t\bar{t}$-ZMF defined in Section II. As discussed in Section II the top (anti)quark rest frame is then defined through a rotation-free Lorentz boost. We study the following spin bases, which are relevant to applications to the Tevatron and the LHC (see Sections VI and VII):

$$\hat{\mathbf{a}} = -\hat{\mathbf{b}} = \hat{\mathbf{k}}, \qquad \text{(helicity basis),} \tag{IV.7}$$

$$\hat{\mathbf{a}} = \hat{\mathbf{b}} = \hat{\mathbf{p}}, \qquad \text{(beam basis),} \tag{IV.8}$$

$$\hat{\mathbf{a}} = \hat{\mathbf{b}} = \hat{\mathbf{d}}, \qquad \text{(off-diagonal basis),} \tag{IV.9}$$

where $\hat{\mathbf{k}}$ denotes the direction of flight of the top quark in the $t\bar{t}$-ZMF and $\hat{\mathbf{p}}$ is the direction of flight of one of the colliding hadrons in that frame. The direction of the hadron beam can be identified to a very good approximation with the direction of flight of one of the initial partons. Thus, at Born level, the beam basis $\hat{\mathbf{a}} = \hat{\mathbf{b}} = \hat{\mathbf{p}}$ coincides with the direction of flight $\hat{\mathbf{p}}^*$ of one of the initial partons in the c.m. frame of the initial partons, and this vector is equal to the unit vector of one of the hadron beams in the laboratory frame. The term 'off-diagonal basis' refers to axes with respect to which the spins of tops and antitops produced by $q\bar{q}$ annihilation are 100% (anti)correlated [19] to leading order in α_s. (For $gg \rightarrow t\bar{t}$ one can show that no spin basis with this property exists.) We use the definition:

$$\hat{\mathbf{d}} = \frac{-\hat{\mathbf{p}} + (1-\gamma)(\hat{\mathbf{p}}\cdot\hat{\mathbf{k}})\hat{\mathbf{k}}}{\sqrt{1 - (\hat{\mathbf{p}}\cdot\hat{\mathbf{k}})^2(1-\gamma^2)}}, \tag{IV.10}$$

where $\gamma = E/m$. The spin bases defined in Eqs. (IV.7)–(IV.9) lead to spin observables (IV.3) that are invariant under spatial rotations of the $t\bar{t}$-ZMF. Thus predictions involving these observables can be unambiguously made without an explicit prescription on how to obtain this frame. If in the case of the beam axis one would use $\hat{\mathbf{a}} = \hat{\mathbf{b}} = \hat{\mathbf{p}}^*$ instead, one would still obtain a collinear-safe observable, which is however not invariant under rotations of the $t\bar{t}$-ZMF. Therefore we do not consider this choice any further.

In addition we find that the observable

$$O' = 4\,\mathbf{S}_t \cdot \mathbf{S}_{\bar{t}}\,, \tag{IV.11}$$

which is also infrared- and collinear-safe, is also sensitive to $t\bar{t}$ spin correlations at both the Tevatron and the LHC. This observable can be expressed in terms of observables of the form of Eq. (IV.3), because

$$O' = 4\sum_{i=1}^{3}(\mathbf{S}_t \cdot \hat{\mathbf{e}}_i)(\hat{\mathbf{e}}_i \cdot \mathbf{S}_{\bar{t}})\,, \tag{IV.12}$$

where $\hat{\mathbf{e}}_{i=1,2,3}$ forms an orthonormal basis.

As mentioned earlier, parity invariance of QCD tells us that the t and $\bar{t}$ ensembles have no polarizations with respect to the reference axes of Eqs. (IV.7)–(IV.9):

$$\langle \mathbf{S}_t \cdot \mathbf{v}\rangle_i = \langle \mathbf{S}_{\bar{t}} \cdot \mathbf{v}\rangle_i = 0, \quad \text{for} \quad \mathbf{v} = \hat{\mathbf{k}}, \hat{\mathbf{p}}, \hat{\mathbf{d}}. \tag{IV.13}$$

Equation (IV.13) holds for any polar vector $\mathbf{v}$. These equations justify the term *spin correlations* for the double spin asymmetries Eq. (IV.6), since a simple calculation shows that

$$4\langle(\mathbf{S}_t \cdot \hat{\mathbf{a}})(\mathbf{S}_{\bar{t}} \cdot \hat{\mathbf{b}})\rangle_i = \text{corr}(\mathbf{S}_t \cdot \hat{\mathbf{a}}, \mathbf{S}_{\bar{t}} \cdot \hat{\mathbf{b}})_i, \tag{IV.14}$$

where for two observables O_1, O_2 the correlation is defined in the standard way by

$$\text{corr}(O_1, O_2) = \frac{\langle O_1 O_2 \rangle - \langle O_1 \rangle \langle O_2 \rangle}{\delta O_1 \delta O_2}, \tag{IV.15}$$

where

$$\delta O_k = \sqrt{\langle O_k^2 \rangle - \langle O_k \rangle^2}. \tag{IV.16}$$

Using the results presented in Sections II and III, let us now discuss the observables defined through Eq. (IV.3), Eqs. (IV.7)–(IV.9) and Eq. (IV.11). The unnormalized expectation value of the observable O at NLO in the QCD coupling — and, as a special case, the NLO cross sections σ^i for the parton reactions in Eq. (IV.1) — is obtained as follows:

$$\begin{aligned}
\sigma^i \langle O \rangle_i &= \frac{\Phi_i}{8\hat{s}} \left\{ \int d\Gamma_2 \, \text{Tr}[(R_B^i + R_V^i + R_{\text{soft}}^{i,g}) O] \right. \\
&\quad + \left. \int d\Gamma_2 dz \, \text{Tr}[(R_{\text{coll}}^{i,g} + R_c^i) O] + \int d\Gamma_3 \, \text{Tr}[R_{\text{res}}^i O] \right\}
\end{aligned} \tag{IV.17}$$

for $i = q\bar{q}, gg$. Here $d\Gamma_3$ is the 3-particle phase-space measure. The contributions to the left-hand side of Eq. (IV.17) from the soft and collinear regions and from the resolved region depend individually on the slicing parameter x_{min}. For $x_{\text{min}} \ll 1$ the leading dependence is, by construction, logarithmic, but in the sum only a residual linear dependence on x_{min} remains, which is due to the approximations made in the soft and collinear regions. By varying x_{min} between 10^{-3} and 10^{-8}, we have checked for the cross sections and for the expectation values of the observables given below that for $x_{\text{min}} \leq 10^{-4}$ this residual dependence is negligible.

For $i = gq, g\bar{q}$ we have

$$\sigma^i \langle O \rangle_i = \frac{\Phi_i}{8\hat{s}} \left\{ \int d\Gamma_2 dz \, \text{Tr}[(R_{\text{coll}}^{i,g} + R_c^i) O] + \int d\Gamma_3 \, \text{Tr}[R_{\text{res}}^i O] \right\}, \tag{IV.18}$$

where $\Phi_{gq} = 1/[2(d-2)N(N^2-1)]$. Of course, $\sigma^{gq} = \sigma^{g\bar{q}}$ and $\langle O \rangle_{gq} = \langle O \rangle_{g\bar{q}}$ within QCD. The statements made below Eq. (IV.17) apply also here.

The unnormalized expectation values Eq. (IV.17) and Eq. (IV.18) are building blocks for computing the distributions (I.16) and (I.17) (see Section VI). In computing the cross sections and these expectation values we have performed the phase-space integration of the resolved parts numerically. If one identifies the renormalization and mass factorization scales, and puts $\mu_R = \mu_F = \mu$, then the NLO parton cross sections and the above expectation values are of the form

$$\sigma^i(\hat{s}, m^2) = \frac{\alpha_s^2}{m^2}[f_i^{(0)}(\rho) + 4\pi\alpha_s(f_i^{(1)}(\rho) + \tilde{f}_i^{(1)}(\rho)\ln(\mu^2/m^2))], \quad i = q\bar{q}, gg, gq \tag{IV.19}$$

$$\sigma^i \langle O_a \rangle_i = \frac{\alpha_s^2}{m^2}[g_{i,a}^{(0)}(\rho) + 4\pi\alpha_s(g_{i,a}^{(1)}(\rho) + \tilde{g}_{i,a}^{(1)}(\rho)\ln(\mu^2/m^2))], \quad i = q\bar{q}, gg, gq \tag{IV.20}$$

and $a = 1, \ldots, 4$. The label $a = 1$ refers to the observable Eq. (IV.11) and $a = 2, 3, 4$ to the helicity, beam, and off-diagonal basis. The variable ρ is defined by

$$\rho = \frac{4m^2}{\hat{s}}. \tag{IV.21}$$

16

For the beam and off-diagonal basis, one has to compute *two* contributions for the gq initial state: either the quark or the gluon direction of flight in the $t\bar{t}$-ZMF can correspond to the direction used to define the axes $\hat{\mathbf{a}}$, $\hat{\mathbf{b}}$, and the contribution from hard gluon emission is different for these two cases. We have

$$f_{gq}^{(0)} = g_{gq,a}^{(0)} = 0. \tag{IV.22}$$

The lowest order scaling functions $f_i^{(0)}$ and $g_{i,a}^{(0)}$ ($i = q\bar{q}, gg$) can be computed analytically. In order to write these functions in a compact form it is advantageous to introduce the following functions:

$$
\begin{aligned}
\ell_1 &= \frac{1}{\beta}\left[\ln(x) + 2\beta\right], \\[4pt]
\ell_2 &= \frac{1}{\beta^3}\left[\ln(x) + 2\beta + \frac{2}{3}\beta^3\right], \\[4pt]
\ell_3 &= \frac{1}{\beta^5}\left[\ln(x) + 2\beta + \frac{2}{3}\beta^3 + \frac{2}{5}\beta^5\right], \\[4pt]
r_1 &= \frac{1}{\beta}\left[\arctan\left(\frac{\beta}{\sqrt{\rho}}\right) - \beta\right],
\end{aligned}
\tag{IV.23}
$$

where $\beta = \sqrt{1-\rho}$ and $x = (1-\beta)/(1+\beta)$.
We then get:

$$f_{q\bar{q}}^{(0)}(\rho) = \frac{\pi\beta\rho}{27}(2+\rho), \tag{IV.24}$$

$$f_{gg}^{(0)}(\rho) = \frac{\pi\beta\rho}{192}\left[4+\rho+2\rho^2 - (16+16\rho+\rho^2)\ell_1\right] \tag{IV.25}$$

$$g_{q\bar{q},1}^{(0)}(\rho) = f_{q\bar{q}}^{(0)}(\rho), \tag{IV.26}$$

$$g_{q\bar{q},2}^{(0)}(\rho) = \frac{\pi\beta\rho}{27}(-2+\rho), \tag{IV.27}$$

$$g_{q\bar{q},3}^{(0)}(\rho) = \frac{\pi\beta\rho}{27}\frac{8+3\rho+4\sqrt{\rho}}{5}, \tag{IV.28}$$

$$g_{q\bar{q},4}^{(0)}(\rho) = f_{q\bar{q}}^{(0)}(\rho) \tag{IV.29}$$

$$g_{gg,1}^{(0)}(\rho) = \frac{\pi\beta\rho}{192}\left[-28+5\rho+2\rho^2 - (16+18\rho+\rho^2)\ell_1\right], \tag{IV.30}$$

$$g_{gg,2}^{(0)}(\rho) = \frac{\pi\beta\rho}{192}\left[\frac{52-7\rho-22\rho^2-2\rho^3}{3} + (16+2\rho+14\rho^2+\rho^3)\ell_2\right], \tag{IV.31}$$

$$
\begin{aligned}
g_{gg,3}^{(0)}(\rho) = \frac{\pi\beta\rho}{192}&\left[-\frac{96}{5}+\frac{248}{15}\sqrt{\rho}+25\rho-\frac{44}{15}\rho^{3/2}-\frac{482}{15}\rho^2-\frac{68}{5}\rho^{5/2}+\frac{284}{15}\rho^3+\frac{2}{5}\rho^4\right.\\
&\left.- (16+34\rho-64\rho^{3/2}-2\rho^2-34\rho^{5/2}+49\rho^3+\rho^4)\ell_3\right],
\end{aligned}
\tag{IV.32}
$$

$$
\begin{aligned}
g_{gg,4}^{(0)}(\rho) = \frac{\pi\beta\rho}{192}\frac{1}{(1+\rho)^2}&\left[-28-35\rho+14\rho^{3/2}+30\rho^2-18\rho^{5/2}+7\rho^3+2\rho^4\right.\\
&\left.- (16+50\rho+68\rho^2+19\rho^3+\rho^4)\ell_1+2\rho^{3/2}(7-9\rho)r_1\right].
\end{aligned}
\tag{IV.33}
$$

The functions $\tilde{f}_i^{(1)}$ and $\tilde{g}_{i,a}^{(1)}$ that determine the scale dependence are obtained from the next formula, which follows from the renormalization group equations:

$$\tilde{f}_{ij}^{(1)}(\rho) = \frac{1}{8\pi^2}\left[\beta_0 f_{ij}^{(0)}(\rho) - \int_\rho^1 dz f_{ik}^{(0)}\left(\frac{\rho}{z}\right)P_{kj}(z) - \int_\rho^1 dz f_{jk}^{(0)}\left(\frac{\rho}{z}\right)P_{ki}(z)\right],\qquad\text{(IV.34)}$$

and likewise for the functions $\tilde{g}_{i,a}^{(1)}(\rho)$. Here,

$$\beta_0 = \frac{1}{3}(11N - 2N_f),\qquad\text{(IV.35)}$$

and the evolution kernels P_{kj} are given in Eqs. (III.26)–(III.29).
For the $q\bar{q}$ initial state we obtain the following results for the μ-dependence:

$$\tilde{f}_{q\bar{q}}^{(1)} = \frac{\beta\rho}{648\pi}\left\{\kappa_1(2+\rho) - 16\frac{\ln(x)}{\beta}\right\},$$

$$\tilde{g}_{q\bar{q},1}^{(1)} = \tilde{f}_{q\bar{q}}^{(1)},\qquad\text{(IV.36)}$$

$$\tilde{g}_{q\bar{q},2}^{(1)} = \frac{\beta\rho}{648\pi}\left\{\kappa_1(-2+\rho) + 16\beta\ln(x) - \frac{32}{3}\right\},\qquad\text{(IV.37)}$$

$$\tilde{g}_{q\bar{q},3}^{(1)} = \frac{\beta\rho}{3240\pi}\left\{\kappa_1(8+3\rho+4\sqrt{\rho}) + \frac{8(-8+\rho)\ln(x)}{\beta} + \frac{32(2\rho-1)}{\beta}\arctan\left(\frac{\beta}{\sqrt{\rho}}\right)\right.$$

$$\left. - 64\sqrt{\rho}\ln(\rho) + \frac{32}{3}\sqrt{\rho} + \frac{16}{3}\right\},\qquad\text{(IV.38)}$$

$$\tilde{g}_{q\bar{q},4}^{(1)} = \tilde{f}_{q\bar{q}}^{(1)},\qquad\text{(IV.39)}$$

where

$$\kappa_1 = 16\ln\left(\frac{\rho}{4\beta^2}\right) + \frac{127}{3} - 2N_f.\qquad\text{(IV.40)}$$

For the gg initial state, we only give analytic results for the simple cases. With

$$\kappa_2 = \ln(x)\ln(\frac{\rho}{4}) - 2\mathrm{Li}_2\left(\frac{1+\beta}{2}\right) + 2\mathrm{Li}_2\left(\frac{1-\beta}{2}\right),$$

$$\kappa_3 = -3\ln(x)^2 + 2\pi^2 - 12\mathrm{Li}_2(x),\qquad\text{(IV.41)}$$

we have

$$\tilde{f}_{gg}^{(1)} = \frac{\rho}{768\pi}\left\{-6\ln\left(\frac{\rho}{4\beta^2}\right)(28+31\rho)\beta + 3\kappa_2(32-16\rho+\rho^2) + \kappa_3(16+16\rho+\rho^2)\right.$$

$$\left. - \frac{2\beta}{15\rho}(724 - 3328\rho + 7449\rho^2) - (198\rho + 59\rho^2 - 288)\ln(x)\right\} - \frac{f_{gg}^{(0)}}{12\pi^2},\qquad\text{(IV.42)}$$

$$\tilde{g}_{gg,1}^{(1)} = \frac{\rho}{768\pi}\left\{-6\ln\left(\frac{\rho}{4\beta^2}\right)(60+31\rho)\beta + 3\kappa_2(-2+\rho)(-16+\rho) + \kappa_3(16+18\rho+\rho^2)\right.$$

18

$$- \frac{2\beta}{15\rho}(-176 - 6118\rho + 7179\rho^2) - (108\rho + 77\rho^2 - 672)\ln(x)\Big\} - \frac{g_{gg,1}^{(0)}}{12\pi^2}, \qquad \text{(IV.43)}$$

$$\tilde{g}_{gg,2}^{(1)} = \frac{\rho}{768\pi}\Big\{\frac{6}{\beta}\ln\left(\frac{\rho}{4\beta^2}\right)(60 - 25\rho + 31\rho^2) - 6\kappa_2(16 - 9\rho + 16\rho^2)$$

$$- (16 + 2\rho + 14\rho^2 + \rho^3)\frac{\kappa_3}{\beta^2} - \frac{2\beta}{15\rho}(7384 + 1127\rho + 3399\rho^2)$$

$$- (-231\rho + 329\rho^2 + 870)\ln(x) - \frac{396(\rho^2 - \rho + 1)^2}{\rho\beta^2}[\text{Li}_2(-\beta) - \text{Li}_2(\beta)]\Big\} - \frac{g_{gg,2}^{(0)}}{12\pi^2}. \text{(IV.44)}$$

For the remaining two functions $\tilde{g}_{gg,3,4}^{(1)}$ we give simple fits in Appendix E.
For the gq initial state, we obtain:

$$\tilde{f}_{gq}^{(1)} = \frac{1}{8\pi^2}\frac{\pi}{192}\Big\{\frac{32}{3}\rho(2 - \rho)\kappa_2 - \frac{4}{9}\rho(14\rho^2 + 27\rho - 136)\ln(x)$$

$$- \frac{8\beta}{135}(1319\rho^2 - 3468\rho + 724)\Big\}, \qquad \text{(IV.45)}$$

$$\tilde{g}_{gq,1}^{(1)} = \frac{1}{8\pi^2}\frac{\pi}{192}\Big\{\frac{4}{3}\rho(16 - 9\rho)\kappa_2 - \frac{4}{9}\rho(14\rho^2 - 27\rho - 328)\ln(x)$$

$$- \frac{8\beta}{135}(1319\rho^2 - 6258\rho - 176)\Big\}, \qquad \text{(IV.46)}$$

$$\tilde{g}_{gq,2}^{(1)} = \frac{1}{8\pi^2}\frac{\pi}{192}\Big\{\frac{4}{3}\rho(-16 + 9\rho)\kappa_2 - \frac{8}{9}\rho(3\rho^2 - 26\rho + 263)\ln(x)$$

$$+ 88(\rho^2 - 2\rho + 2)[\text{Li}_2(\beta) - \text{Li}_2(-\beta)] - \frac{8\beta}{135}(1439\rho^2 + 1347\rho + 7384)\Big\}. \qquad \text{(IV.47)}$$

Again we give simple fits in Appendix E for the more complicated functions $\tilde{g}_{gq,3,4}^{(1)}$.

The scaling functions $f_i^{(1)}$ and $g_{i,a}^{(1)}$ are obtained by numerical integration. As a check we computed the spin-averaged NLO $t\bar{t}$ production cross sections σ^i as functions of ρ. We found excellent agreement with the results of Refs. [2, 4, 5]. Our result for $\tilde{f}_{gq}^{(1)}$ also agrees with the one of Ref. [2]. In the comparison of $\tilde{f}_j^{(1)}$ one has to take into account that Ref. [2] uses a renormalization scheme where heavy and light quark loops are subtracted differently according to the scheme of Ref. [50], while we use the standard $\overline{\text{MS}}$ definition of α_s of $N_f = 6$ flavour QCD. This implies that our scaling functions $\tilde{f}_j^{(1)}$ are related to the functions $(\tilde{f}_j^{(1)})_\text{N}$ of Nason, Dawson and Ellis by

$$\tilde{f}_j^{(1)} = (\tilde{f}_j^{(1)})_\text{N} - \frac{1}{12\pi^2}f_j^{(0)}, \quad j = q\bar{q}, gg. \qquad \text{(IV.48)}$$

Performing the conversion we again find perfect agreement with Ref. [2].
For the functions $f_i^{(1)}$ and $g_{i,a}^{(1)}$ we give fits to the results of our numerical integrations in Appendix E. To account for the richer structure of the functions $g_{i,a}$ — compared with the results for the unpolarized cross sections — we have used a more general ansatz than in Ref. [2]. All scaling functions for the initial
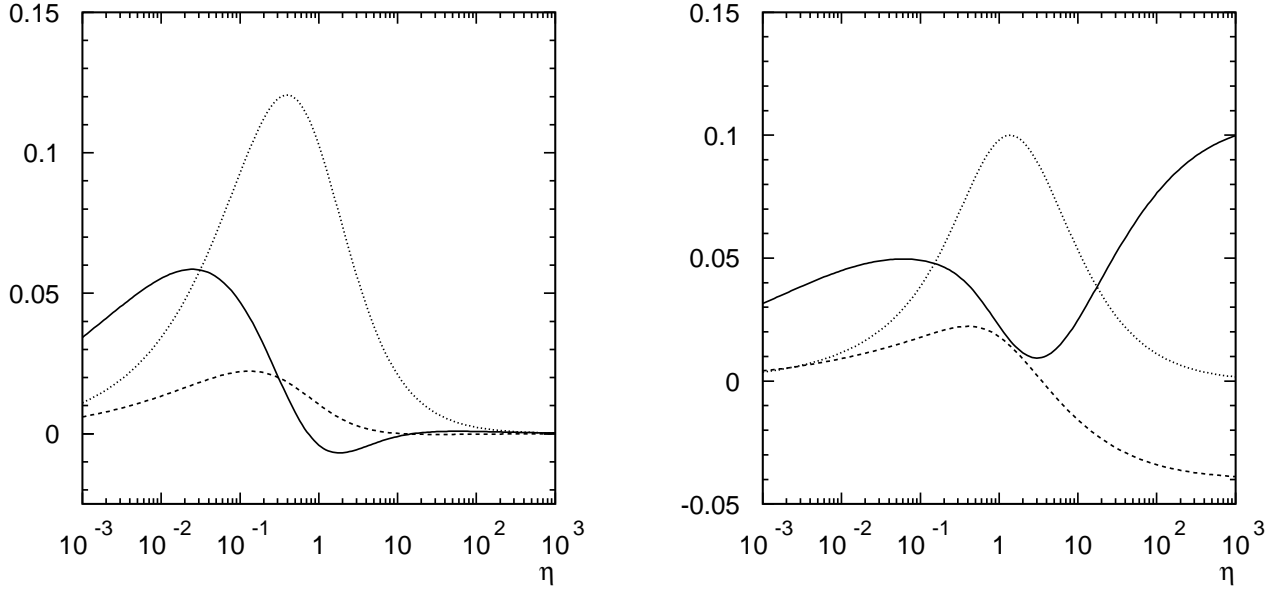
Figure 1: *Left: Scaling functions $f_{q\bar{q}}^{(0)}(\eta)$ (dotted), $f_{q\bar{q}}^{(1)}(\eta)$ (full), and $\tilde{f}_{q\bar{q}}^{(1)}(\eta)$ (dashed). Right: The same for the process $gg \to t\bar{t}(g)$.*
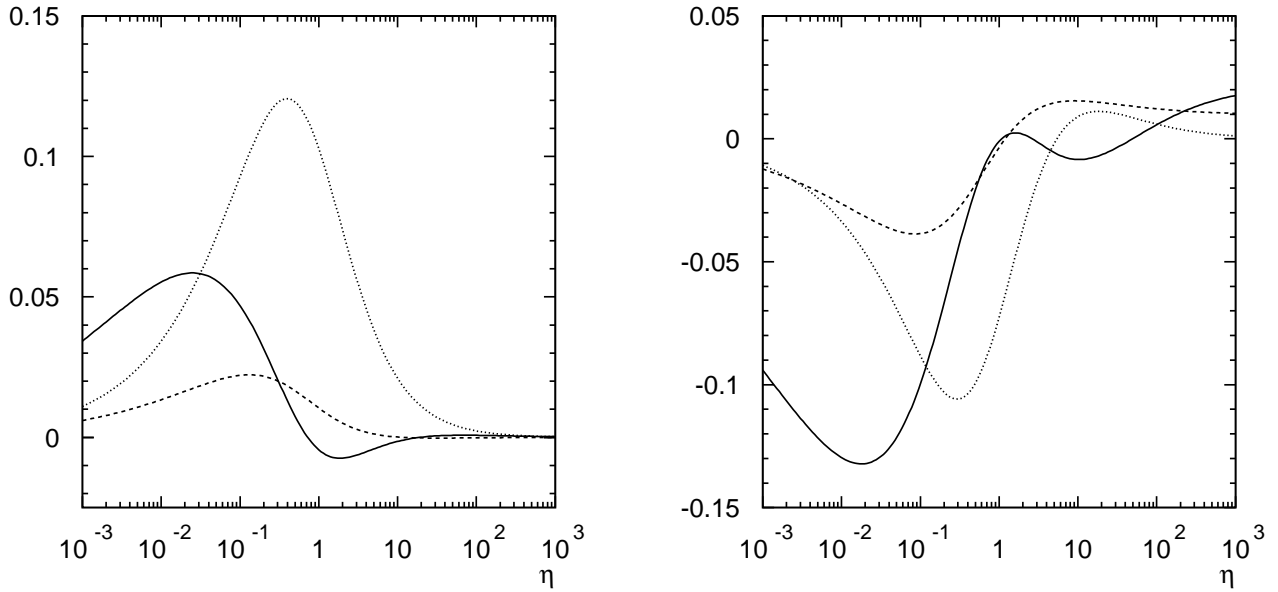

Figure 2: *Left: Scaling functions $g_{q\bar{q},1}^{(0)}(\eta)$ (dotted), $g_{q\bar{q},1}^{(1)}(\eta)$ (full), and $\tilde{g}_{q\bar{q},1}^{(1)}(\eta)$ (dashed). Right: The same for the process $gg \to t\bar{t}(g)$.*

states $q\bar{q}$ and gg are plotted in Figs. 1–5 as a function of

$$\eta = \frac{1}{\rho} - 1. \qquad (IV.49)$$

20

Figure 3: *Left: Scaling functions $g^{(0)}_{q\bar{q},2}(\eta)$ (dotted), $g^{(1)}_{q\bar{q},2}(\eta)$ (full), and $\tilde{g}^{(1)}_{q\bar{q},2}(\eta)$ (dashed). Right: The same for the process $gg \to t\bar{t}(g)$.*
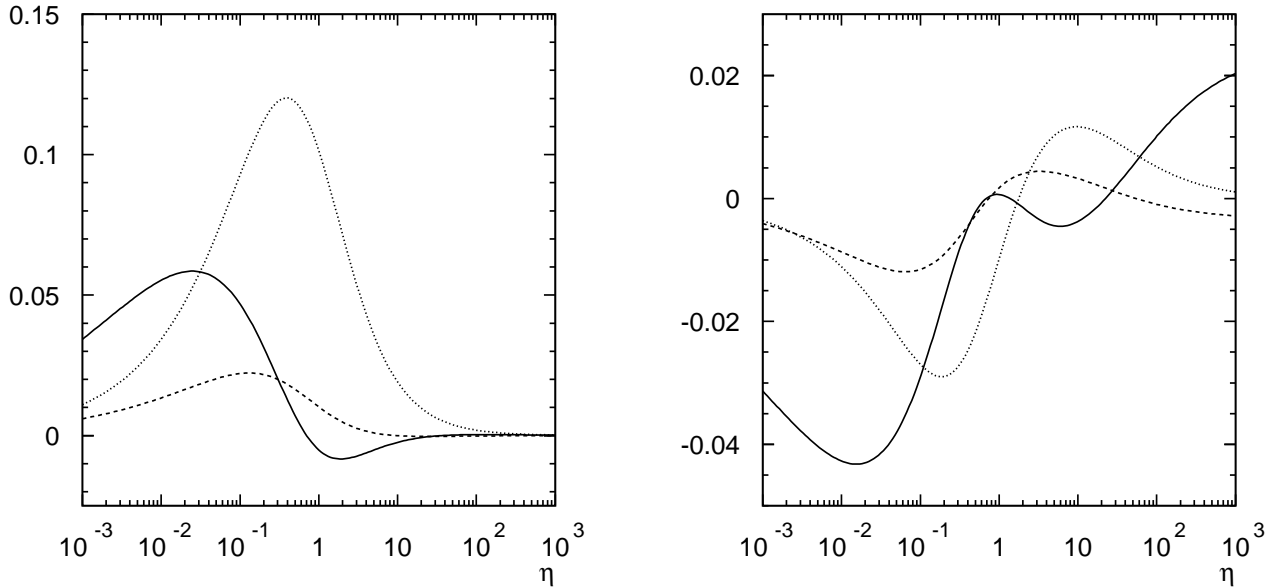
Figure 4: *Left: Scaling functions $g^{(0)}_{q\bar{q},3}(\eta)$ (dotted), $g^{(1)}_{q\bar{q},3}(\eta)$ (full), and $\tilde{g}^{(1)}_{q\bar{q},3}(\eta)$ (dashed). Right: The same for the process $gg \to t\bar{t}(g)$.*

For large values of η, the results for the functions $g^{(1)}_{i,a}$ and $\tilde{g}^{(1)}_{i,a}$ differ from the corresponding results in Refs. [33, 34], since in those papers the spin axes were defined using the initial-state parton c.m.s. rather than the $t\bar{t}$-ZMF.
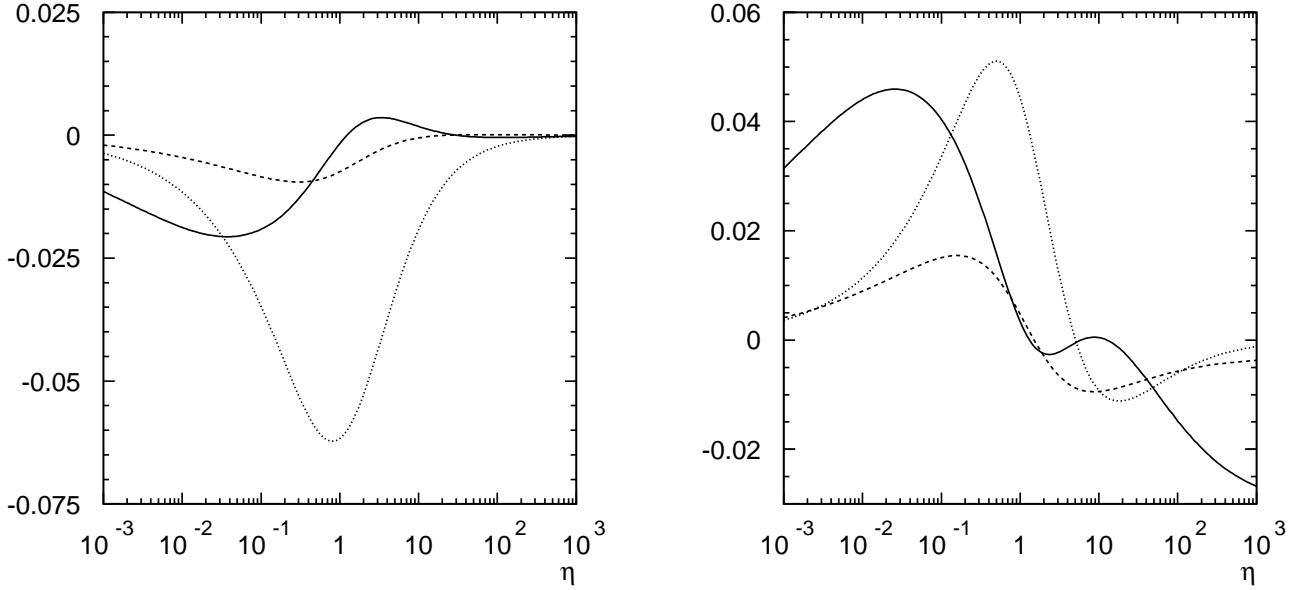
Figure 5: *Left: Scaling functions* $g_{q\bar{q},4}^{(0)}(\eta)$ *(dotted),* $g_{q\bar{q},4}^{(1)}(\eta)$ *(full), and* $\tilde{g}_{q\bar{q},4}^{(1)}(\eta)$ *(dashed). Right: The same for the process* $gg \to t\bar{t}(g)$.

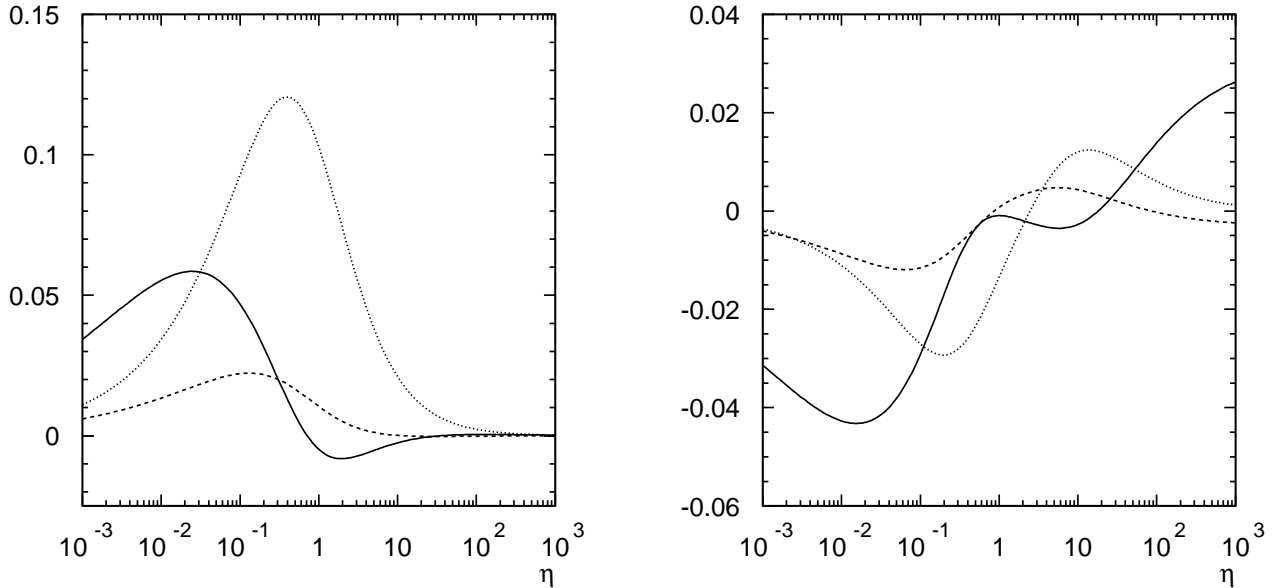# V. Decays of polarized top quarks

In the leading pole approximation for the intermediate top and antitop quarks the NLO QCD analysis of the reactions Eq. (I.8)–Eq. (I.10) involves also the matrix elements to order α_s of the main SM decay modes of the (anti)top quark in a given spin state, that is, the semileptonic modes

$$t \to b\ell^+ \nu_\ell, b\ell^+ \nu_\ell g \tag{V.1}$$

$(\ell = e, \mu, \tau)$, and the non-leptonic decays

$$t \to bq\bar{q}', bq\bar{q}'g, \tag{V.2}$$

where $q\bar{q}' = u\bar{d}, c\bar{s}$ for the dominant channels. Specifically, for computing the angular distributions (I.16) and (I.17), we need the matrix elements for the parton reactions

$$i \xrightarrow{t\bar{t}} a_1 + a_2 + X, \tag{V.3}$$

where a_1, a_2 denotes a lepton or a jet. Thus we require, in addition to the above production density matrices, the one-particle inclusive angular distributions $d\Gamma/d\cos\theta$ for the decays

$$\begin{aligned} t(s_t) &\to a_1(q_1) + X_1, \\ \bar{t}(s_{\bar{t}}) &\to a_2(q_2) + X_2, \end{aligned} \tag{V.4}$$

at NLO in α_s. Here q_1 and q_2 are the momenta of a_1 and a_2, respectively, which we define in the rest frame of the (anti)top quark, and θ is the angle between the polarization vector of the (anti)top quark and

22

the direction of flight of $a_1(a_2)$. For a fully polarized ensemble of top quarks these distributions are of the form

$$\frac{d\Gamma^{(1)}}{d\cos\theta} = \frac{\Gamma^{(1)}}{2}(1 + \kappa^{(1)}\cos\theta), \tag{V.5}$$

where $\Gamma^{(1)}$ is the partial width of the respective decay channel and $\kappa^{(1)}$ is the top-spin analysing power of a_1. For the case of the standard $(V-A)$ charged current interactions these distributions were computed to order α_s for the semileptonic and non-leptonic channels in Refs. [36] and [37], respectively. ¿From these results the corresponding unnormalized one-particle inclusive decay density matrices ρ and $\bar{\rho}$ integrated over the energies can be extracted. These matrices have the form

$$\rho_{\alpha'\alpha}^{t\to a_1} = \frac{\Gamma^{(1)}}{2}(\mathbb{1} + \kappa^{(1)}\tau\cdot\hat{\mathbf{q}}_1)_{\alpha'\alpha}, \tag{V.6}$$

$$\bar{\rho}_{\alpha'\alpha}^{\bar{t}\to a_2} = \frac{\Gamma^{(2)}}{2}(\mathbb{1} - \kappa^{(2)}\tau\cdot\hat{\mathbf{q}}_2)_{\alpha'\alpha}, \tag{V.7}$$

where $\hat{\mathbf{q}}_{1,2}$ are the directions of flight of a_1 and a_2 in the rest frame of the top and antitop quarks, respectively. As we work to lowest order in the electroweak couplings, $\Gamma^{(2)} = \Gamma^{(1)}$ and $\kappa_2 = \kappa_1$ to all orders in α_s, if the channel $a_2 + X_2$ is the charge-conjugate of $a_1 + X_1$.

For semileptonic top decays, the charged lepton is the most efficient analyser of the spin of the top quark. In the case of non-leptonic decays $t \to bq\bar{q}'(g)$ this role is taken by the weak isospin $I_W = -1/2$ quark from W decay. Tagging of the flavor of q or $\bar{q}'$, besides those of the b quark, is feasible, as far as the dominant channels are concerned, only for $q = c$, albeit with low efficiency. The non-b jets in non-leptonic top decay may be used as analysers of the top spin in the following, more efficient way: angular momentum conservation and the $(V-A)$ structure enforce that the fermion with $I_W = -1/2$ from W decay is, on average, less energetic than its partner with $I_W = +1/2$. This implies that the least-energetic light quark jet is a good top spin analyser. As far as the W boson is concerned notice that its analysing power is practically the same as that of the b quark:

$$\kappa_W = -\kappa_b + O(\alpha_s). \tag{V.8}$$

In Ref. [37] the coefficients $\kappa^{(f)}$ were given to NLO accuracy. In Section VI we need, however, the unnormalized density matrices (V.6) and (V.7); that is, we require, apart from the partial widths

$$\Gamma^{(f)} = a_0^{(f)} + 4\pi\alpha_s a_1^{(f)}, \tag{V.9}$$

the dimensionful coefficients

$$\Gamma^{(f)}\kappa^{(f)} = b_0^{(f)} + 4\pi\alpha_s b_1^{(f)}. \tag{V.10}$$

For the determination of these coefficients we use the Fermi constant $G_F = 1.16639 \times 10^{-5} \text{ GeV}^{-2}$, $m = 175$ GeV, $m_W = 80.41$ GeV, $\Gamma_W = 2.06$ GeV, $m_b = 5$ GeV, and all other quark and lepton masses are put to zero. (We do not use the narrow width approximation for the intermediate W boson.) We obtain, for the hadronic (h) and semileptonic (sl) decays $t \to bq\bar{q}'$, $b\ell\nu$, putting the CKM matrix elements

$|V_{tb}| = |V_{qq'}| = 1$:

$$
\begin{aligned}
a_0^{\mathrm{h}} &= 0.50645 \ \mathrm{GeV}, \\
a_0^{\mathrm{sl}} &= \frac{a_0^{\mathrm{h}}}{N}, \\
a_1^{\mathrm{h}} &= -0.01900(8) \ \mathrm{GeV}, \\
a_1^{\mathrm{sl}} &= -0.01061(2) \ \mathrm{GeV}.
\end{aligned}
\tag{V.11}
$$

For the LO coefficients b_0 we obtain:

$$
\begin{aligned}
b_0^d &= a_0^h = N b_0^\ell, \\
b_0^{b,\mathrm{h}} &= -0.20663 \ \mathrm{GeV} = N \, b_0^{b,\mathrm{sl}}, \\
b_0^u &= -0.15819 \ \mathrm{GeV} = N \, b_0^{\mathrm{v}}, \\
b_0^j &= 0.25840 \ \mathrm{GeV}, \\
b_0^T &= -0.16040 \ \mathrm{GeV}.
\end{aligned}
\tag{V.12}
$$

Here j stands for least energetic non-b jet, and T for an oriented thrust axis (for details, compare Ref. [37]). In Table 1 we give the corresponding NLO coefficients b_1. The numbers in the first columns are for 'bare' quarks, while in the second and third columns the E-algorithm and Durham algorithm were used, respectively, as jet clustering schemes [37]. We demand that the four final-state partons in $t \to b q \bar{q}' g$ be always clustered into three jets, i.e. no jet resolution parameter is involved. This is possible because the leading order matrix elements are free from soft and collinear singularities.

Table 1: *NLO coefficients b_1. Numbers are in units of GeV.*

	Partons	Jets, E-algo.	Jets, D-algo.	Semileptonic decay
b_1^d [GeV]	$-0.03154(22)$	$-0.04218(22)$	$-0.04410(22)$	$-$
b_1^ℓ [GeV]	$-$	$-$	$-$	$-0.01074(7)$
$b_1^{b,\mathrm{h}}$ or $b_1^{b,\mathrm{sl}}$ [GeV]	$0.01354(23)$	$0.01420(23)$	$0.01412(23)$	$0.00626(7)$
b_1^u or b_1^{v} [GeV]	$0.00431(21)$	$0.00935(22)$	$0.00852(22)$	$0.00120(7)$
b_1^j [GeV]	$-$	$-0.02336(23)$	$-0.02342(23)$	$-$
b_1^T [GeV]	$0.00915(22)$	$-$	$-$	$-$

Higher-dimensional distributions for t and/or $\bar{t}$ decays such as $d\Gamma/(dx_i d\cos\theta)$, where x_i the scaled lepton or jet energy are also known. Together with the production density matrices of Sections II–IV, they can be used for predictions of higher-dimensional distributions for the 2-particle inclusive reactions (I.12)–(I.15).

VI. Angular correlations in hadronic collisions

Let us now discuss the hadronic reactions Eqs. (I.12)–(I.15). In particular we derive the distributions of Eq. (I.16) and Eq. (I.17) at NLO in α_s, using the narrow-width approximation for the intermediate top and antitop quarks and taking into account only the factorizable QCD corrections. Recall that in this approximation the squared matrix elements of the parton reactions (I.8)–(I.10) are of the form shown in Eq. (I.11). We postpone the discussion of the non-factorizable QCD corrections until the end of this section. There we show that, at NLO in α_s, they are irrelevant for the distributions defined in Eqs. (I.16) and (I.17).

With the ingredients of Sections II–V we can first determine the two-fold differential ($\overline{\text{MS}}$-subtracted) cross sections

$$\frac{d\sigma(i \to a_1 a_2 + X)}{d\cos\theta_1 d\cos\theta_2} \tag{VI.1}$$

for the parton reactions $i \to a_1 a_2 + X$, where $\theta_1 (\theta_2)$ refers to the angle between the direction of flight $\hat{\mathbf{q}}_1$ ($\hat{\mathbf{q}}_2$) of particle a_1 (a_2) in the t ($\bar{t}$) rest frame and an arbitrary direction $\hat{\mathbf{a}}$ ($\hat{\mathbf{b}}$) that may be used as z axis in the (anti)top rest frame. Recall that we define the $t(\bar{t})$ rest frame by performing a rotation-free Lorentz boost from the $t\bar{t}$-ZMF. For the reactions (I.12)–(I.15), i.e.

$$h_1(P_1)\, h_2(P_2) \to t\bar{t} + X \to a_1\, a_2 + X\,, \tag{VI.2}$$

where $h_1, h_2 = p$ or $\bar{p}$, the differential cross sections are obtained in the usual way:

$$\frac{d\sigma(h_1(P_1)h_2(P_2) \to a_1 a_2 + X)}{d\cos\theta_1 d\cos\theta_2} = \sum_{a,b} \int dx_1 dx_2\, f_a^{h_1}(x_1,\mu_F) f_b^{h_2}(x_2,\mu_F)$$
$$\times\ \frac{d\sigma(a(x_1 P_1)b(x_2 P_2) \to a_1 a_2 + X)}{d\cos\theta_1 d\cos\theta_2}\,, \tag{VI.3}$$

where $f_a^h(x,\mu_F)$ denotes the parton distribution function (PDF) of parton a in hadron h.

The following analysis is based on integrating over the full phase-space of the particles in the final state. What then is the structure of the normalized distributions

$$\frac{1}{\sigma}\frac{d\sigma}{d\cos\theta_1 d\cos\theta_2} \tag{VI.4}$$

if we choose as reference axes $\hat{\mathbf{a}}, \hat{\mathbf{b}}$ one of the sets Eq. (IV.7)–Eq. (IV.9)? Each of the contributions to $d\sigma(i \to a_1 a_2 + X)$ is of the form $\text{Tr}\,[\rho R_s^i \bar\rho]$ ($s = B, V, \text{soft}, \text{col}, \text{c}, \text{res}$, depending on i), where the R_s^i have the structure as given in Eq. (IV.2) and ρ and $\bar\rho$ are given by Eqs. (V.6) and (V.7), respectively. All contributions are bilinear in $\hat{\mathbf{q}}_1$ and $\hat{\mathbf{q}}_2$. Thus the differential cross section Eq. (VI.3) is bilinear in $\cos\theta_1$ and $\cos\theta_2$. Parity invariance of QCD dictates that the top and antitop quarks have no polarization along the above reference axes $\hat{\mathbf{a}}$ and $\hat{\mathbf{b}}$, see Eq. (IV.13). This implies that in QCD

$$\langle\cos\theta_1\rangle = \langle\cos\theta_2\rangle = 0\,. \tag{VI.5}$$

Here the expectation value refers to reaction (VI.2), i.e. $\langle O \rangle = \sigma^{-1} \int d\sigma O$. (Equation (VI.5) applies also to cuts that are parity-invariant.) Thus for these reference axes the coefficients B_1 and B_2 in Eq. (IV.2)

are absent in the double distribution Eq. (I.16), and we obtain

$$\frac{1}{\sigma}\frac{d\sigma(h_1 h_2 \to a_1 a_2 + X)}{d\cos\theta_1 d\cos\theta_2} = \frac{1}{4}(1 - C_i \cos\theta_1 \cos\theta_2). \tag{VI.6}$$

with $i = \text{hel, beam, off}$ for the helicity, beam, and off-diagonal bases. Non-zero $B_{1,2}$ are generated by parity-violating contributions to $i \to t\bar{t}X$. Computations indicate [51, 52, 53] that they are small within the standard model.

Next we consider the distribution of the angle φ between the directions of flight $\hat{\mathbf{q}}_{1,2}$ of particle/jet a_1 and a_2, defined in the t and $\bar{t}$ rest frames, respectively. Using CP invariance of QCD and arguments analogous to those above, we find that this distribution is of the form

$$\frac{1}{\sigma}\frac{d\sigma(h_1 h_2 \to a_1 a_2 + X)}{d\cos\varphi} = \frac{1}{2}(1 - D\cos\varphi). \tag{VI.7}$$

Defining, for $\mu_R = \mu_F = m$,

$$
\begin{aligned}
N_r &= \frac{\alpha_s^2}{m^2}\frac{1}{\Gamma_t^2}\sum_{a,b}\int dx_1 dx_2\, f_a^{h_1}(x_1,\mu_F) f_b^{h_2}(x_2,\mu_F) \\
&\times \left\{ g_{ab,r}^{(0)} b_0^{(1)} b_0^{(2)} + 4\pi\alpha_s[g_{ab,r}^{(1)} b_0^{(1)} b_0^{(2)} + g_{ab,r}^{(0)} b_1^{(1)} b_0^{(2)} + g_{ab,r}^{(0)} b_0^{(1)} b_1^{(2)}] \right\},
\end{aligned} \tag{VI.8}
$$

$$
\begin{aligned}
\sigma &= \frac{\alpha_s^2}{m^2}\frac{1}{\Gamma_t^2}\sum_{a,b}\int dx_1 dx_2\, f_a^{h_1}(x_1,\mu_F) f_b^{h_2}(x_2,\mu_F) \\
&\times \left\{ f_{ab}^{(0)} a_0^{(1)} a_0^{(2)} + 4\pi\alpha_s[f_{ab}^{(1)} a_0^{(1)} a_0^{(2)} + f_{ab}^{(0)} a_1^{(1)} a_0^{(2)} + f_{ab}^{(0)} a_0^{(1)} a_1^{(2)}] \right\},
\end{aligned} \tag{VI.9}
$$

we obtain to NLO in the QCD coupling:

$$D = \frac{N_1}{\sigma}, \quad C_{\text{hel}} = \frac{N_2}{\sigma}, \quad C_{\text{beam}} = \frac{N_3}{\sigma}, \quad C_{\text{off}} = \frac{N_4}{\sigma}. \tag{VI.10}$$

Here $f_i^{(0,1)}(\rho)$ and $g_{i,r}^{(0,1)}(\rho)$ are the scaling functions defined in Eqs. (IV.19) and (IV.20), and collected in Appendix E, with $\rho = 4m^2/\hat{s}$, where the partonic c.m. energy $\sqrt{\hat{s}}$ is given in terms of the hadronic c.m. energy $\sqrt{s}$ through

$$\hat{s} = x_1 x_2 s. \tag{VI.11}$$

The total top quark width is denoted by Γ_t.

Finally, we discuss the issue of non-factorizable corrections. At NLO in α_s, such corrections are present in the one-loop contributions to the $q\bar{q}$ and gg fusion processes Eq. (I.8) and in the squared matrix elements for the corresponding processes Eq. (I.9) with real gluon radiation. These non-factorizable corrections correspond, at this order in the QCD coupling, to gluon exchange that interconnects the different stages of the off-shell $t\bar{t}$ production and decay process. These corrections were studied in the semi-soft gluon approximation in Ref. [42]. This approximation consists in taking into account only virtual, respectively real gluons with energies E_g of the order of Γ_t. This is adequate because

26

the contribution of a hard gluon to this correction is suppressed by Γ_t/E_g. The contributions $d\sigma_{nf}^{q\bar{q}}$ and $d\sigma_{nf}^{gg}$ to the respective differential cross sections are important for calculating a number of distributions, such as invariant mass distributions of the t, $\bar{t}$ quarks and of $t\bar{t}$ pairs. However, the non-factorizable corrections do not contribute to observables, which are inclusive in both the top and antitop invariant masses [38, 39, 40, 41, 42]. A well-known example for such a case is the total cross section.

It is straightforward to show that this result applies also to the distributions shown in Eqs. (VI.6) and (VI.7). The non-factorizable contributions $d\sigma_{nf}^{q\bar{q}}$ and $d\sigma_{nf}^{gg}$ (which contain both virtual and real gluon exchanges with momenta being integrated over) are proportional to the respective differential Born cross sections, decomposed into colour singlet and octet pieces. We represent the Lorentz-invariant phase-space element $d\Gamma_6$ for the 6-particle final states in Eq. (I.8) as

$$d\Gamma_6 \propto d\Gamma_{t\bar{t}} d\Gamma_t d\Gamma_{\bar{t}} dM_t^2 dM_{\bar{t}}^2, \tag{VI.12}$$

where M_t $(M_{\bar{t}})$ is the invariant mass of the top (anti)quark, $d\Gamma_{t\bar{t}}$ is the phase-space element of the intermediate $t\bar{t}$ state, and $d\Gamma_t$ $(d\Gamma_{\bar{t}})$ is the 3-particle phase-space element of t $(\bar{t})$ decay in its rest frame, where the z axis is identified with the reference axis $\hat{\mathbf{a}}$ $(\hat{\mathbf{b}})$. From this decomposition, it is clear that one has to integrate out the top and antitop invariant masses in calculating the contribution of $d\sigma_{nf}^i$ to the distribution (VI.6). But then the theorem of Refs. [38, 39, 40] applies.

In order to show that the opening angle distribution (VI.7) receives no contribution from $d\sigma_{nf}^i$ either, we recall that this distribution is due to $\langle \mathbf{S}_t \cdot \mathbf{S}_{\bar{t}} \rangle$, and $\mathbf{S}_t \cdot \mathbf{S}_{\bar{t}}$ can be decomposed as given below Eq. (IV.11). Thus, to NLO in the QCD coupling the above angular distributions are determined solely by the Born contributions and the factorizable QCD corrections.

VII. Numerical results

In this section we present the numerical results for the angular distributions (VI.6) and (VI.7). In the absence of cuts the spin correlation coefficients can be computed in terms of expectation values:

$$\begin{aligned} C &= -9\langle \cos\theta_1 \cos\theta_2 \rangle, \\ D &= -3\langle \cos\varphi \rangle. \end{aligned} \tag{VII.1}$$

In the following we present the NLO results for the coefficients C and D in the absence of phase-space cuts, using Eq. (VI.8) and Eq. (VI.9). It is convenient to rewrite these formulae:

$$N_r = \frac{\alpha_s^2}{m^2} \frac{1}{\Gamma_t^2} \sum_i \left\{ N_{i,r}^{(0)} b_0^{(1)} b_0^{(2)} + 4\pi\alpha_s [N_{i,r}^{(1)} b_0^{(1)} b_0^{(2)} + N_{i,r}^{(0)} b_1^{(1)} b_0^{(2)} + N_{i,r}^{(0)} b_0^{(1)} b_1^{(2)}] \right\}, \tag{VII.2}$$

$$\sigma = \frac{\alpha_s^2}{m^2} \frac{1}{\Gamma_t^2} \sum_i \left\{ Z_i^{(0)} a_0^{(1)} a_0^{(2)} + 4\pi\alpha_s [Z_i^{(1)} a_0^{(1)} a_0^{(2)} + Z_i^{(0)} a_1^{(1)} a_0^{(2)} + Z_i^{(0)} a_0^{(1)} a_1^{(2)}] \right\}, \tag{VII.3}$$

where $i = q\bar{q}, gg, gq, g\bar{q}$. For the evaluation of Eqs. (VII.2), (VII.3) we use the NLO parton distribution functions of Ref. [54] (CTEQ6.1M) and of Ref. [55] (MRST2003). In addition we also use the PDFs

Table 2: *Results for the quantities $Z_i^{(0)}$ and $N_{i,r}^{(0)}$ defined in Eqs. (VII.2), (VII.3) for different PDFs at the Tevatron and the LHC.*

Tevatron		$i = q\bar{q}$	$i = gg$
$Z_i^{(0)}$	CTEQ6.1M	0.032162	$3.9358 \cdot 10^{-3}$
	MRST2003	0.033193	$3.9751 \cdot 10^{-3}$
	GRV98	0.033528	$5.0460 \cdot 10^{-3}$
$N_{i,1}^{(0)}$	CTEQ6.1M	0.010721	$-1.6864 \cdot 10^{-3}$
	MRST2003	0.011064	$-1.7534 \cdot 10^{-3}$
	GRV98	0.011176	$-2.2477 \cdot 10^{-3}$
$N_{i,2}^{(0)}$	CTEQ6.1M	-0.016695	$2.3820 \cdot 10^{-3}$
	MRST2003	-0.017240	$2.4585 \cdot 10^{-3}$
	GRV98	-0.017436	$3.1438 \cdot 10^{-3}$
$N_{i,3}^{(0)}$	CTEQ6.1M	0.031849	$-1.2099 \cdot 10^{-3}$
	MRST2003	0.032869	$-1.2774 \cdot 10^{-3}$
	GRV98	0.033199	$-1.6457 \cdot 10^{-3}$
$N_{i,4}^{(0)}$	CTEQ6.1M	0.032162	$-1.2959 \cdot 10^{-3}$
	MRST2003	0.033193	$-1.3606 \cdot 10^{-3}$
	GRV98	0.033528	$-1.7497 \cdot 10^{-3}$
LHC		$i = q\bar{q}$	$i = gg$
$Z_i^{(0)}$	CTEQ6.1M	0.46482	3.2048
	MRST2003	0.49789	3.5616
	GRV98	0.48075	4.1237
$N_{i,1}^{(0)}$	CTEQ6.1M	0.15494	-0.92015
	MRST2003	0.16596	-1.0163
	GRV98	0.16025	-1.1620
$N_{i,2}^{(0)}$	CTEQ6.1M	-0.26645	1.3931
	MRST2003	-0.28604	1.5401
	GRV98	-0.27709	1.7621

Table 3: *Results for the quantities $Z_i^{(1)}$ and $N_{i,r}^{(1)}$ defined in Eqs. (VII.2), (VII.3) for different PDFs at the Tevatron and the LHC.*

Tevatron		$i = q\bar{q}$	$i = gg$	$i = qg + g\bar{q}$
$Z_i^{(1)}$	CTEQ6.1M	$4.699 \cdot 10^{-3}$	$2.312 \cdot 10^{-3}$	$-3.627 \cdot 10^{-4}$
	MRST2003	$4.836 \cdot 10^{-3}$	$2.423 \cdot 10^{-3}$	$-3.926 \cdot 10^{-4}$
	GRV98	$4.854 \cdot 10^{-3}$	$3.113 \cdot 10^{-3}$	$-4.442 \cdot 10^{-4}$
$N_{i,1}^{(1)}$	CTEQ6.1M	$1.539 \cdot 10^{-3}$	$-1.070 \cdot 10^{-3}$	$1.216 \cdot 10^{-4}$
	MRST2003	$1.583 \cdot 10^{-3}$	$-1.143 \cdot 10^{-3}$	$1.289 \cdot 10^{-4}$
	GRV98	$1.589 \cdot 10^{-3}$	$-1.478 \cdot 10^{-3}$	$1.456 \cdot 10^{-4}$
$N_{i,2}^{(1)}$	CTEQ6.1M	$-2.643 \cdot 10^{-3}$	$1.458 \cdot 10^{-3}$	$-1.970 \cdot 10^{-4}$
	MRST2003	$-2.721 \cdot 10^{-3}$	$1.552 \cdot 10^{-3}$	$-2.065 \cdot 10^{-4}$
	GRV98	$-2.734 \cdot 10^{-3}$	$2.004 \cdot 10^{-3}$	$-2.331 \cdot 10^{-4}$
$N_{i,3}^{(1)}$	CTEQ6.1M	$4.459 \cdot 10^{-3}$	$-8.647 \cdot 10^{-4}$	$2.066 \cdot 10^{-5}$
	MRST2003	$4.587 \cdot 10^{-3}$	$-9.246 \cdot 10^{-4}$	$1.995 \cdot 10^{-5}$
	GRV98	$4.602 \cdot 10^{-3}$	$-1.195 \cdot 10^{-3}$	$2.258 \cdot 10^{-5}$
$N_{i,4}^{(1)}$	CTEQ6.1M	$4.515 \cdot 10^{-3}$	$-9.117 \cdot 10^{-4}$	$3.033 \cdot 10^{-5}$
	MRST2003	$4.645 \cdot 10^{-3}$	$-9.725 \cdot 10^{-4}$	$2.975 \cdot 10^{-5}$
	GRV98	$4.660 \cdot 10^{-3}$	$-1.256 \cdot 10^{-3}$	$3.363 \cdot 10^{-5}$
LHC		$i = q\bar{q}$	$i = gg$	$i = qg + g\bar{q}$
$Z_i^{(1)}$	CTEQ6.1M	0.04197	1.277	0.04565
	MRST2003	0.04415	1.411	0.05120
	GRV98	0.04194	1.625	0.06018
$N_{i,1}^{(1)}$	CTEQ6.1M	0.01329	-0.4330	0.03077
	MRST2003	0.01396	-0.4760	0.03307
	GRV98	0.01324	-0.5423	0.03082
$N_{i,2}^{(1)}$	CTEQ6M	-0.02417	0.5927	-0.07905
	MRST2003	-0.02550	0.6513	-0.08540
	GRV98	-0.02419	0.7402	-0.08181

of Ref. [56] (GRV98), to illustrate the dependence on the gluon distribution function. We put $\mu_R = \mu_F = m_t = 175$ GeV, $N_f = 5$ and use the following values for $\alpha_s^{N_f=5}$: $\alpha_s(m_t) = 0.1074$ for CTEQ6.1M, $\alpha_s(m_t) = 0.1062$ for MRST2003, and $\alpha_s(m_t) = 0.1041$ for GRV98. (The values of α_s are those used by the different groups when fitting the PDFs.) In Table 2 we present the values of $Z_i^{(0)}$ and $N_{i,r}^{(0)}$ for $p\bar{p}$ collisions at $\sqrt{s} = 1.96$ GeV (Tevatron) and pp collisions at $\sqrt{s} = 14$ TeV (LHC). In the latter case, we only show results for the D coefficient and the C_{hel} coefficient, since the spin correlations in the beam and the off-diagonal basis are very small at the LHC [35]. Table 3 lists the NLO coefficients $Z_i^{(1)}$ and $N_{i,r}^{(1)}$. We observe the following generic features: For the coefficients $N_{i,a}$ the two initial states $q\bar{q}$ and gg always contribute with opposite signs. For the gg initial state the GRV98 PDF systematically gives a larger contribution, while the other two PDFs agree quite well in most of the cases.

Adding all contributions as in Eqs. (VII.2), (VII.3) and taking the ratios N_r/σ, we obtain LO and NLO predictions for the spin correlation coefficients. The results are listed in Table 4 for the Tevatron and in Table 5 for the LHC, for the different decay modes of the top and antitop quarks. In these two tables we use the CTEQ6L (LO) and CTEQ6.1M (NLO) PDFs. As spin analysers we use the charged lepton and/or the least energetic non-b-quark jet defined in the Durham jet clustering scheme.

At the Tevatron, the helicity basis is not the best choice, since the t and $\bar{t}$ are only moderately relativistic in this case. The spin correlations are large both in the beam and off-diagonal basis. In fact, since the results are almost the same in these two bases, the beam basis is probably the best choice since it is easier to determine experimentally. The QCD corrections decrease the LO results at the Tevatron. The relative size of the corrections varies between $\sim 16\%$ ($C_{beam,off}$) and $\sim 28\%$ (D) for the dilepton channel and between $\sim 27\%$ ($C_{beam,off}$) and $\sim 38\%$ (D) in the all-jets channel.

At the LHC, where the gg initial state gives the dominant contribution, the helicity correlation is the best choice from the four distributions. Here the spin correlations in the dilepton channel are of the order of 30%. The QCD corrections are much smaller than at the Tevatron. In the dilepton channel they enhance the spin correlation by $\sim 2\%$ in the helicity basis and by $\sim 10\%$ for the opening angle correlation coefficient D. In the all-jet channel, the QCD corrections decrease the LO results for C_{hel} by $\sim 8\%$ and for D by $\sim 1\%$.

In Table 6 we compare the NLO results for the spin correlation coefficients evaluated for the 3 different PDFs that we used. The CTEQ6.1M and MRST2003 distributions give almost identical results, which is remarkable since the individual contributions from the $q\bar{q}$ and gg initial states differ in some cases significantly (see Tables 2, 3). (For previous versions of these distribution functions, the agreement for the spin correlations was not so striking [35].) Using the GRV98 PDF, however, leads to spin correlations that are up to $\sim 13\%$ smaller at the Tevatron and up to $\sim 4\%$ larger at the LHC as compared to the other two PDFs. This shows that the spin correlations are very sensitive to the relative quark and gluon content of the proton. Future measurements of these correlations may help to pin down the parton distributions further.

To estimate higher order corrections to our predictions, we now study the dependence on the renormalization and factorization scales. For simplicity, we keep $\mu = \mu_F = \mu_R$ and vary μ between $m_t/10$ and $10m_t$. The results for the quantities σC_{beam} (Tevatron) and σC_{hel} (LHC) are shown in Fig. 6 for the dilepton decay channel, where we sum over $\ell = e, \mu, \tau$. The inclusion of the QCD corrections reduces the scale dependence significantly. The correlation coefficients C and D are ratios in which a factor α_s^2 drops out. Therefore, at LO, the coefficients only depend on μ_F but not on μ_R. A comparison between

30

Table 4: *LO and NLO results for the spin correlation coefficients* C *and* D *of the distributions (VI.6) and (VI.7) in the case of* $p\bar{p}$ *collisions at* $\sqrt{s} = 1.96$ *TeV for different* $t\bar{t}$ *decay modes. The PDF CTEQ6L (LO) and CTEQ6.1M (NLO) of Ref. [54] were used, and* $\mu_F = \mu_R = m_t$.

		Dilepton	Lepton–jet	Jet–jet
C_{hel}	LO	-0.471	-0.240	-0.123
	NLO	-0.352	-0.168	-0.080
C_{beam}	LO	0.928	0.474	0.242
	NLO	0.777	0.370	0.176
C_{off}	LO	0.937	0.478	0.244
	NLO	0.782	0.372	0.177
D	LO	0.297	0.151	0.0773
	NLO	0.213	0.101	0.0480

Table 5: *Results for* C_{hel} *and* D *for* pp *collisions at* $\sqrt{s} = 14$ *TeV using the same PDF and parameters as in Table 4.*

		Dilepton	Lepton–jet	Jet–jet
C_{hel}	LO	0.319	0.163	0.083
	NLO	0.326	0.158	0.076
D	LO	-0.217	-0.111	-0.0567
	NLO	-0.237	-0.115	-0.0560

Table 6: *Spin correlation coefficients at NLO for different PDFs for the Tevatron (upper part) and the LHC (lower part) for dilepton final states.*

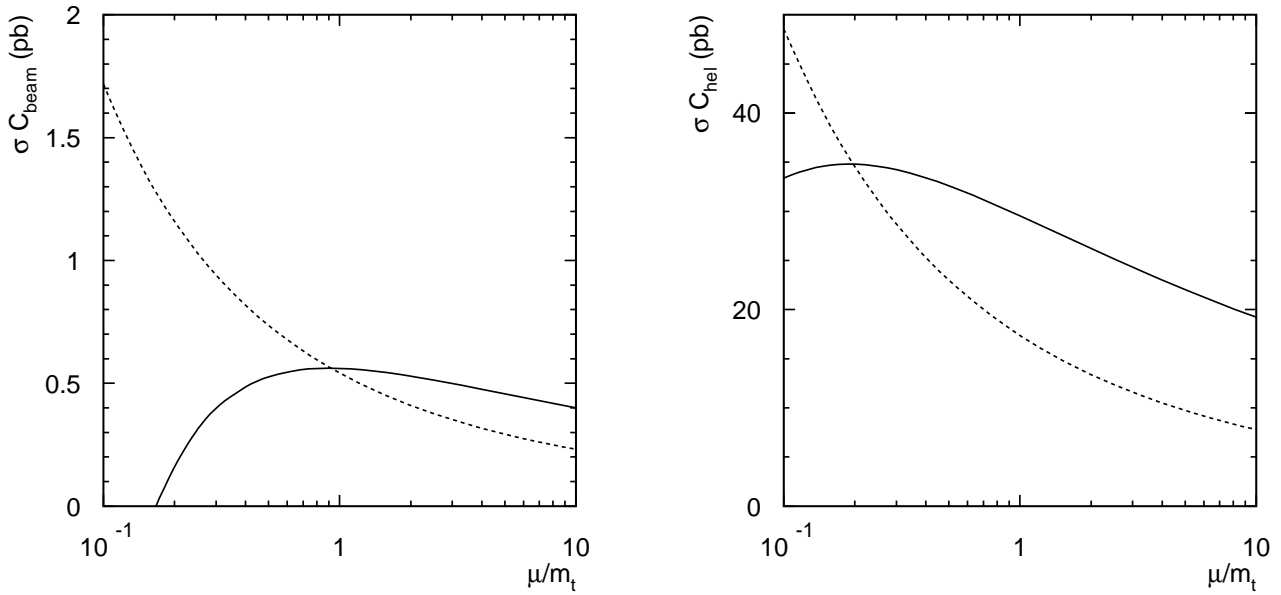|	Tevatron		
	CTEQ6.1M	MRST2003	GRV98
C_{hel}	-0.352	-0.352	-0.313
C_{beam}	0.777	0.777	0.732
C_{off}	0.782	0.782	0.736
D	0.213	0.212	0.185
	LHC		
C_{hel}	0.326	0.327	0.339
D	-0.237	-0.237	-0.243

Figure 6: *Left: Dependence of σC_{beam} on $\mu = \mu_F = \mu_R$ for $p\bar{p}$ collisions at $\sqrt{s} = 1.96$ TeV in the dilepton decay channel. The dashed line shows the LO result, the full line shows the result at NLO. Right: The same for σC_{hel} for pp collisions at $\sqrt{s} = 14$ TeV.*

Table 7: *Dependence of the correlation coefficients, computed with the PDF CTEQ6.1M, on $\mu = \mu_R = \mu_F$ at NLO for the dilepton decay channel.*

$\mu_R = \mu_F$	Tevatron				LHC	
	C_{hel}	C_{beam}	C_{off}	D	C_{hel}	D
$m_t/2$	-0.326	0.735	0.740	0.191	0.329	-0.244
m_t	-0.352	0.777	0.782	0.213	0.326	-0.237
$2m_t$	-0.370	0.804	0.810	0.227	0.324	-0.232

the scale dependence at LO and NLO is thus meaningless for these coefficients. Table 7 therefore only lists the NLO scale dependence. At the Tevatron, a variation of μ between $m_t/2$ and $2m_t$ changes the results at $\mu = m_t$ by $\sim \pm (5\text{–}10)\%$, while at the LHC the change of C_{hel} is less than a per cent and D varies by $\sim \pm 3\%$.

Before closing this section, we summarize how an experimental measurement of the distributions (VI.6) and (VI.7) that matches our predictions should proceed:

i. Reconstruct the top and antitop 4-momenta in the laboratory frame (= c.m. frame of the colliding hadrons).

ii. Perform a rotation-free boost from the laboratory frame to the $t\bar{t}$-ZMF. Compute $\hat{\mathbf{a}}$ and $\hat{\mathbf{b}}$ in that frame.

iii. Perform rotation-free boosts from the $t\bar{t}$-ZMF to the top quark rest frame and the antitop quark rest frame. Compute the direction $\hat{\mathbf{q}}_1$ of the top quark decay product a_1 in the t rest frame and the direction $\hat{\mathbf{q}}_2$ of the antitop quark decay product a_2 in the $\bar{t}$ rest frame. Finally, compute $\cos\theta_1 = \hat{\mathbf{a}} \cdot \hat{\mathbf{q}}_1$, $\cos\theta_2 = \hat{\mathbf{b}} \cdot \hat{\mathbf{q}}_2$ and $\cos\phi = \hat{\mathbf{q}}_1 \cdot \hat{\mathbf{q}}_2$.

Note that in this prescription the t and $\bar{t}$ rest frames are obtained by first boosting into the $t\bar{t}$-ZMF. If this step is left out, and the t and $\bar{t}$ rest frames are constructed by directly boosting from the lab frame, a Wigner rotation has to be taken into account.

The results in this paper were obtained without imposing kinematic cuts. Such cuts will in general distort the distributions, i.e. C and D will in general depend on the angles θ_1, θ_2 and φ, respectively. The expectation values on the r.h.s. of Eqs. (VII.1) may still be used as measures of the $t\bar{t}$ spin correlations in the presence of cuts. They are then no longer directly related to these differential distributions. One strategy, followed for instance in Ref. [62], is to correct for these distortions by Monte Carlo methods before extracting the spin correlation coefficient and comparing with theoretical predictions. A future aim will be to directly include the cuts in an NLO event generator to be constructed with the above results for all relevant $2 \to 6$ and $2 \to 7$ processes.

VIII. Conclusions

We have determined the differential cross sections for top quark pair production in a general spin configuration by $q\bar{q}$ annihilation, gg, qg, and $\bar{q}g$ fusion to order α_s^3. These cross sections provide, together with the differential rates of polarized top and antitop decays at order α_s, the NLO factorizable contributions to the reactions given in Eqs. (I.8) to Eq. (I.10). We have evaluated the corresponding spin density matrices for on-shell intermediate top and antitop quarks. However, our results can also be employed as building blocks for taking the finite top quark width at NLO into account. (For studies at the Born level, see for instance Refs. [63, 64].)

As an application of the above results we have studied a number of distributions due to top–antitop spin correlations. The QCD-induced spin correlations are large effects, which are easily visible in distributions of the final-state particles. Given the size of the spin correlations, they are expected to become a good tool for analysing in detail top quark pair production and decay dynamics. They can be studied at the Tevatron and — in view of the expected large $t\bar{t}$ data samples — especially at the LHC, in the dilepton, single lepton and all-hadronic decay channels, by measuring suitably defined double angular distributions. In fact, a first measurement of spin correlations in the off-diagonal basis was already performed by the D0 collaboration for the dilepton decay channel [65]. While this analysis was limited by the very small event sample, it clearly demonstrated the possibility of the experimental study of these effects. For the LHC a simulation was performed [62], showing that the experimental accuracy of a measurement of C_{hel} at the LHC can be expected to be better than 10%.

On the theoretical side, we have shown in this paper that the NLO QCD corrections to the double angular distributions are of the order of 15 to 40% for the Tevatron, and below 10% for the LHC. A study of the scale dependence of our NLO predictions indicates that the residual theoretical uncertainty due to higher order corrections should be $\lesssim 10\%$. Work on soft gluon and threshold resummations will further reduce the theoretical uncertainties.

In particular for pp collisions at $\sqrt{s} = 14$ TeV, the theoretical uncertainties are quite small. By the time the LHC will start operating it may therefore be expected that further theoretical progress will have turned top quark spin correlations into a precision tool for the analysis of $t\bar{t}$ events.

A. One-loop integrals

In this appendix, we collect a number of functions that appear in the virtual corrections given in Section II.2 and in Appendices B, C. Only the real parts of the integrals are given. It proves useful to express the integrals in terms of the following variables:

$$
\begin{aligned}
y_\pm &= \frac{1}{2}(1 \pm \beta), \\
y_t &= \frac{1}{2}(1 - \beta y), \\
\xi &= \frac{m^2}{\hat{s}}, \\
x &= \frac{1-\beta}{1+\beta}.
\end{aligned}
\tag{A.1}
$$

1) The six-dimensional box integrals are defined by

$$
\begin{aligned}
&D_0^6(q_1, q_2, q_3, m_1, m_2, m_3, m_4) \\
&= \frac{1}{i\pi^2} \int \frac{d^6 l}{(l^2 - m_1^2)((l+q_1)^2 - m_2^2)((l+q_1+q_2)^2 - m_3^2)((l+q_1+q_2+q_3)^2 - m_4^2)}.
\end{aligned}
\tag{A.2}
$$

The following integrals appear in our results:

$$
\begin{aligned}
D_0^6(p_1, p_2, -k_2, 0, 0, 0, m) =\ & \frac{\pi}{\hat{s}(y_t - 1)} \left\{ \frac{1}{1 - \frac{\xi}{y_t(1-y_t)}} \left[-\mathrm{Li}_2\left(1 - \frac{\xi}{y_t}\right) + \frac{1}{2}\ln^2(y_t) \right] \right. \\
& + \frac{y_-}{(y_+ - y_-)} \frac{1}{(1 - \frac{y_+}{1-y_t})} \left[-\mathrm{Li}_2(y_-) + \frac{1}{2}\ln^2(y_-) \right] \\
& \left. + \frac{y_+}{(y_- - y_+)} \frac{1}{(1 - \frac{y_-}{1-y_t})} \left[-\mathrm{Li}_2(y_+) + \frac{1}{2}\ln^2(y_+) \right] \right\}.
\end{aligned}
\tag{A.3}
$$

$$
\begin{aligned}
D_0^6(-k_1, p_1, p_2, 0, m, m, m) =\ & \frac{2\pi}{\hat{s}\beta(1-y^2)} \left\{ \frac{(1+\beta)(1-y)}{4} \left[\frac{\pi^2}{3} - \ln^2(x) \right] \right. \\
& \left. + 2y_t \left[\mathrm{Li}_2(-x) - \ln(x)\ln\left(\frac{y_t}{y_-}\right) \right] + (\beta - y)\mathrm{Li}_2\left(1 - \frac{y_t}{\xi}\right) \right\}.
\end{aligned}
\tag{A.4}
$$

$$
\begin{aligned}
D_0^6(p_1, -k_1, p_2, 0, 0, m, m) =\ & \frac{\pi}{\hat{s}} \left\{ \frac{\pi^2}{2} + \frac{4\xi}{\beta^2(1-y^2)} \left[\frac{\pi^2}{6} + \frac{y_t(1-y_t)}{2\xi} \ln^2\left(\frac{y_t}{1-y_t}\right) \right. \right. \\
& \left. \left. + \mathrm{Li}_2\left(1 - \frac{y_t}{\xi}\right) + \mathrm{Li}_2\left(1 - \frac{1-y_t}{\xi}\right) \right] \right\}.
\end{aligned}
\tag{A.5}
$$

$$
\begin{aligned}
D_0^6(p_1, p_2, -k_1, 0, 0, 0, m) &= D_0^6(p_1, p_2, -k_2, 0, 0, 0, m)|_{y \to -y}. \tag{A.6} \\
D_0^6(-k_2, p_1, p_2, 0, m, m, m) &= D_0^6(-k_1, p_1, p_2, 0, m, m, m)|_{y \to -y}. \tag{A.7}
\end{aligned}
$$

2) The 3-point integrals are defined by

$$
C_0(q_1, q_2, m_1, m_2, m_3) = \frac{1}{i\pi^2} \int \frac{(2\pi\mu)^{2\varepsilon} d^{4-2\varepsilon} l}{(l^2 - m_1^2)((l+q_1)^2 - m_2^2)((l+q_1+q_2)^2 - m_3^2)}.
\tag{A.8}
$$

The following integrals appear in our results (they agree with those listed in [4]):

$$C_0(p_1,p_2,0,0,0) = \frac{C_\varepsilon}{\hat{s}}\left[\frac{1}{\varepsilon^2}+\frac{1}{\varepsilon}\ln(\xi)\right]+\overline{C}_0(p_1,p_2,0,0,0),$$

$$\overline{C}_0(p_1,p_2,0,0,0) = \frac{1}{\hat{s}}\left[\frac{1}{2}\ln^2(\xi)-\frac{7\pi^2}{12}\right]. \tag{A.9}$$

$$C_0(-p_1,k_1,0,0,m) = -\frac{C_\varepsilon}{y_t\hat{s}}\left[\frac{1}{2\varepsilon^2}-\frac{1}{\varepsilon}\ln\left(\frac{y_t}{\xi}\right)\right]+\overline{C}_0(-p_1,k_1,0,0,m),$$

$$\overline{C}_0(-p_1,k_1,0,0,m) = -\frac{1}{y_t\hat{s}}\left[\ln^2\left(\frac{y_t}{\xi}\right)+\mathrm{Li}_2\left(1-\frac{y_t}{\xi}\right)+\frac{\pi^2}{24}\right]. \tag{A.10}$$

$$C_0(-p_1,k_2,0,0,m) = C_0(-p_1,k_1,0,0,m)|_{y\to-y}. \tag{A.11}$$

$$C_0(k_1,k_2,0,m,0) = \frac{1}{\hat{s}\beta}\left[2\mathrm{Li}_2(-x)+\frac{1}{2}\ln^2(x)+\frac{\pi^2}{6}\right]. \tag{A.12}$$

$$C_0(k_1,k_2,m,0,m) = \frac{C_\varepsilon}{\hat{s}\beta}\left[\frac{1}{\varepsilon}\ln(x)\right]+\overline{C}_0(k_1,k_2,m,0,m),$$

$$\overline{C}_0(k_1,k_2,m,0,m) = \frac{1}{\hat{s}\beta}\left[-2\ln(x)\ln(1-x)-2\mathrm{Li}_2(x)+\frac{1}{2}\ln^2(x)-\frac{2\pi^2}{3}\right]. \tag{A.13}$$

$$C_0(k_1,-p_1,0,m,m) = \frac{1}{y_t\hat{s}}\left[\frac{\pi^2}{6}-\mathrm{Li}_2\left(1-\frac{y_t}{\xi}\right)\right]. \tag{A.14}$$

$$C_0(k_2,-p_1,0,m,m) = C_0(k_1,-p_1,0,m,m)|_{y\to-y}. \tag{A.15}$$

$$C_0(p_1,p_2,m,m,m)) = \frac{1}{2\hat{s}}\left[\ln^2(x)-\pi^2\right]. \tag{A.16}$$

3) The two-point integrals are defined by

$$B_0(q,m_1,m_2) = \frac{1}{i\pi^2}\int\frac{(2\pi\mu)^{2\varepsilon}d^{4-2\varepsilon}l}{(l^2-m_1^2)((l+q)^2-m_2^2)} = \frac{C_\varepsilon}{\varepsilon}+\overline{B}_0(q,m_1,m_2). \tag{A.17}$$

The following finite parts of these integrals are needed:

$$\overline{B}_0(k_1+k_2,0,0) = 2+\ln(\xi). \tag{A.18}$$

$$\overline{B}_0(k_1,0,m) = 2. \tag{A.19}$$

$$\overline{B}_0(k_1-p_1,0,m) = 2+\frac{y_t}{y_t-\xi}\ln\left(\frac{\xi}{y_t}\right). \tag{A.20}$$

$$\overline{B}_0(k_2-p_1,0,m) = \overline{B}_0(k_1-p_1,0,m)|_{y\to-y}. \tag{A.21}$$

$$\overline{B}_0(k_1+k_2,m,m) = 2+\beta\ln(x). \tag{A.22}$$

4) Finally, the one-point integral is given by

$$A_0(m) = \frac{1}{i\pi^2}\int\frac{(2\pi\mu)^{2\varepsilon}d^{4-2\varepsilon}l}{(l^2-m^2)} = \frac{C_\varepsilon}{\varepsilon}m^2+m^2. \tag{A.23}$$

36

B. Virtual corrections to $q\bar{q} \to t\bar{t}$

Here we list the coefficients $A_V^{q\bar{q}}$ and e_a^V, defined in (II.28), which appear in the one-loop contributions to $q\bar{q} \to t\bar{t}$ (note that the contributions proportional to the finite part of the one-point integral ($= m^2$) and those of $\overline{B}_0(k_1, 0, m) = 2$ are added to those terms that are not multiplied by an n-point integral):

$$
\begin{aligned}
A_V^{q\bar{q}} = e_0^V = {} & \frac{D_0^6(p_1, p_2, -k_2, 0, 0, 0, m)}{\pi} \hat{s}\beta^2(1 - y^2)\frac{N^2 - 2}{4N}\left(\frac{\beta^2 - 3}{1 - \beta y} + 2\beta y\right) \\
& + \frac{D_0^6(p_1, p_2, -k_1, 0, 0, 0, m)}{\pi}\hat{s}\beta^2(1 - y^2)\frac{1}{2N}\left(\frac{\beta^2 - 3}{1 + \beta y} - 2\beta y\right) \\
& - \frac{m^2}{\beta^2}C_0(k_1, k_2, 0, m, 0)\left\{\frac{N}{2}(2y^2\beta^2 - 3y^2 + 2\beta^3 y - 2\beta y + 1) + \frac{4\beta y(1 - \beta^2)}{N}\right. \\
& + \left.\beta^2(\beta^2 - 3)\left[\frac{N^2 - 2}{N(1 - \beta y)} + \frac{2}{N(1 + \beta y)}\right]\right\} \\
& - \frac{\overline{B}_0(k_1 + k_2, 0, 0)}{4\beta^2}\left\{N(1 - 3y^2 - \beta^4 + y^2\beta^4 - 2\beta y + 4y^2\beta^2)\right. \\
& - \left.\frac{\beta}{N}(-8y + 6\beta - 3\beta^3 + 3y^2\beta^3)\right\} + \frac{N^2 - 2}{2N}\overline{B}_0(k_1 - p_1, 0, m)\left\{\frac{2(1 - \beta^2)}{1 - \beta y} - (1 + \beta y)\right\} \\
& + \frac{1}{N}\overline{B}_0(k_2 - p_1, 0, m)\left\{\frac{2(1 - \beta^2)}{1 + \beta y} - (1 - \beta y)\right\} \\
& + \frac{1}{4N}\overline{B}_0(k_1 + k_2, m, m)(y^2 + 2y^2\beta^2 + 5 - 2\beta^2) \\
& + \frac{1}{2\beta^2}\left\{(2\beta^3 y + 5y^2\beta^2 + \beta^2 - 2\beta y + 1 - 3y^2)N + \frac{\beta(1 - \beta^2)}{N}(\beta - \beta y^2 + 8y)\right. \\
& - \left.4\beta^2(1 - \beta^2)\left[\frac{N^2 - 2}{N(1 - \beta y)} + \frac{2}{N(1 + \beta y)}\right]\right\}.
\end{aligned}
$$
(B.1)

$$
\begin{aligned}
e_1^V = {} & -\frac{\hat{s}D_0^6(p_1, p_2, -k_2, 0, 0, 0, m)}{\pi}\frac{N^2 - 2}{2N}\left(2 - \frac{1 - \beta^2}{1 - \beta y}\right) \\
& - \frac{\hat{s}D_0^6(p_1, p_2, -k_1, 0, 0, 0, m)}{\pi N}\left(2 - \frac{1 - \beta^2}{1 + \beta y}\right) \\
& + \frac{m^2}{\beta^2}C_0(k_1, k_2, 0, m, 0)\left\{N + 2\beta^2\left[\frac{N^2 - 2}{N(1 - \beta y)} + \frac{2}{N(1 + \beta y)}\right]\right\} \\
& + \frac{\overline{B}_0(k_1 + k_2, 0, 0)}{2\beta^2}\left\{(1 - \beta^2)N + \frac{3\beta^2}{N}\right\} - \frac{\overline{B}_0(k_1 - p_1, 0, m)\beta\left(N^2 - 2\right)(\beta - y)}{N(1 - \beta y)} \\
& - \frac{2\overline{B}_0(k_2 - p_1, 0, m)\beta\left(\beta + y\right)}{N(1 + \beta y)} + \frac{3\overline{B}_0(k_1 + k_2, m, m)}{2N}
\end{aligned}
$$

$$+ \quad \frac{1}{\beta^2}\left\{N(3\beta^2-1)-2\beta^2(1-\beta^2)\left[\frac{N^2-2}{N(1-\beta y)}+\frac{2}{N(1+\beta y)}\right]\right\}. \tag{B.2}$$

$$
\begin{aligned}
e_2^V &= -\frac{\hat{s}D_0^6(p_1,p_2,-k_2,0,0,0,m)}{\pi}\frac{N^2-2}{2N}\left\{1+\beta^2-3\beta y+3\beta^3 y-2\beta^3 y^3+\frac{(1-\beta^2)^2}{1-\beta y}\right\}\\
&\quad - \frac{\hat{s}D_0^6(p_1,p_2,-k_1,0,0,0,m)}{\pi N}\left\{1+\beta^2+3\beta y-3\beta^3 y+2\beta^3 y^3+\frac{(1-\beta^2)^2}{1+\beta y}\right\}\\
&\quad + \frac{m^2}{\beta^2}C_0(k_1,k_2,0,m,0)\left\{N(2y^2\beta^2-3y^2+2\beta^3 y-2\beta y+3)+\frac{8y\beta(1-\beta^2)}{N}\right.\\
&\quad - \left. 2\beta^2(1-\beta^2)\left[\frac{N^2-2}{N(1-\beta y)}+\frac{2}{N(1+\beta y)}\right]\right\}\\
&\quad + \frac{\overline{B}_0(k_1+k_2,0,0)}{2\beta^2}\left\{N(3-2\beta y-3y^2-\beta^4+y^2\beta^4-2\beta^2+4y^2\beta^2)+\frac{\beta}{N}(8y+3\beta^3-3y^2\beta^3)\right\}\\
&\quad - \frac{\overline{B}_0(k_1-p_1,0,m)\left(N^2-2\right)(1-\beta y)}{N}-\frac{2\overline{B}_0(k_2-p_1,0,m)(1+\beta y)}{N}\\
&\quad + \frac{\overline{B}_0(k_1+k_2,m,m)\left(1+2\beta^2\right)\left(1-y^2\right)}{2N}\\
&\quad - \frac{1}{\beta^2}\left\{(3-2\beta y+2\beta^3 y-3y^2-5\beta^2+5y^2\beta^2)N+\frac{\beta}{N}(1-\beta^2)(\beta-\beta y^2+8y)\right\}. \tag{B.3}
\end{aligned}
$$

$$
\begin{aligned}
e_3^V &= \sqrt{(1-y^2)(1-\beta^2)}\left\{\frac{m^2}{2\beta^2}C_0(k_1,k_2,0,m,0)\left[-(2\beta+3y)N+\frac{8\beta}{N}\right]\right.\\
&\quad + \frac{\overline{B}_0(k_1+k_2,0,0)}{4\beta^2}\left[(-2\beta-3y+2\beta^2 y)N+\frac{8\beta}{N}\right]\\
&\quad + \frac{\overline{B}_0(k_1-p_1,0,m)\left(N^2-2\right)\beta}{2N\left(1-\beta y\right)}-\frac{\overline{B}_0(k_2-p_1,0,m)\beta}{N(1+\beta y)}-\frac{\overline{B}_0(k_1+k_2,m,m)y}{4N}\\
&\quad - \left. \frac{1}{2\beta^2}\left[N(3\beta^2 y-3y-2\beta)+\frac{\beta(8-\beta y)}{N}+2\beta^3\left(\frac{N^2-2}{N(1-\beta y)}-\frac{2}{N(1+\beta y)}\right)\right]\right\}. \tag{B.4}
\end{aligned}
$$

C. Virtual corrections to $gg \to t\bar{t}$

We list here the coefficients $A_V^{gg}, C_V^{gg}, D_V^{gg}$ and E_V^{gg} of Eq. (II.34), which are part of the IR-finite terms of the one-loop corrections to $gg \to t\bar{t}$.

$$
\begin{aligned}
A_V^{gg} &= \frac{\beta^2 D_0^6(p_1, p_2, -k_2, 0, 0, 0, m)N^2 \hat{s}\left(1-y^2\right)}{2\pi}\left\{ -1-\beta y + \frac{4-\beta^2}{1-\beta y} - 2\frac{2-\beta^2}{(1-\beta y)^2} + \frac{2(1-\beta^2)^2}{(1-\beta y)^3} \right\} \\
&+ \frac{D_0^6(-k_1, p_1, p_2, 0, m, m, m)\hat{s}\left(2+N^2\left(1-\beta y\right)\right)}{4\pi N^2 \beta^2\left(1+\beta y\right)}\left\{ \beta^2 y^2 + \beta^5 y - 3\beta^3 y + 2\beta y - \beta^4 - 2\beta^2 + 6 \right. \\
&- \frac{\beta^6 + 12 - 2\beta^4 - 3\beta^2}{1-\beta y} + \frac{2(4-3\beta^2)(1-\beta^4)}{(1-\beta y)^2} - \left. \frac{2(1+\beta^2)(1-\beta^2)^3}{(1-\beta y)^3} \right\} \\
&+ \frac{2\beta^4 D_0^6(p_1, -k_1, p_2, 0, 0, m, m)\hat{s}\left(1-y^2\right)}{\pi(1-\beta^2 y^2)^3}\left\{ -4 + 3y^2 + \beta^4 y^2 + \beta^2(1-y^2)(3-y^2) \right\} \\
&+ \frac{m^2 C_0(k_1, k_2, 0, m, 0)N^2}{2\beta^4}\left\{ 2(2+y^2)\beta^4 + 3(1-y^2)\beta^2 - 3 + \frac{6\beta^6 - 22\beta^4 - 3\beta^2 + 3}{1-\beta y} \right. \\
&+ \left. \frac{8\beta^4(3-2\beta^2)}{(1-\beta y)^2} - \frac{8\beta^4(1-\beta^2)^2}{(1-\beta y)^3} \right\} \\
&- \frac{m^2 C_0(k_1, -p_1, 0, m, m)}{\beta^2 N^2}\left\{ (\beta^3 y - \beta y + \beta^2 y^2 - \beta^4 + 4)N^2 - 2\beta^2 - 2\beta y \right. \\
&+ \frac{(-1+\beta^4 + 3\beta^6 - 7\beta^2)N^2 - 4\beta^4 + 4\beta^2 + 5 - \beta^6}{1-\beta y} + \frac{2(1-\beta^2)(\beta^2(1-2\beta^2)N^2 + \beta^4 + \beta^2 - 1)}{(1-\beta y)^2} \\
&+ \frac{(-3-5\beta^4 + 3\beta^6 + 17\beta^2)N^2 - 2\beta^4 + 2\beta^2 - 3 - \beta^6}{1+\beta y} + \frac{4N^2(2\beta^2 + \beta^4 - 5)\beta^2}{(1+\beta y)^2} \\
&+ \left. \frac{8N^2(1-\beta^2)^2\beta^2}{(1+\beta y)^3} \right\} + \frac{m^2 C_0(p_1, p_2, m, m, m)}{N^2 \beta^2}\left\{ -\beta^2(1-\beta^2)N^3 - N^2\beta^2 + 2 \right. \\
&+ \frac{\beta^2(1-\beta^2)N^3 + (1-\beta^2)(1+4\beta^2 + \beta^4)N^2 - \beta^6 + \beta^2 - 3\beta^4 - 5}{1-\beta y} \\
&- \left. \frac{(1+\beta^2)((1-\beta^2)^2 N^2 + \beta^4 + 2\beta^2 - 5)}{(1-\beta y)^2} - \frac{2(1+\beta^2)(1-\beta^2)^2}{(1-\beta y)^3} \right\} \\
&+ \frac{\overline{B}_0(k_1 - p_1, 0, m)\left[2 - N^2(1+\beta y)\right]}{8N^2\left(1+\beta y\right)}\left\{ -(10\beta y + 31 - 9\beta^2)N^2 + 2\beta y + 23 - 9\beta^2 \right. \\
&+ \frac{(1-\beta^2)(\beta^2 - 5)(N^2 - 1)}{1-2\beta y + \beta^2} + 4\frac{(\beta^4 - 13\beta^2 + 18)N^2 - 14 - \beta^4 + 9\beta^2}{1-\beta y} \\
&+ \left. \frac{8(1-\beta^2)((3\beta^2 - 5)N^2 - 3\beta^2 + 3)}{(1-\beta y)^2} + \frac{8(1-\beta^2)^2((1-\beta^2)N^2 + \beta^2)}{(1-\beta y)^3} \right\} \\
&+ \frac{\overline{B}_0(k_1 + k_2, 0, 0)N^2(1-y^2)\left(-2 + \left(-3+4\beta^2 + 2\beta^4\right)y^2\right)}{4\left(1-\beta^2 y^2\right)}
\end{aligned}
$$

$$+ \quad \frac{\overline{B}_0(k_1+k_2,m,m)}{4N^2(1-\beta^2 y^2)}\left\{2\beta^2 y^2(1-\beta^2)^2 N^3+(1-y^2)(2-\beta^2 y^2-2\beta^4 y^2)N^2+4(1-y^2)\right\}$$

$$+ \quad \frac{1}{24N^2\beta^4}\left\{(-60\beta^4 y^2+23\beta^6+36\beta^2 y^2-41\beta^4-72\beta^2+36)N^4\right.$$

$$- \quad 3\beta^2(9\beta^4-43\beta^2+4-4\beta^2 y^2)N^2+12\beta^4-48\beta^2+\frac{4N^4(6\beta^8-56\beta^6+59\beta^4+18\beta^2-9)}{1-\beta y}$$

$$- \quad \frac{24\beta^4(1-\beta^2)(4(2-\beta^2)N^4+(\beta^4+6\beta^2-13)N^2-\beta^4-3\beta^2+6)}{(1-\beta y)^2}$$

$$+ \quad \frac{48\beta^4(N^2-1)(1-\beta^2)^2((1-\beta^2)N^2+\beta^2)}{(1-\beta y)^3}$$

$$+ \quad \frac{12\beta^2((2\beta^{10}+17\beta^6+3+2\beta^8-115\beta^2+43\beta^4)N^2+24\beta^2-4\beta^6+12-2\beta^{10}-6\beta^8)}{(3+\beta^2)(1-\beta y)}$$

$$+ \quad \frac{3\beta^4(N^2-1)(1-\beta^2)(\beta^2-5)(N^2(3+\beta^2)-4)}{(3+\beta^2)(1+\beta^2+2\beta y)}+\frac{4\beta^6(1-\beta^2)N^3 N_f y^2}{(1-\beta^2 y^2)}\right\}+(y\to -y). \quad \text{(C.1)}$$

$$\begin{aligned}
C_V^{gg} &= \frac{2D_0^6(p_1,p_2,-k_2,0,0,0,m)N^2 m^2}{\pi}\left\{\frac{10-3\beta^2}{1-\beta y}-\frac{6(1-\beta^2)}{(1-\beta y)^2}+\frac{2(1-\beta^2)^2}{(1-\beta y)^3}\right.\\
&+ \quad \left.\frac{-\beta^3 y^3+2\beta^3 y-\beta^2 y^2+4\beta^2-4\beta y-4}{1-\beta^2}\right\}\\
&+ \quad \frac{D_0^6(-k_1,p_1,p_2,0,m,m,m)m^2\left(2+N^2(1-\beta y)\right)(1+\beta^2)}{\pi\beta^2 N^2(1+\beta y)}\left\{\frac{8-\beta^2}{1-\beta y}-\frac{6(1-\beta^2)}{(1-\beta y)^2}\right.\\
&+ \quad \left.\frac{2(1-\beta^2)^2}{(1-\beta y)^3}+\frac{-\beta^5 y+\beta^4+\beta^3 y-\beta^2 y^2-2\beta^2-2\beta y-4}{1-\beta^4}\right\}\\
&+ \quad \frac{4D_0^6(p_1,-k_1,p_2,0,0,m,m)m^2}{\pi}\left\{-\frac{2}{1-\beta^2}+\frac{2\beta^4+5}{1-\beta y}-\frac{2(1-\beta^2)(2+\beta^2)}{(1-\beta y)^2}+\frac{2(1-\beta^2)^2}{(1-\beta y)^3}\right\}\\
&+ \quad \frac{C_0(k_1,k_2,0,m,0)N^2 m^2}{2\beta^4}\left\{-2(2+y^2)\beta^4+(3y^2-7)\beta^2+3-\frac{3+6\beta^6-14\beta^4-7\beta^2}{1-\beta y}\right.\\
&- \quad \left.\frac{16\beta^4(1-\beta^2)}{(1-\beta y)^2}+\frac{8\beta^4(1-\beta^2)^2}{(1-\beta y)^3}\right\}\\
&+ \quad \frac{C_0(k_1,-p_1,0,m,m)m^2}{\beta^2 N^2}\left\{(\beta^3 y-\beta y+\beta^2 y^2+2-\beta^4)N^2-2\beta^2-2\beta y\right.\\
&- \quad \frac{(1-\beta^4)((1+3\beta^2)N^2-3-\beta^2)}{1-\beta y}+\frac{2(1-\beta^2)^2(2N^2\beta^2-\beta^2-1)}{(1-\beta y)^2}+\frac{8N^2(1-\beta^2)^2\beta^2}{(1+\beta y)^3}\\
&+ \quad \left.\frac{(3\beta^6+11\beta^2-5\beta^4-1)N^2-\beta^2-\beta^6-\beta^4-1}{1+\beta y}-\frac{4N^2(1-\beta^2)(3+\beta^2)\beta^2}{(1+\beta y)^2}\right\}\\
&+ \quad \frac{C_0(p_1,p_2,m,m,m)m^2}{\beta^2 N^2}\left\{\beta^2(1-\beta^2)N^3+N^2\beta^2-2\right.
\end{aligned}$$

$$+ \quad \frac{-\beta^2(1-\beta^2)N^3 + (3\beta^4 - \beta^2 + \beta^6 - 1)N^2 + 3 + \beta^2 + 3\beta^4 + \beta^6}{1-\beta y}$$

$$+ \quad \frac{(1-\beta^4)(N^2(1-\beta^2)-3-\beta^2)}{(1-\beta y)^2} + \frac{2(1+\beta^2)(1-\beta^2)^2}{(1-\beta y)^3} \Bigg\}$$

$$+ \quad \frac{\overline{B}_0(k_1-p_1,0,m)(2-N^2(1+\beta y))(1-\beta^2)}{8N^2(1+\beta y)} \Bigg\{ \frac{(-9\beta^2+11+10\beta y)N^2 - 2\beta y - 19 + 9\beta^2}{1-\beta^2}$$

$$+ \quad \frac{(1-\beta^2)(N^2-1)}{1-2\beta y+\beta^2} + \frac{4(\beta^2-8)(N^2-1)}{1-\beta y} + \frac{24(1-\beta^2)(N^2-1)}{(1-\beta y)^2} - \frac{8(1-\beta^2)^2(N^2-1)}{(1-\beta y)^3} \Bigg\}$$

$$- \quad \frac{\overline{B}_0(k_1+k_2,0,0)N^2\left(1-y^2\right)\left(2+\left(-3+4\beta^2+2\beta^4\right)y^2\right)}{4(1-\beta^2 y^2)}$$

$$- \quad \frac{\overline{B}_0(k_1+k_2,m,m)}{4N^2(1-\beta^2 y^2)} \Bigg\{ 2\beta^2 y^2(1-\beta^2)^2 N^3 + (-2-(2+5\beta^2+2\beta^4)y^2 + \beta^2(1+2\beta^2)y^4)N^2$$

$$- \quad 4\left(1+y^2\right) \Bigg\} + \frac{1-\beta^2}{24\beta^4 N^2} \Bigg\{ \frac{(60\beta^4 y^2 - 43\beta^4 + 120\beta^2 - 23\beta^6 - 36\beta^2 y^2 - 36)N^4}{1-\beta^2}$$

$$- \quad \frac{3\beta^2(-9\beta^4 + 31\beta^2 + 4\beta^2 y^2 - 4)N^2 + 12\beta^4 - 48\beta^2}{1-\beta^2} + \frac{4N^4(6\beta^6 - 26\beta^4 - 21\beta^2 + 9)}{1-\beta y}$$

$$+ \quad 12\beta^2 \frac{(4\beta^6 + 13\beta^4 + 54\beta^2 - 3 + 2\beta^8)N^2 - 2\beta^8 - 12 - 38\beta^2 - 6\beta^6 - 12\beta^4}{(3+\beta^2)(1-\beta y)}$$

$$+ \quad \frac{3\beta^4(1-\beta^2)(N^2-1)(3N^2 + N^2\beta^2 - 4)}{(3+\beta^2)(1+\beta^2+2\beta y)} + \frac{24\beta^4(1-\beta^2)(N^2-1)(4N^2-\beta^2-3)}{(1-\beta y)^2}$$

$$- \quad \frac{48\beta^4(1-\beta^2)^2(N^2-1)^2}{(1-\beta y)^3} - \frac{4\beta^6 N^3 N_f y^2}{1-\beta^2 y^2} \Bigg\} + (y \rightarrow -y). \tag{C.2}$$

$$
\begin{aligned}
D_V^{gg} &= (1-\beta^2)\Bigg\{ \frac{D_0^6(p_1,p_2,-k_2,0,0,0,m)N^2}{\pi\beta^2}\left[\frac{\beta^2}{1-\beta y} - \frac{2}{1-y^2}\right] \\
&+ \quad \frac{D_0^6(-k_1,p_1,p_2,0,m,m,m)(2+N^2(1-\beta y))}{\pi\beta^2 N^2(1+\beta y)}\left[\frac{2\beta^2-1}{1-\beta y} + \frac{1-\beta^2}{(1-\beta y)^2} - \frac{2\beta y}{1-y^2}\right] \\
&- \quad \frac{2(1-\beta^2)^2 D_0^6(p_1,-k_1,p_2,0,0,m,m)}{\pi\beta^2(1-y^2)(1-\beta^2 y^2)^2} \\
&+ \quad \frac{C_0(k_1,k_2,0,m,0)N^2}{4\beta^4}\left[3(1-\beta^2) + \frac{(3+\beta^2)(2\beta^2-1)}{1-\beta y} - \frac{4\beta^2}{1-y}\right] \\
&+ \quad \frac{C_0(k_1,-p_1,0,m,m)}{4\beta^2 N^2}\left[\frac{(1-\beta^2)(2N^2\beta^2 + \beta^2 - 4)}{1-\beta y} - \frac{2(1-\beta^2)(N^2-1)\beta^2}{(1-\beta y)^2}\right. \\
&- \quad \left.\frac{2(2-3\beta^2+\beta^4)N^2 + \beta^4 + 3\beta^2 + 4}{1+\beta y} + \frac{4(1-\beta^2)N^2\beta^2}{(1+\beta y)^2} - 4\frac{(1-\beta^2)N^2 + 2\beta y - 2}{1-y^2}\right] \\
&+ \quad \frac{C_0(p_1,p_2,m,m,m)}{\beta^2 N^2}\left[\frac{N^2+\beta^2+1}{1-\beta y} + \frac{1-\beta^2}{(1-\beta y)^2} - \frac{N^2+2}{1-y}\right]
\end{aligned}
$$

$$
\begin{aligned}
+ &\ \frac{\overline{B}_0(k_1-p_1,0,m)(2-N^2(1+\beta y))}{\beta^2 N^2 \hat{s}(1+\beta y)}\left[\frac{N^2-\beta}{1-y}+\frac{N^2+\beta}{1+y}+\frac{2\beta^2}{1-\beta y}-\frac{(1+N^2)\beta^2}{(1-\beta y)^2}\right.\\[4pt]
+ &\ \left.\frac{(1-\beta^2)(2N^2-1)\beta^2}{(1-\beta y)^3}\right]+\frac{\overline{B}_0(k_1+k_2,0,0)N^2}{2\beta^4\hat{s}}\left[3-2\beta^2+\frac{4\beta^2-3}{1-\beta y}\right]\\[4pt]
+ &\ \frac{\overline{B}_0(k_1+k_2,m,m)}{2\beta^2 N^2 \hat{s}}\left[N^2+\frac{(1+7\beta^2)N^2+4\beta^2+4}{(1-\beta^2)(1-\beta y)}-4\frac{N^2\beta^2+N^2+2}{(1-\beta^2)(1-y)}\right]\\[4pt]
+ &\ \frac{1}{N^2\beta^4\hat{s}}\left[-N^2(3N^2(1-\beta^2)+\beta^2)+\frac{4(N^4-N^2+2)\beta^2}{1+y}\right.\\[4pt]
- &\ \frac{(5\beta^2-3)N^4-\beta^2(2\beta^4+6\beta^2-1)N^2+5\beta^4+\beta^6+4\beta^2}{1-\beta y}\\[4pt]
- &\ \left.\frac{\beta^4(4N^4-2N^2\beta^2-3+\beta^2)}{(1-\beta y)^2}+\frac{2\beta^4(1-\beta^2)(N^2-1)(2N^2-1)}{(1-\beta y)^3}\right]+(y\to-y)\Bigg\}. \qquad\text{(C.3)}
\end{aligned}
$$

$$
\begin{aligned}
E_V^{gg} = &\ \frac{N^2 D_0^6(p_1,p_2,-k_2,0,0,0,m)}{\pi}\Bigg\{2\beta^2-2\beta^2 y^2-4\beta y-10-2\frac{1+2\beta y+\beta^2}{\beta^2(1-y^2)}-\frac{7\beta^2-19}{1-\beta y}\\[4pt]
- &\ \frac{(1-\beta^2)(9-\beta^2)}{(1-\beta y)^2}+4\frac{(1-\beta^2)^2}{(1-\beta y)^3}\Bigg\}+\frac{N^2 D_0^6(p_1,p_2,-k_1,0,0,0,m)}{\pi}\Bigg\{-2\beta^2+2\beta^2 y^2+6\\[4pt]
- &\ 5\frac{1-\beta^2}{1+\beta y}+\frac{(1-\beta^2)^2}{(1+\beta y)^2}-2\frac{1+2\beta y+\beta^2}{\beta^2(1-y^2)}\Bigg\}\\[4pt]
- &\ \frac{D_0^6(-k_1,p_1,p_2,0,m,m,m)(2+N^2(1-\beta y))}{4\pi\beta^2 N^2(1-\beta y)}\Bigg\{2\beta^2-4\beta y-6+\frac{(1-\beta^2)(3\beta^4+4\beta^2+9)}{1-\beta y}\\[4pt]
- &\ 4\frac{(1-\beta^4)(1-\beta^2)}{(1-\beta y)^2}-\frac{(1+\beta^2)(3\beta^4+6\beta^2-1)}{1+\beta y}+8\frac{(1-\beta^2)\beta y}{1-y^2}\Bigg\}\\[4pt]
+ &\ \frac{D_0^6(-k_2,p_1,p_2,0,m,m,m)(2+N^2(1+\beta y))}{4\pi\beta^2 N^2(1+\beta y)}\Bigg\{2\beta^2+4\beta y+2+\frac{(3-\beta^2)(1-\beta^2)^2}{(1+\beta y)}\\[4pt]
+ &\ \frac{(1+\beta^2)(\beta^6-15\beta^4-13\beta^2-5)}{(1-\beta^2)(1-\beta y)}+4\frac{\beta(1+\beta)^3}{(1-\beta)(1-y)}-4\frac{(1-\beta)^3\beta}{(1+\beta)(1+y)}\Bigg\}\\[4pt]
+ &\ \frac{2D_0^6(p_1,-k_1,p_2,0,0,m,m)}{\pi}\Bigg\{\frac{2\beta^4+\beta^2+9}{1-\beta y}-\frac{(1-\beta^2)(5+3\beta^2)}{(1-\beta y)^2}+4\frac{(1-\beta^2)^2}{(1-\beta y)^3}\\[4pt]
- &\ \frac{(1-\beta^2)(3+2\beta^2)}{1+\beta y}+\frac{(1-\beta^2)^2}{(1+\beta y)^2}-2\frac{1+2\beta y+\beta^2}{\beta^2(1-y^2)}\Bigg\}\\[4pt]
- &\ \frac{(1-\beta^2)C_0(k_1,k_2,0,m,0)N^2}{4\beta^4}\Bigg\{-2(3-\beta^2)(1+\beta y)+\frac{15\beta^6-13\beta^2-24\beta^4+6}{(1-\beta^2)(1-\beta y)}\\[4pt]
+ &\ 4\beta^4\frac{5-\beta^2}{(1-\beta y)^2}-16\beta^4\frac{1-\beta^2}{(1-\beta y)^3}+\beta^2\frac{1+11\beta^2}{1+\beta y}-4\beta^4\frac{1-\beta^2}{(1+\beta y)^2}+8\beta^2\frac{1+2\beta y+\beta^2}{(1-\beta^2)(1-y^2)}\Bigg\}\\[4pt]
+ &\ \frac{(1-\beta^2)C_0(k_1,-p_1,0,m,m)}{2\beta^2 N^2}\Bigg\{N^2(1+2\beta y+\beta^2)-4-\frac{(2+3\beta^2+3\beta^4)N^2-5-2\beta^2-\beta^4}{(1-\beta y)}
\end{aligned}
$$

$$
\begin{aligned}
- \;& \frac{2(1-\beta^2)(2+\beta^2-3\beta^2 N^2)}{(1-\beta y)^2} - \frac{(1+\beta^2)(1+3\beta^2)N^2+1-4\beta^2-\beta^4}{1+\beta y} \\
+ \;& \frac{4\beta^2 N^2(1-\beta^2)}{(1+\beta y)^2} - 2\frac{N^2(1+2\beta y+\beta^2)-2(1+\beta y)}{1-y^2}\Bigg\} \\
+ \;& \frac{C_0(k_2,-p_1,0,m,m)}{2\beta^2 N^2}\Bigg\{(1-\beta^2)(3+2\beta y-\beta^2)N^2+4(1-\beta^2)-3\frac{(1-\beta^2)^2(1-N^2\beta^2)}{(1+\beta y)} \\
- \;& \frac{(5-3\beta^2)(1-\beta^2)^2 N^2+5+2\beta^2+9\beta^4}{1-\beta y} - \frac{4\beta^2 N^2(1-\beta^2)(3+\beta^2)}{(1-\beta y)^2} \\
+ \;& \frac{16\beta^2 N^2(1-\beta^2)^2}{(1-\beta y)^3} - 2\frac{(1-\beta^2)(1+2\beta y+\beta^2)N^2-2-2\beta(3y+3\beta+\beta^2 y)}{1-y^2}\Bigg\} \\
+ \;& \frac{C_0(p_1,p_2,m,m,m)(1-\beta^2)}{2N^2\beta^2}\Bigg\{-\frac{4(2+N^2)(1+2\beta y+\beta^2)}{(1-\beta^2)(1-y^2)}+\frac{(1-\beta^2)(3-\beta^2)}{(1+\beta y)^2} \\
- \;& \frac{\beta^2(1-\beta^2)^2 N^3-\beta^2(1+\beta^2)(3+\beta^2)N^2-7-3\beta^2-5\beta^4-\beta^6}{(1-\beta^2)(1-\beta y)}+4\frac{(1-\beta^4)}{(1-\beta y)^3} \\
- \;& \frac{5+3\beta^4-2N^2(1-\beta^4)}{(1-\beta y)^2}+\frac{(N^3\beta^2(1-\beta^2)+(2-3\beta^2-\beta^4)N^2-1-6\beta^2-\beta^4)}{(1+\beta y)}\Bigg\} \\
+ \;& \frac{\overline{B}_0(k_1-p_1,0,m)(2-N^2(1+\beta y))}{4N^2\hat{s}}\Bigg\{-\frac{(25-2\beta^2+\beta^4)N^2-17-\beta^4-6\beta^2}{1-\beta y} \\
+ \;& \frac{2(1-\beta^2)((9+\beta^2)N^2-\beta^2-5)}{(1-\beta y)^2}+\frac{4(1-2N^2)(1-\beta^2)^2}{(1-\beta y)^3}+\frac{32(N^2-1)}{(3+\beta^2)(1-2\beta y+\beta^2)} \\
- \;& \frac{(-25+\beta^4-9\beta^2+\beta^6)N^2+1-23\beta^2-9\beta^4-\beta^6}{(3+\beta^2)(1+\beta y)}+8\frac{N^2(1+\beta y)-\beta(\beta+y)}{\beta^2(1-y^2)}\Bigg\} \\
+ \;& \frac{\overline{B}_0(k_2-p_1,0,m)(2-N^2(1-\beta y))}{N^2\hat{s}(1-\beta y)}\Bigg\{1-5N^2+\frac{(5N^2-3)(1-\beta^2)}{1+\beta y}-\frac{N^2(1-\beta^2)^2}{(1+\beta y)^2} \\
+ \;& 2\frac{N^2(1+2\beta y+\beta^2)+\beta(\beta^2 y+2\beta+y)}{\beta^2(1-y^2)}\Bigg\} \\
+ \;& \frac{\overline{B}_0(k_1+k_2,0,0)N^2}{2\beta^4\hat{s}}\Bigg\{6(1+\beta^2)(1-2\beta^2)(1+\beta y)-\frac{(6-11\beta^2-19\beta^4+4\beta^6)}{1-\beta y} \\
- \;& \frac{\beta^2(1-\beta^2)(1+4\beta^2)}{1+\beta y}\Bigg\}+\frac{\overline{B}_0(k_1+k_2,m,m)}{2\beta^2 N^2\hat{s}}\Bigg\{2N^2(1+5\beta^2)(1+\beta y) \\
+ \;& \beta^2\frac{2(1-\beta^2)^2 N^3-(3+5\beta^2)N^2-8}{(1+\beta y)}-\frac{8(N^2\beta^2+2+N^2)(1+2\beta y+\beta^2)}{(1-\beta^2)(1-y^2)} \\
+ \;& \frac{(-2\beta^2(1-\beta^2)^3 N^3+(2+11\beta^2+24\beta^4-5\beta^6)N^2+8(1+3\beta^2))}{(1-\beta^2)(1-\beta y)}\Bigg\} \\
+ \;& \frac{1}{3\hat{s}N^2\beta^4}\Bigg\{6N^2(1+\beta y)((3\beta^4+4\beta^2-3)N^2-\beta^2-\beta^4)+\frac{(32\beta^6-107\beta^4-39\beta^2+18)N^4}{1-\beta y}
\end{aligned}
$$

$$
\begin{aligned}
&+ \frac{3\beta^2(39\beta^2 + 3\beta^4 + 2\beta^6 - 2)N^2 - 3\beta^2(8 + 27\beta^2 + 10\beta^4 + \beta^6)}{1 - \beta y} \\
&- \frac{6\beta^4(1 - \beta^2)((\beta^2 - 7)N^4 + (\beta^2 + 9)N^2 - \beta^2 - 3)}{(1 - \beta y)^2} - \frac{12\beta^4(1 - \beta^2)^2(N^2 - 1)(2N^2 - 1)}{(1 - \beta y)^3} \\
&+ \frac{(1 - \beta^2)\beta^2 N^4(32\beta^2 + 3)}{1 + \beta y} - \frac{3(1 - \beta^2)\beta^4((\beta^2 + 5)(2\beta^2 + 7)N^2 - \beta^4 - 14\beta^2 - 35)}{(3 + \beta^2)(1 + \beta y)} \\
&- \frac{6N^2\beta^4(1 - \beta^2)^2(N^2 - 1)}{(1 + \beta y)^2} + \frac{24(N^4 - N^2 + 2)\beta^2(1 + \beta^2 + 2\beta y)}{1 - y^2} \\
&+ \frac{12\beta^4(N^2 - 1)(N^2\beta^2 + 3N^2 - 4)}{(3 + \beta^2)(1 - 2\beta y + \beta^2)} - \left. \frac{2\beta^5(1 - \beta^2)N^3 N_f y}{1 - \beta^2 y^2} \right\} .
\end{aligned}
\tag{C.4}
$$

D. Helicity amplitudes for the real emission processes

In this section we give explicit results in terms of helicity amplitudes for all real emission processes needed to compute the $2 \to 3$ spin density matrices R_{res}^i, $i = q\bar{q}, gg, qg, \bar{q}g$, discussed in sections III and IV. Generically, the matrices R_{res}^i can be obtained from

$$
\sum |\mathcal{T}|^2 \propto \text{Tr}\left[R_{\text{res}}^i(\mathbb{1} + \hat{\mathbf{s}}_t \cdot \boldsymbol{\tau}) \otimes (\mathbb{1} + \hat{\mathbf{s}}_{\bar{t}} \cdot \boldsymbol{\tau}) \right],
\tag{D.1}
$$

where the amplitudes $\mathcal{T}$ are given below and the sum stands for averaging or summing over colours and unobserved spins of the initial- or final-state particles. For the evaluation of the spin correlation observables introduced in Eq. (IV.3) one can also use the right-hand side of Eq. (IV.6).

D.1. The process $gg \to t\bar{t}g$

In this subsection we present the Born amplitudes for the process

$$
g(p_1)g(p_2)g(p_3) \to t(k_1)\bar{t}(k_2)
\tag{D.2}
$$

for all possible gluon helicity, and for t and $\bar{t}$ spin configurations in 4 dimensions. The gluon 4-momenta in (D.2) are incoming, and the $t, \bar{t}$ momenta are outgoing. The amplitudes for the process $gg \to t\bar{t}g$ can be easily obtained by crossing from the amplitudes given below. It is convenient to decompose the amplitude for (D.2) with respect to its colour structure. Performing this decomposition the $\mathcal{T}$ matrix element is then of the form:

$$
\mathcal{T}(ggg \to t\bar{t}) = \sum_{\{i,j,k\} \in P(1,2,3)} (T_{a_i} T_{a_j} T_{a_k})_{c_t c_{\bar{t}}} A(p_i, p_j, p_k, k_1, s_t, k_2, s_{\bar{t}}),
\tag{D.3}
$$

where the sum runs over all permutations of the indices $\{1, 2, 3\}$. The T_a are the generators of colour SU(N) in the fundamental representation. The indices $a_i, c_t,$ and $c_{\bar{t}}$ label the colour of the gluons, quarks, and antiquarks, respectively. The amplitudes $A(p_1, p_2, p_3, k_1, s_t, k_2, s_{\bar{t}})$ are the so-called colour-ordered

44

subamplitudes. They can be computed in a very compact way by using spinor helicity methods [57, 58, 59, 60]. We use the following notation [57] for massless spinors u, v of helicity $\pm\frac{1}{2}$:

$$
\begin{aligned}
u(p, \pm) &= v(p, \mp) = |p\pm\rangle, \\
\bar{u}(p, \pm) &= \bar{v}(p, \mp) = \langle p\pm|.
\end{aligned}
\tag{D.4}
$$

For the spinor products we use the short-hand notation:

$$
\begin{aligned}
\langle p_i p_j \rangle &= \langle p_i - | p_j + \rangle, \\
[p_i p_j] &= \langle p_i + | p_j - \rangle, \\
\langle p_i \pm | p_j | p_k \pm \rangle &= \langle p_i \pm | \not{p}_j | p_k \pm \rangle = \langle p_i \pm | p_j \mp \rangle \langle p_j \mp | p_k \pm \rangle,
\end{aligned}
\tag{D.5}
$$

for $p_i^2 = p_j^2 = p_k^2 = 0$. The polarization vector of a gluon with momentum k can be written in the 4-dimensional helicity scheme as follows:

$$
\varepsilon_\mu^\pm(k, q) = \pm \frac{\langle q^\mp | \gamma_\mu | k^\mp \rangle}{\sqrt{2} \langle q^\mp | k^\pm \rangle}.
\tag{D.6}
$$

The momentum q denotes a 'massless' ($q^2 = 0$) reference momentum, which is otherwise arbitrary. For a top quark with mass m and spin vector s_t we use the formalism of Ref. [58]:

$$
u(k_1, s_t) = \frac{[q_1 q_2]}{m} |q_1^+\rangle + |q_2^-\rangle,
\tag{D.7}
$$

with

$$
k_1 = q_1 + q_2, \quad \text{and} \quad s_t = (q_1 - q_2)/m
\tag{D.8}
$$

and

$$
v(k_2, s_{\bar{t}}) = \frac{[r_1 r_2]}{m} |r_1^+\rangle - |r_2^-\rangle,
\tag{D.9}
$$

with

$$
k_2 = r_1 + r_2, \quad \text{and} \quad s_{\bar{t}} = (r_2 - r_1)/m.
\tag{D.10}
$$

Note that q_1, q_2, r_1, and r_2 are massless momenta with

$$
2(q_1 \cdot q_2) = 2(r_1 \cdot r_2) = m^2.
\tag{D.11}
$$

We use the short-hand notation

$$
\langle p_i \pm | \sum_j p_j | p_k \pm \rangle \equiv \sum_j \langle p_i \pm | p_j | p_k \pm \rangle.
\tag{D.12}
$$

(If the momentum of the top or antitop quark is sandwiched between two spinors one must first decompose it into the sum of massless momenta $q_1 + q_2$ or $r_1 + r_2$.) For specific gluon helicity states we

obtain:

$$A(1^-,2^-,3^-) = \frac{[q_1 r_2]\langle q_1{}^+|p_1+p_2+p_3|q_2{}^+\rangle}{[p_1 q_1][p_1 p_2][p_2 p_3][p_3 q_1]} + \frac{[q_1 r_2]}{[p_1 q_1][p_2 q_1][p_3 q_1]}\Big($$

$$\frac{1}{4(p_1\cdot k_1)(p_3\cdot k_2)}\langle q_1{}^+|k_2|p_3{}^+\rangle\Big[\langle p_2 q_2\rangle\langle q_1{}^+|k_1|p_1{}^+\rangle - \langle p_1 p_2\rangle\langle q_1{}^+|p_1|q_2{}^+\rangle\Big]$$

$$-\frac{1}{2(p_3\cdot k_2)}\frac{1}{[p_1 p_2]}\langle q_1{}^+|p_1+p_2|q_2{}^+\rangle\langle q_1{}^+|k_2|p_3{}^+\rangle$$

$$+\frac{1}{2(p_1\cdot k_1)}\frac{1}{[p_2 p_3]}\Big[\langle q_1{}^+|p_3+p_2|q_2{}^+\rangle\langle q_1{}^+|k_1|p_1{}^+\rangle + \langle q_1{}^+|p_1|q_2{}^+\rangle\langle q_1{}^+|p_2+p_3|p_1{}^+\rangle\Big]\Big), \quad \text{(D.13)}$$

$$A(1^+,2^-,3^-) = -\frac{1}{2}\frac{\langle p_2 p_3\rangle(\langle r_1 r_2\rangle[p_1 r_2]\langle p_1{}^+|p_2+p_3|q_2{}^+\rangle - \langle q_1 q_2\rangle[p_1 q_1]\langle p_1{}^+|p_2+p_3|r_1{}^+\rangle)}{(m^2+(k_1\cdot k_2))\langle p_1 p_2\rangle[p_1 p_2][p_2 p_3]\langle r_1 r_2\rangle}$$

$$+\frac{1}{4}\frac{\langle p_1{}^+|k_1|p_2{}^+\rangle}{(p_1\cdot k_1)\langle p_1 p_2\rangle[p_1 p_2][p_1 p_3]}\Big(\frac{2}{[p_2 p_3]}\frac{\langle q_1 q_2\rangle}{\langle r_1 r_2\rangle}[p_1 q_1]\langle p_1{}^+|p_2+p_3|r_1{}^+\rangle$$

$$+\frac{1}{(p_3\cdot k_2)}\frac{\langle q_1 q_2\rangle}{\langle r_1 r_2\rangle}[p_1 q_1](\langle p_2 p_3\rangle\langle p_3 r_1\rangle[p_1 p_3] + \langle p_2 r_1\rangle\langle p_1{}^+|k_2|p_3{}^+\rangle)$$

$$-\frac{1}{(p_3\cdot k_2)}\langle p_2 q_2\rangle[p_1 r_2]\langle p_1{}^+|k_2|p_3{}^+\rangle - \frac{2}{[p_2 p_3]}[p_1 r_2]\langle p_1{}^+|p_2+p_3|q_2{}^+\rangle\Big), \quad \text{(D.14)}$$

$$A(1^-,2^+,3^-) = -\frac{1}{2}\frac{\langle p_1 p_3\rangle^2([p_2 r_2]\langle q_2{}^-|p_1+p_3|p_2{}^-\rangle\langle r_1 r_2\rangle - \langle q_1 q_2\rangle[p_2 q_1]\langle r_1{}^-|p_1+p_3|p_2{}^-\rangle)}{\langle p_1 p_2\rangle\langle p_2 p_3\rangle[p_2 p_3]\langle r_1 r_2\rangle[p_1 p_2](k_1\cdot k_2)+m^2}$$

$$+\frac{1}{2}\frac{\langle p_1 p_3\rangle}{\langle p_1 p_2\rangle\langle p_2 p_3\rangle[p_2 p_3]\langle r_1 r_2\rangle[p_1 p_2](p_1\cdot k_1)}\Big(\langle p_1 q_1\rangle\langle p_3 q_2\rangle[p_2 q_1][p_2 r_2]\langle r_1 r_2\rangle$$

$$+\langle p_1 q_2\rangle[p_2 r_2]\langle p_3{}^-|p_1-q_2|p_2{}^-\rangle\langle r_1 r_2\rangle + \langle p_3 r_1\rangle\langle q_1 q_2\rangle[p_2 q_1]\langle p_1{}^-|q_1+q_2|p_2{}^-\rangle\Big)$$

$$+\frac{1}{4}\frac{\langle p_1{}^-|k_1|p_2{}^-\rangle}{[p_1 p_2]\langle p_1 p_2\rangle[p_2 p_3]\langle r_1 r_2\rangle(p_1\cdot k_1)(p_3\cdot k_2)}\Big(\langle p_1 p_3\rangle\langle p_3 r_1\rangle\langle q_1 q_2\rangle[p_2 q_1][p_2 p_3]$$

$$-\langle p_3{}^-|k_2|p_2{}^-\rangle(\langle p_1 q_2\rangle[p_2 r_2]\langle r_1 r_2\rangle - [p_2 q_1]\langle q_1 q_2\rangle\langle p_1 r_1\rangle)\Big), \quad \text{(D.15)}$$

$$A(1^-,2^-,3^+) = -\frac{1}{2}\frac{\langle p_1 p_2\rangle([p_3 r_2]\langle q_2{}^-|p_1+p_2|p_3{}^-\rangle\langle r_1 r_2\rangle - \langle q_1 q_2\rangle[p_3 q_1]\langle r_1{}^-|p_1+p_2|p_3{}^-\rangle)}{[p_2 p_3]\langle p_2 p_3\rangle[p_1 p_2]\langle r_1 r_2\rangle(k_1\cdot k_2)+m^2}$$

$$-\frac{1}{2}\frac{\langle p_2{}^-|k_2|p_3{}^-\rangle([p_3 r_2]\langle q_2{}^-|p_1+p_2|p_3{}^-\rangle\langle r_1 r_2\rangle - \langle q_1 q_2\rangle[p_3 q_1]\langle r_1{}^-|p_1+p_2|p_3{}^-\rangle)}{[p_1 p_3]\langle p_2 p_3\rangle[p_1 p_2]\langle r_1 r_2\rangle[p_2 p_3](p_3\cdot k_2)}$$

$$+\frac{1}{4}\frac{\langle p_2{}^-|k_2|p_3{}^-\rangle}{[p_1 p_3][p_2 p_3]\langle p_2 p_3\rangle\langle r_1 r_2\rangle(p_1\cdot k_1)(p_3\cdot k_2)}([p_3 r_2]\langle p_1 p_2\rangle\langle p_1 q_2\rangle[p_1 p_3]\langle r_1 r_2\rangle$$

$$+\langle p_1{}^-|k_1|p_3{}^-\rangle([p_3 r_2]\langle p_2 q_2\rangle\langle r_1 r_2\rangle - \langle p_2 r_1\rangle\langle q_1 q_2\rangle[p_3 q_1])). \quad \text{(D.16)}$$

The subamplitudes for the remaining gluon helicity configurations can be obtained by exploiting, for example, CPT invariance. Calculating the squared amplitude in terms of colour-ordered subamplitudes, we have:

$$|\mathcal{T}(ggg\to t\bar{t})|^2 = N^3\frac{N^2-1}{N}\Big\{\sum_{\{i,j,k\}\in P(1,2,3)}|A(i,j,k)|^2$$

46

$$-\frac{1}{N^2}\sum_{\{i,j,k\}\in P(1,2,3)}|A(i,j,k)+A(i,k,j)+A(k,i,j)|^2+\frac{N^2+1}{N^4}\left|\sum_{\{i,j,k\}\in P(1,2,3)}A(i,j,k)\right|^2\Big\}. \quad \text{(D.17)}$$

The structure of (D.17) must be the same as that of the $\mathcal{T}$ matrix element squared of the reaction $Z,\gamma\to t\bar{t}ggg$, which was computed in Ref. [61]. We find agreement with this result.

D.2. The process $q\bar{q}\to t\bar{t}g$

Here we give the Born amplitudes for the reaction

$$q(p_1)\bar{q}(p_2)\to t(k_1)\bar{t}(k_2)g(p_3). \quad \text{(D.18)}$$

The colour decomposition of the corresponding $\mathcal{T}$ matrix element is given by

$$\mathcal{T}(q\bar{q}\to t\bar{t}g)=\frac{1}{N}\delta_{\bar{q}q}(T_a)_{t\bar{t}}A_1+\frac{1}{N}\delta_{t\bar{t}}(T_a)_{\bar{q}q}A_2+\delta_{\bar{q}\bar{t}}(T_a)_{tq}A_3+\delta_{tq}(T_a)_{\bar{q}\bar{t}}A_4, \quad \text{(D.19)}$$

with $q,\bar{q}$ denoting the colour indices of the massless quarks, while $t,\bar{t}$ denote the colour indices of the top quarks. The amplitudes for the processes

$$qg\to t\bar{t}q,\quad \bar{q}g\to t\bar{t}\bar{q} \quad \text{(D.20)}$$

can be obtained by crossing from (D.19). Using the above colour decomposition, the squared matrix element is given by

$$|\mathcal{T}(q\bar{q}\to t\bar{t}g)|^2=(N^2-1)\left(N\left(|A_3|^2+|A_4|^2\right)-\frac{1}{N}\left(A_1A_1^*+A_2A_2^*+2A_1^*A_2+2A_2^*A_1\right)\right), \quad \text{(D.21)}$$

where we have used

$$A_1+A_2+A_3+A_4=0 \quad \text{(D.22)}$$

in order to simplify the term that is subleading in the number of colours. Using again the 4-dimensional spinor helicity methods as in the previous section, we obtain the following results for specific helicity configurations of the massless partons:

$$A_1(p_1^-,p_2^-,p_3^+)=+\frac{1}{4}\frac{1}{(p_1\cdot p_2)}\frac{1}{(p_3\cdot k_1)}\left(-\frac{1}{\langle p_1p_3\rangle}\langle p_3^+|k_1|p_1^+\rangle\langle p_1q_2\rangle[p_2r_2]\right.$$
$$+\frac{1}{\langle p_1p_3\rangle}\frac{1}{\langle r_1r_2\rangle}\langle p_3^+|k_1|p_1^+\rangle\langle p_1r_1\rangle\langle q_1q_2\rangle[p_2q_1]-\frac{1}{\langle r_1r_2\rangle}\langle p_1r_1\rangle\langle q_1q_2\rangle[p_2p_3][p_3q_1]\right)$$
$$+\frac{1}{4}\frac{1}{(p_1\cdot p_2)}\frac{1}{(p_3\cdot k_2)}\left(-\langle p_1q_2\rangle[p_2p_3][p_3r_2]+\frac{1}{\langle p_1p_3\rangle}\langle p_3^+|k_2|p_1^+\rangle\langle p_1q_2\rangle[p_2r_2]\right.$$
$$\left.-\frac{1}{\langle p_1p_3\rangle}\frac{1}{\langle r_1r_2\rangle}\langle p_3^+|k_2|p_1^+\rangle\langle p_1r_1\rangle\langle q_1q_2\rangle[p_2q_1]\right), \quad \text{(D.23)}$$

$$A_2(p_1^-,p_2^-,p_3^+)=+\frac{1}{4}\frac{1}{(p_2\cdot p_3)}\frac{1}{(k_1\cdot k_2)+m^2}\left(\frac{1}{\langle p_1p_3\rangle}\frac{1}{\langle r_1r_2\rangle}\langle p_1p_2\rangle\langle p_1r_1\rangle\langle q_1q_2\rangle[p_2p_3][p_2q_1]\right.$$

$$+\langle p_1 q_2\rangle [p_2 p_3][p_3 r_2] - \frac{1}{\langle p_1 p_3\rangle}\langle p_1 p_2\rangle\langle p_1 q_2\rangle [p_2 p_3][p_2 r_2]$$

$$-\frac{1}{\langle r_1 r_2\rangle}\langle p_1 r_1\rangle\langle q_1 q_2\rangle [p_2 p_3][p_3 q_1]\Big), \tag{D.24}$$

$$A_3(p_1{}^-, p_2{}^-, p_3{}^+) = +\frac{1}{4}\frac{1}{(p_1\cdot p_2)}\frac{1}{(k_1\cdot k_2)+m^2}\Big(-\frac{\langle p_1 p_2\rangle\langle p_1 r_1\rangle}{\langle p_1 p_3\rangle\langle r_1 r_2\rangle}\langle q_1 q_2\rangle [p_2 p_3][p_2 q_1]$$

$$-\langle p_1 q_2\rangle [p_2 p_3][p_3 r_2] + \frac{1}{\langle p_1 p_3\rangle}\langle p_1 p_2\rangle\langle p_1 q_2\rangle [p_2 p_3][p_2 r_2] + \frac{1}{\langle r_1 r_2\rangle}\langle p_1 r_1\rangle\langle q_1 q_2\rangle [p_2 p_3][p_3 q_1]\Big)$$

$$+\frac{1}{4}\frac{1}{(p_1\cdot p_2)}\frac{1}{(p_3\cdot k_1)}\Big(+\frac{1}{\langle p_1 p_3\rangle}\langle p_3{}^+|k_1|p_1{}^+\rangle\langle p_1 q_2\rangle [p_2 r_2]$$

$$-\frac{1}{\langle p_1 p_3\rangle}\frac{1}{\langle r_1 r_2\rangle}\langle p_3{}^+|k_1|p_1{}^+\rangle\langle p_1 r_1\rangle\langle q_1 q_2\rangle [p_2 q_1] + \frac{1}{\langle r_1 r_2\rangle}\langle p_1 r_1\rangle\langle q_1 q_2\rangle [p_2 p_3][p_3 q_1]\Big), \tag{D.25}$$

$$A_1(p_1{}^-, p_2{}^-, p_3{}^-) = +\frac{1}{4}\frac{1}{(p_1\cdot p_2)}\frac{1}{(p_3\cdot k_1)}\Big(-\langle p_1 p_3\rangle\langle p_3 q_2\rangle [p_2 r_2]$$

$$+\frac{1}{[p_2 p_3]}\langle p_2{}^+|k_1|p_3{}^+\rangle\langle p_1 q_2\rangle [p_2 r_2] - \frac{1}{[p_2 p_3]}\frac{1}{\langle r_1 r_2\rangle}\langle p_2{}^+|k_1|p_3{}^+\rangle\langle p_1 r_1\rangle\langle q_1 q_2\rangle [p_2 q_1]\Big)$$

$$+\frac{1}{4}\frac{1}{(p_1\cdot p_2)}\frac{1}{(p_3\cdot k_2)}\Big(-\frac{1}{\langle r_1 r_2\rangle}\langle p_1 p_3\rangle\langle p_3 r_1\rangle\langle q_1 q_2\rangle [p_2 q_1]$$

$$-\frac{1}{[p_2 p_3]}\langle p_2{}^+|k_2|p_3{}^+\rangle\langle p_1 q_2\rangle [p_2 r_2] + \frac{1}{[p_2 p_3]}\frac{1}{\langle r_1 r_2\rangle}\langle p_2{}^+|k_2|p_3{}^+\rangle\langle p_1 r_1\rangle\langle q_1 q_2\rangle [p_2 q_1]\Big), \tag{D.26}$$

$$A_2(p_1{}^-, p_2{}^-, p_3{}^-) = \frac{1}{4}\frac{1}{(p_1\cdot p_3)}\frac{1}{(k_1\cdot k_2)+m^2}\Big(-\frac{1}{[p_2 p_3]}\frac{1}{\langle r_1 r_2\rangle}\langle p_1 p_3\rangle\langle p_1 r_1\rangle\langle q_1 q_2\rangle [p_1 p_2][p_2 q_1]$$

$$+\langle p_1 p_3\rangle\langle p_3 q_2\rangle [p_2 r_2] - \frac{1}{\langle r_1 r_2\rangle}\langle p_1 p_3\rangle\langle p_3 r_1\rangle\langle q_1 q_2\rangle [p_2 q_1]$$

$$+\frac{1}{[p_2 p_3]}\langle p_1 p_3\rangle\langle p_1 q_2\rangle [p_1 p_2][p_2 r_2]\Big), \tag{D.27}$$

$$A_3(p_1{}^-, p_2{}^-, p_3{}^-) = \frac{1}{4}\frac{1}{(p_1\cdot p_2)}\frac{1}{(k_1\cdot k_2)+m^2}\Big(-\frac{1}{[p_2 p_3]}\frac{1}{\langle r_1 r_2\rangle}\langle p_1 p_3\rangle\langle p_1 r_1\rangle\langle q_1 q_2\rangle [p_1 p_2][p_2 q_1]$$

$$-\frac{1}{\langle r_1 r_2\rangle}\langle p_1 p_3\rangle\langle p_3 r_1\rangle\langle q_1 q_2\rangle [p_2 q_1] + \frac{1}{[p_2 p_3]}\langle p_1 p_3\rangle\langle p_1 q_2\rangle [p_1 p_2][p_2 r_2] + \langle p_1 p_3\rangle\langle p_3 q_2\rangle [p_2 r_2]\Big)$$

$$+\frac{1}{2(p_1\cdot p_2)}\frac{1}{2(p_3\cdot k_1)}\Big(+\langle p_1 p_3\rangle\langle p_3 q_2\rangle [p_2 r_2] - \frac{1}{[p_2 p_3]}\langle p_2{}^+|k_1|p_3{}^+\rangle\langle p_1 q_2\rangle [p_2 r_2]$$

$$+\frac{1}{[p_2 p_3]}\frac{1}{\langle r_1 r_2\rangle}\langle p_2{}^+|k_1|p_3{}^+\rangle\langle p_1 r_1\rangle\langle q_1 q_2\rangle [p_2 q_1]\Big)$$

$$+\frac{1}{4}\frac{1}{(p_1\cdot p_3)}\frac{1}{(k_1\cdot k_2)+m^2}\Big(-\langle p_1 p_3\rangle\langle p_3 q_2\rangle [p_2 r_2] + \frac{1}{\langle r_1 r_2\rangle}\langle p_1 p_3\rangle\langle p_3 r_1\rangle\langle q_1 q_2\rangle [p_2 q_1]$$

$$-\frac{1}{[p_2 p_3]}\langle p_1 p_3\rangle\langle p_1 q_2\rangle [p_1 p_2][p_2 r_2] + \frac{1}{[p_2 p_3]}\frac{1}{\langle r_1 r_2\rangle}\langle p_1 p_3\rangle\langle p_1 r_1\rangle\langle q_1 q_2\rangle [p_1 p_2][p_2 q_1]\Big). \tag{D.28}$$

The remaining two helicity configurations can be obtained by exploiting the parity invariance of QCD. The amplitudes A determined in this way may get an additional phase, which cancels, however, when

48

calculating (D.21).

E. Fits to NLO results

In the following we give results in the form of fits for those functions discussed in Section IV that are not given in analytic form. These fits can be used to obtain predictions at the hadron level by convoluting with the corresponding parton distribution functions. At small β values, the accuracy of the fits is at the per cent level. For larger β values, they are less precise — but still precise enough for all phenomenological applications. Note that because of cancellations between different contributions, the 8 digits of precision of the parameters a_i are sometimes important.

For the scale-independent part in the reaction $gg \to t\bar{t}X$ we choose an ansatz similar to that used in Ref. [2]:

$$
\begin{aligned}
f_{gg}^{(1)}, g_{gg,a}^{(1)} &= c_{gg,i}\frac{7}{1536\pi}\left[12\beta\ln(8\beta^2)^2 - \frac{366}{7}\beta\ln(8\beta^2) + \frac{11}{42}\pi^2\right] \\
&+ \beta[a_1 + \beta^2(a_2\ln(8\beta^2) + a_3) + a_4\beta^4\ln(8\beta^2) + \rho^2(a_5\ln(\rho) + a_6\ln(\rho)^2) \\
&+ \rho(a_7\ln(\rho) + a_8\ln(\rho)^2)] \\
&+ a_9\beta^5 + a_{10}\beta^7\ln(\beta) + \rho^3(a_{11}\ln(\rho) + a_{12}\ln(\rho)^2).
\end{aligned}
\tag{E.1}
$$

The coefficients $c_{gg,i}$ are determined from the behaviour for small β. Fitting this function to our theoretical prediction, we obtain the values given in Table 8.

For the reaction $q\bar{q} \to t\bar{t}X$ we chose an ansatz similar to that of Ref. [2]:

$$
\begin{aligned}
f_{q\bar{q}}^{(1)}, g_{q\bar{q},a}^{(1)} &= c_{q\bar{q},i}\frac{\rho}{72\pi}\left[\frac{16}{3}\beta\ln(8\beta^2)^2 - \frac{82}{3}\beta\ln(8\beta^2) - \frac{\pi^2}{6}\right] \\
&+ \beta\rho[a_1 + \beta^2(a_2\ln(8\beta^2) + a_3) + \beta^4(a_4\ln(8\beta^2) + a_5) \\
&+ a_6\beta^6\ln(8\beta^2) + a_7\ln(\rho) + a_8\ln(\rho)^2].
\end{aligned}
\tag{E.2}
$$

The fitted parameters are given in Table 9. For the reaction $qg \to t\bar{t}X$ one has to consider two possibilities: either the quark or the gluon direction of flight in the $t\bar{t}$-ZMS corresponds to the direction used to define the axes $\hat{\mathbf{a}}, \hat{\mathbf{b}}$. In the case of the beam and off-diagonal bases, these two choices give different results at the parton level for the contribution from hard gluon emission. We denote the scaling functions for the first case by $g_{qg,3,4}^{(1)}$ and for the second case by $g_{gq,3,4}^{(1)}$. As fit ansatz we choose

$$
\begin{aligned}
f_{qg}^{(1)}, g_{qg(gq),a}^{(1)} &= \beta[\beta^2(a_1\ln(\beta) + a_2) + \beta^4(a_3\ln(\beta) + a_4) + \rho^2(a_5\ln(\rho) + a_6\ln(\rho)^2) \\
&+ \rho(a_7\ln(\rho) + a_8\ln(\rho)^2)] + \beta^4[a_9 + a_{10}\ln(\eta) + a_{11}\ln(\eta)^2] \\
&+ \rho^3[a_{12}\ln(\rho) + a_{13}\ln(\rho)^2].
\end{aligned}
\tag{E.3}
$$

The fitted values are shown in Tables 10 and 11.

¿From the analytic expressions for the leading-order results, the scaling functions determining the μ dependence can be obtained by a simple convolution with the corresponding Altarelli–Parisi evolution

Table 8: *Fit parameters as defined in Eq. (E.1) for the functions $f_{gg}^{(1)}, g_{gg,a}^{(1)}$.*

	$f_{gg}^{(1)}$	$g_{gg,1}^{(1)}$	$g_{gg,2}^{(1)}$	$g_{gg,3}^{(1)}$	$g_{gg,4}^{(1)}$
$c_{gg,i}$	1	-3	1	-1	-1
a_1	0.10981761	-0.31527984	0.10618585	-0.10654108	-0.10708321
a_2	-1.0630975	-0.27483778	-0.1722542	-0.091362874	0.062373685
a_3	-1.2553496	-0.98582485	0.053571485	-1.4480832	-0.31938862
a_4	-9.4872673	-4.7958679	0.46063565	-1.7773284	0.34555702
a_5	-3.6880817	-1.9966529	0.40949176	-1.5264395	0.038824512
a_6	-5.4736051	-2.8306013	1.3268284	-1.3615869	0.052584228
a_7	2.0430787	1.0567063	-0.66333002	0.12455129	-0.35180567
a_8	$6.8070238 \cdot 10^{-3}$	$-9.6117859 \cdot 10^{-3}$	0.034668583	-0.082780239	-0.13230861
a_9	23.269583	11.630659	-0.71127314	5.3857605	-0.46984803
a_{10}	-0.91120803	-1.5749174	4.1212869	-2.14052	-0.4187379
a_{11}	0.2999526	-0.32863816	0.12551445	-0.17836516	-0.21912773
a_{12}	-5.3509101	-2.2770031	-0.66992889	-0.64180163	0.22150197

Table 9: *Fit parameters as defined in Eq. (E.2) for the functions $f_{q\bar{q}}^{(1)}, g_{q\bar{q},a}^{(1)}$.*

	$f_{q\bar{q}}^{(1)}$	$g_{g\bar{q},1}^{(1)}$	$g_{q\bar{q},2}^{(1)}$	$g_{q\bar{q},3}^{(1)}$	$g_{q\bar{q},4}^{(1)}$
$c_{q\bar{q},i}$	1	1	$-1/3$	1	1
a_1	0.18272533	0.18271262	-0.061287765	0.18253142	0.18262171
a_2	0.18635401	0.18719675	0.015656292	0.1756192	0.18665363
a_3	-0.16337335	-0.15894226	-0.07245742	-0.17432802	-0.14086689
a_4	0.26381224	0.27417865	-0.089475628	0.22222852	0.27777792
a_5	-0.76180191	-0.78525268	0.21303639	-0.6620887	-0.78622279
a_6	-0.030248112	-0.034023724	0.020746502	-0.021337505	-0.033873638
a_7	0.012349472	0.013843671	-0.022717427	0.014090792	0.030078002
a_8	$7.7073036 \cdot 10^{-3}$	$7.85052 \cdot 10^{-3}$	$-8.1364483 \cdot 10^{-3}$	$5.9573824 \cdot 10^{-3}$	$8.8545826 \cdot 10^{-3}$

Table 10: *Fit parameters as defined in Eq. (E.3) for the functions* $f^{(1)}_{qg}$, $g^{(1)}_{qg,1,2}$.

	$f^{(1)}_{qg}$	$g^{(1)}_{qg,1}$	$g^{(1)}_{qg,2}$
a_1	0.01532878	$-7.5038708 \cdot 10^{-3}$	$2.1881981 \cdot 10^{-3}$
a_2	-0.45170812	-0.29554484	0.23254702
a_3	-0.1287014	-0.048548285	0.022275599
a_4	0.52370186	0.30790838	-0.23459259
a_5	-0.26811216	-0.15956101	0.12225428
a_6	0.022340876	0.018846548	-0.017627
a_7	-0.19533856	-0.14177144	0.11350417
a_8	-0.054689213	-0.02584021	0.021535027
a_9	-0.045358797	-0.013097499	$1.5210124 \cdot 10^{-3}$
a_{10}	$-7.7692908 \cdot 10^{-4}$	$1.3753108 \cdot 10^{-3}$	$-1.5369012 \cdot 10^{-3}$
a_{11}	$5.6252092 \cdot 10^{-5}$	$-8.811281 \cdot 10^{-5}$	$9.6359945 \cdot 10^{-5}$
a_{12}	$-8.8107179 \cdot 10^{-5}$	$-5.0153667 \cdot 10^{-5}$	$2.1289443 \cdot 10^{-5}$
a_{13}	-0.03501338	-0.013967759	$7.2211643 \cdot 10^{-3}$

Table 11: *Fit parameters as defined in Eq. (E.3) for the functions* $g^{(1)}_{qg,3,4}$ $g^{(1)}_{gq,3,4}$ *discussed in the text.*

	$g^{(1)}_{qg,3}$	$g^{(1)}_{qg,4}$	$g^{(1)}_{gq,3}$	$g^{(1)}_{gq,4}$
a_1	$1.8239099 \cdot 10^{-3}$	$2.0186389 \cdot 10^{-3}$	$1.6574875 \cdot 10^{-3}$	$1.8413674 \cdot 10^{-3}$
a_2	0.011452419	-0.025864066	-0.25682763	-0.26685522
a_3	-0.015540536	-0.022761156	-0.019640631	-0.025869178
a_4	$-6.5191297 \cdot 10^{-3}$	0.031656197	0.25770922	0.2732
a_5	0.012121019	$-7.5126124 \cdot 10^{-3}$	-0.13514839	-0.13361839
a_6	$-4.8820211 \cdot 10^{-3}$	$-3.8773834 \cdot 10^{-3}$	0.024057235	0.018832676
a_7	$-2.9631254 \cdot 10^{-3}$	-0.021304475	-0.12327878	-0.13543713
a_8	$-6.6094881 \cdot 10^{-3}$	-0.010139352	-0.018603959	-0.025245484
a_9	$-3.8199452 \cdot 10^{-3}$	$-4.3853099 \cdot 10^{-3}$	$-4.0261913 \cdot 10^{-3}$	$-6.6003001 \cdot 10^{-3}$
a_{10}	$1.8172768 \cdot 10^{-3}$	$1.8737765 \cdot 10^{-3}$	$1.065926 \cdot 10^{-3}$	$9.7391848 \cdot 10^{-4}$
a_{11}	$-1.0969205 \cdot 10^{-4}$	$-1.1280442 \cdot 10^{-4}$	$-5.9556692 \cdot 10^{-5}$	$-5.5377984 \cdot 10^{-5}$
a_{12}	$-2.2922513 \cdot 10^{-5}$	$-2.6895291 \cdot 10^{-5}$	$-2.100388 \cdot 10^{-5}$	$-2.4470893 \cdot 10^{-5}$
a_{13}	$-2.8989325 \cdot 10^{-3}$	$-5.9168202 \cdot 10^{-3}$	$-4.9177402 \cdot 10^{-3}$	$-6.3797473 \cdot 10^{-3}$

kernels, see Eq. (IV.34). In most cases the convolution integrals can be done analytically. For the remaining functions we use as ansatz for the process $gg \to t\bar{t}X$:

$$
\begin{aligned}
\tilde{g}^{(1)}_{gg,3,4} &= a_1 + a_2\beta + a_3\beta^2 + a_4\beta^3 + a_5\beta^4 + a_6\beta\ln(\beta) + a_7\beta^2\ln(\beta) + a_8\beta\ln(\beta)^2 + a_9\beta^2\ln(\beta)^2 \\
&+ a_{10}\beta^3\ln(\beta) + a_{11}\beta^3\ln(\beta)^2 + a_{12}\rho\ln(\rho) + a_{13}\rho^2\ln(\rho) + a_{14}\rho\ln(\rho)^2 \\
&+ a_{15}\rho^2\ln(\rho)^2 + a_{16}\beta\rho\ln(\rho). \quad (\text{E.4})
\end{aligned}
$$

The fitted values for the two functions $\tilde{g}^{(1)}_{gg,3,4}$ are given in Table 12.
For the scale-dependent part in the reaction $qg \to t\bar{t}X$ we use

$$
\begin{aligned}
\tilde{g}^{(1)}_{qg,3,4} = \tilde{g}^{(1)}_{gq,3,4} &= \beta(\beta^2(a_1\ln(\beta) + a_2) + \beta^4(a_3\ln(\beta) + a_4) + \rho^2(a_5\ln(\rho) + a_6\ln(\rho)^2) \\
&+ \rho(a_7\ln(\rho) + a_8\ln(\rho)^2)) + \beta^4 a_9 + \beta^4 a_{10}\ln(\eta) + \beta^4 a_{11}\ln(\eta)^2 \\
&+ \rho^3(a_{12}\ln(\rho) + a_{13}\ln(\rho)^2) + a_{14}\beta\ln(\eta) + a_{15}\beta^3\ln(\eta) + a_{16}\beta\ln(\eta)^2 \\
&+ a_{17}\beta^3\ln(\eta)^2 + a_{18}\beta\rho\ln(\eta) + a_{19}\beta^3\rho\ln(\eta) + a_{20}\beta\rho\ln(\eta)^2. \quad (\text{E.5})
\end{aligned}
$$

The fitted values for the two functions $\tilde{g}^{(1)}_{gq,3,4}$ are shown in Table 13.

Table 12: *Fit parameters as defined in Eq. (E.4) for the two functions $\tilde{g}_{gg,3,4}^{(1)}$.*

	$\tilde{g}_{gg,3}^{(1)}$	$\tilde{g}_{gg,4}^{(1)}$
a_1	$3.600512 \cdot 10^{-4}$	$9.8339551 \cdot 10^{-4}$
a_2	-0.89103071	-2.1615978
a_3	4.1432564	-2.4383759
a_4	-5.652246	-1.7863628
a_5	2.396262	6.3822522
a_6	-0.26139117	-0.7174869
a_7	0.55643278	-4.634966
a_8	-0.029004255	-0.076074349
a_9	0.44754783	0.26832936
a_{10}	-0.39236517	-8.4049829
a_{11}	-0.52419439	1.3153541
a_{12}	1.9909471	7.6847524
a_{13}	-0.8099637	-2.9175181
a_{14}	0.013395378	0.023018999
a_{15}	0.031263952	0.035390606
a_{16}	-1.9746581	-7.5775663

Table 13: *Fit parameters as defined in Eq. (E.5) for the two functions $\tilde{g}^{(1)}_{gq,3,4}$.*

	$\tilde{g}^{(1)}_{gq,3}$	$\tilde{g}^{(1)}_{gq,4}$
a_1	0.016955545	$-2.7829949 \cdot 10^{-3}$
a_2	0.057599714	0.03597281
a_3	0.012017294	$1.5756308 \cdot 10^{-3}$
a_4	-0.061168008	-0.043921612
a_5	0.025443918	0.023078656
a_6	$-2.4972922 \cdot 10^{-3}$	$-2.5244529 \cdot 10^{-3}$
a_7	0.019870969	0.019474128
a_8	$5.0330984 \cdot 10^{-3}$	$4.949093 \cdot 10^{-3}$
a_9	$2.216736 \cdot 10^{-3}$	$7.0180624 \cdot 10^{-3}$
a_{10}	$7.7028477 \cdot 10^{-3}$	$-1.6586156 \cdot 10^{-3}$
a_{11}	$-1.8013666 \cdot 10^{-4}$	$1.1083146 \cdot 10^{-4}$
a_{12}	$3.666881 \cdot 10^{-5}$	$-3.7800956 \cdot 10^{-5}$
a_{13}	$1.7202878 \cdot 10^{-3}$	$1.3536538 \cdot 10^{-3}$
a_{14}	$-4.2292913 \cdot 10^{-6}$	$2.2933896 \cdot 10^{-6}$
a_{15}	$-7.5513607 \cdot 10^{-3}$	$1.7188112 \cdot 10^{-3}$
a_{16}	$8.349152 \cdot 10^{-7}$	$8.6710055 \cdot 10^{-7}$
a_{17}	$1.6975408 \cdot 10^{-4}$	$-1.1585369 \cdot 10^{-4}$
a_{18}	$4.1704783 \cdot 10^{-6}$	$-2.2181371 \cdot 10^{-6}$
a_{19}	$1.645701 \cdot 10^{-3}$	$-1.7941491 \cdot 10^{-3}$
a_{20}	$-8.3995838 \cdot 10^{-7}$	$-8.6053362 \cdot 10^{-7}$

References

[1] I. I. Y. Bigi, Y. L. Dokshitzer, V. A. Khoze, J. H. Kühn and P. M. Zerwas, Phys. Lett. B **181** (1986) 157.

[2] P. Nason, S. Dawson and R. K. Ellis, Nucl. Phys. B **303** (1988) 607.

[3] P. Nason, S. Dawson and R. K. Ellis, Nucl. Phys. B **327** (1989) 49.

[4] W. Beenakker, H. Kuijf, W. L. van Neerven and J. Smith, Phys. Rev. D **40** (1989) 54.

[5] W. Beenakker, W. L. van Neerven, R. Meng, G. A. Schuler and J. Smith, Nucl. Phys. B **351** (1991) 507.

[6] E. Laenen, J. Smith and W. L. van Neerven, Phys. Lett. B **321** (1994) 254 [arXiv:hep-ph/9310233].

[7] N. Kidonakis and G. Sterman, Nucl. Phys. B **505** (1997) 321 [arXiv:hep-ph/9705234].

[8] R. Bonciani, S. Catani, M. L. Mangano and P. Nason, Nucl. Phys. B **529** (1998) 424 [arXiv:hep-ph/9801375].

[9] N. Kidonakis, E. Laenen, S. Moch and R. Vogt, Phys. Rev. D **64** (2001) 114001 [arXiv:hep-ph/0105041].

[10] D. Chakraborty, J. Konigsberg and D. Rainwater, Ann. Rev. Nucl. Part. Sci. **53** (2003) 301 [arXiv:hep-ph/0303092].

[11] J. H. Kühn, Nucl. Phys. B **237** (1984) 77.

[12] V. D. Barger, J. Ohnemus and R. J. Phillips, Int. J. Mod. Phys. A **4** (1989) 617.

[13] T. Arens and L. M. Sehgal, Nucl. Phys. B **393** (1993) 46.

[14] T. Arens and L. M. Sehgal, Phys. Lett. B **302** (1993) 501.

[15] G. Mahlon and S. Parke, Phys. Rev. D **53** (1996) 4886 [arXiv:hep-ph/9512264].

[16] T. Stelzer and S. Willenbrock, Phys. Lett. B **374** (1996) 169 [arXiv:hep-ph/9512292].

[17] D. Chang, S. C. Lee and A. Sumarokov, Phys. Rev. Lett. **77** (1996) 1218 [arXiv:hep-ph/9512417].

[18] A. Brandenburg, Phys. Lett. B **388** (1996) 626 [arXiv:hep-ph/9603333].

[19] G. Mahlon and S. Parke, Phys. Lett. B **411** (1997) 173 [arXiv:hep-ph/9706304].

[20] D. Atwood, A. Aeppli and A. Soni, Phys. Rev. Lett. **69** (1992) 2754.

[21] G. L. Kane, G. A. Ladinsky and C. P. Yuan, Phys. Rev. D **45** (1992) 124.

[22] C. R. Schmidt and M. E. Peskin, Phys. Rev. Lett. **69** (1992) 410.

[23] A. Brandenburg and J. P. Ma, Phys. Lett. B **298** (1993) 211.

[24] W. Bernreuther and A. Brandenburg, Phys. Lett. B **314** (1993) 104.

[25] W. Bernreuther and A. Brandenburg, Phys. Rev. D **49** (1994) 4481 [arXiv:hep-ph/9312210].

[26] P. Haberl, O. Nachtmann and A. Wilch, Phys. Rev. D **53** (1996) 4875 [arXiv:hep-ph/9505409].

[27] K. Cheung, Phys. Rev. D **55** (1997) 4430 [arXiv:hep-ph/9610368].

[28] B. Grzadkowski, B. Lampe and K. J. Abraham, Phys. Lett. B **415** (1997) 193 [arXiv:hep-ph/9706489].

[29] W. Bernreuther, M. Flesch and P. Haberl, Phys. Rev. D **58** (1998) 114031 [arXiv:hep-ph/9709284].

[30] W. Bernreuther, A. Brandenburg and M. Flesch, arXiv:hep-ph/9812387.

[31] D. Atwood, S. Bar-Shalom, G. Eilam and A. Soni, Phys. Rep. **347** (2001) 1 [arXiv:hep-ph/0006032].

[32] W. Khater and P. Osland, Nucl. Phys. B **661** (2003) 209 [arXiv:hep-ph/0302004].

[33] W. Bernreuther, A. Brandenburg and Z. G. Si, Phys. Lett. B **483** (2000) 99 [arXiv:hep-ph/0004184].

[34] W. Bernreuther, A. Brandenburg, Z. G. Si and P. Uwer, Phys. Lett. B **509** (2001) 53 [arXiv:hep-ph/0104096].

[35] W. Bernreuther, A. Brandenburg, Z. G. Si and P. Uwer, Phys. Rev. Lett. **87** (2001) 242002 [arXiv:hep-ph/0107086].

[36] A. Czarnecki, M. Jezabek and J. H. Kühn, Nucl. Phys. B **351** (1991) 70.

[37] A. Brandenburg, Z. G. Si and P. Uwer, Phys. Lett. B **539** (2002) 235 [arXiv:hep-ph/0205023].

[38] V. S. Fadin, V. A. Khoze and A. D. Martin, Phys. Rev. D **49** (1994) 2247.

[39] V. S. Fadin, V. A. Khoze and A. D. Martin, Phys. Lett. B **320** (1994) 141 [arXiv:hep-ph/9309234].

[40] K. Melnikov and O. I. Yakovlev, Phys. Lett. B **324** (1994) 217 [arXiv:hep-ph/9302311].

[41] W. Beenakker, A. P. Chapovsky and F. A. Berends, Nucl. Phys. B **508** (1997) 17 [arXiv:hep-ph/9707326].

[42] W. Beenakker, F. A. Berends and A. P. Chapovsky, Phys. Lett. B **454** (1999) 129 [arXiv:hep-ph/9902304].

[43] W. Bernreuther, A. Brandenburg and P. Uwer, Phys. Lett. B **368** (1996) 153 [arXiv:hep-ph/9510300].

[44] W. G. Dharmaratna and G. R. Goldstein, Phys. Rev. D **53** (1996) 1073.

[45] V. N. Gribov and L. N. Lipatov, Yad. Fiz. **15** (1972) 1218 [Sov. J. Nucl. Phys. **15** (1972) 675].

[46] V. N. Gribov and L. N. Lipatov, Yad. Fiz. **15** (1972) 781 [Sov. J. Nucl. Phys. **15** (1972) 438].

[47] L. N. Lipatov, Yad. Fiz. **20** (1974) 181 [Sov. J. Nucl. Phys. **20** (1975) 94].

[48] G. Altarelli and G. Parisi, Nucl. Phys. B **126** (1977) 298.

[49] Y. L. Dokshitzer, Sov. Phys. JETP **46** (1977) 641 [Zh. Eksp. Teor. Fiz. **73** (1977) 1216].

[50] J. C. Collins, F. Wilczek and A. Zee, Phys. Rev. D **18** (1978) 242.

[51] W. Beenakker, A. Denner, W. Hollik, R. Mertig, T. Sack and D. Wackeroth, Nucl. Phys. B **411** (1994) 343.

[52] C. Kao, G. A. Ladinsky and C. P. Yuan, Int. J. Mod. Phys. A **12** (1997) 1341.

[53] C. Kao and D. Wackeroth, Phys. Rev. D **61** (2000) 055009 [arXiv:hep-ph/9902202].

[54] J. Pumplin, D. R. Stump, J. Huston, H. L. Lai, P. Nadolsky and W. K. Tung, JHEP **0207** (2002) 012 [arXiv:hep-ph/0201195].

[55] A. D. Martin, R. G. Roberts, W. J. Stirling and R. S. Thorne, arXiv:hep-ph/0308087.

[56] M. Glück, E. Reya and A. Vogt, Eur. Phys. J. C **5** (1998) 461 [arXiv:hep-ph/9806404].

[57] Z. Xu, D. H. Zhang and L. Chang, Nucl. Phys. B **291** (1987) 392.

[58] R. Kleiss and W. J. Stirling, Nucl. Phys. B **262** (1985) 235.

[59] J. F. Gunion and Z. Kunszt, Phys. Lett. B **161** (1985) 333.

[60] M. L. Mangano and S. J. Parke, Phys. Rep. **200** (1991) 301.

[61] J. M. Campbell and E. W. Glover, Nucl. Phys. B **527** (1998) 264 [arXiv:hep-ph/9710255].

[62] S. R. Slabospitsky and L. Sonnenschein, Comput. Phys. Commun. **148** (2002) 87 [arXiv:hep-ph/0201292].

[63] N. Kauer and D. Zeppenfeld, Phys. Rev. D **65** (2002) 014021 [arXiv:hep-ph/0107181].

[64] N. Kauer, Phys. Rev. D **67** (2003) 054013 [arXiv:hep-ph/0212091].

[65] B. Abbott *et al.* [D0 Collaboration], Phys. Rev. Lett. **85** (2000) 256 [arXiv:hep-ex/0002058].